

TRPML1 REGULATES PROSTATE CANCER CELL PROLIFERATION THROUGH THE  
MODULATION OF OXIDATIVE STRESS AND CELL CYCLE

by

Andra Mihaela Sterea

Submitted in partial fulfilment of the requirements  
for the degree of Master of Science

at  
Dalhousie University  
Halifax, Nova Scotia  
August 2018

**Dedicated to Mușca și Stuf**

## Table of Contents

<b>List of Tables .....</b>	<b>vii</b>
<b>List of Figures.....</b>	<b>viii</b>
<b>Abstract.....</b>	<b>x</b>
<b>List of Abbreviations and Symbols Used .....</b>	<b>xi</b>
<b>Acknowledgements .....</b>	<b>xiv</b>
<b>CHAPTER I: INTRODUCTION .....</b>	<b>1</b>
<b>    1.1 Subchapter I: Cancer, A Historical Account and Current Knowledge.....</b>	<b>1</b>
1.1.1 History of Cancer .....	1
1.1.2 Current Knowledge and Challenges .....	2
1.1.3 The Molecular Mechanisms of Cancer and the Basis for the Famous “Hallmarks of Cancer” .....	5
1.1.3.1 PI3K/AKT/mTOR Pathway .....	6
1.1.3.2 JNK Signaling Pathway .....	7
1.1.3.3 ERK Pathway .....	8
1.1.3.4 Autophagy .....	8
1.1.3.5 Generation of Reactive Oxygen and Nitrogen Species.....	9
1.1.3.6 DNA Damage and Repair .....	11
1.1.3.6.1 Homologous Recombination .....	12
1.1.3.6.2 Mismatch Repair.....	12
1.1.3.6.3 Nucleotide Excision Repair .....	13
1.1.3.6.4 DNA Strand Crosslink Repair .....	13
1.1.3.6.5 Nonhomologous End-Joining .....	14
1.1.3.7 Apoptosis .....	14
<b>    1.2 Subchapter II: A Comprehensive Description of Prostate Cancer .....</b>	<b>19</b>
1.2.1 Physiology of the Prostate Gland.....	19
1.2.2 Prostate Cancer Epidemiology.....	20
1.2.3 Diagnosis.....	21
1.2.4 Biomarkers .....	22

1.2.4.1 PSA Testing .....	22
1.2.4.2 Emerging “omics”-Related Biomarkers .....	27
1.2.4.3 Immune System-Based Biomarkers.....	28
1.2.5 Tumor Biopsy Analysis .....	29
1.2.5.1 Grading .....	29
1.2.5.2 Staging .....	29
1.2.6 Driver Mutations.....	30
1.2.6.1 Genes Alterations in PCa and Other Cancers .....	30
1.2.6.3 Mutations Specific to PCa .....	32
<b>1.3 Subchapter III: Prostate Cancer Therapies and Patient Care.....</b>	<b>33</b>
1.3.1 Current Treatments .....	34
1.3.2 Emerging Therapies .....	34
1.3.2.1 TRP Ion Channel-Based Therapies for Cancer.....	35
1.3.2.2 TRP Ion Channel-Based Therapies for Prostate Cancer.....	36
<b>1.4 Subchapter IV: Lysosomal TRP Channels and Their Role in Carcinogenesis.....</b>	<b>36</b>
1.4.1 Lysosome Physiology .....	36
1.4.2 TRP Channels .....	42
1.4.2.1 TRPML1 .....	42
<b>1.5 Subchapter V: Project Rationale and Objectives .....</b>	<b>48</b>
1.5.1 Rationale and Hypothesis .....	48
1.5.2 Objectives .....	49
<b>CHAPTER II: MATERIALS AND METHODS .....</b>	<b>50</b>
<b>2.1 Cell Lines.....</b>	<b>50</b>
<b>2.2 Reagents.....</b>	<b>50</b>
<b>2.3 Mucolipin-Specific Inhibitor (ML-SI) Treatment .....</b>	<b>51</b>
<b>2.4 TRPML1 Knockdown .....</b>	<b>52</b>
<b>2.5 RT-qPCR.....</b>	<b>52</b>
2.5.1 Primer Sequence Table .....	53

<b>2.6 Western Blot .....</b>	<b>53</b>
<b>2.7 Flow Cytometry .....</b>	<b>55</b>
2.7.1 CFSE (5(6)-Carboxyfluorescein N-Hydroxysuccinimidyl Ester) Staining .....	55
2.7.2 Propidium Iodide (PI) Staining .....	56
2.7.3 DAF-FM and H <sub>2</sub> DCFDA Staining.....	57
2.7.4 Annexin V/7AAD Staining.....	57
<b>2.8 MTS Assay .....</b>	<b>58</b>
<b>2.9 Confocal Microscopy .....</b>	<b>59</b>
<b>2.10 Calcium Imaging .....</b>	<b>59</b>
<b>2.11 Bioinformatics Analysis .....</b>	<b>60</b>
2.11.1 Kaplan Meier Survival Analysis .....	61
2.11.2 CCLE Gene Expression .....	61
2.11.3 Co-Expression Analysis.....	61
<b>2.12 Statistics.....</b>	<b>61</b>
<b>CHAPTER III: RESULTS.....</b>	<b>63</b>
<b>3.1 The Loss of TRPML1 Decreases Cell Proliferation in PCa Cell Lines in a Dose-Dependent Manner .....</b>	<b>63</b>
<b>3.2 Knockdown of TRPML1 in PCa Leads to G2/M Cell Cycle Arrest due to DNA Damage .....</b>	<b>81</b>
<b>3.3 TRPML1 KD Results in the Accumulation of Reactive Oxygen and Nitrogen Species in PCa Cells .....</b>	<b>92</b>
<b>3.4 TRPML1 Knockdown Inhibits Autophagy Through the Activation of AKT .....</b>	<b>97</b>
<b>3.5 Analysis of TRPML1 as a Potential Biomarker for Prostate Cancer .....</b>	<b>103</b>
<b>CHAPTER IV: SUMMARY .....</b>	<b>111</b>
<b>CHAPTER V: LIMITATIONS AND FUTURE DIRECTIONS.....</b>	<b>114</b>
<b>5.1 In Vitro Model.....</b>	<b>114</b>
<b>5.2 Specificity of ML-SI.....</b>	<b>115</b>

<b>5.3 Presence of TRPML1 in Newly Synthesized Lysosomes .....</b>	<b>115</b>
<b>5.4 Assessment of Lysosomal Functionality.....</b>	<b>116</b>
<b>5.5 Identification of Molecular Mechanism.....</b>	<b>116</b>
<b>5.6 Univariate Analysis vs. Multivariate Analysis.....</b>	<b>117</b>
<b>CHAPTER VI: DISCUSSION.....</b>	<b>114</b>
<b>APPENDIX A: SUPPLEMENTAL FIGURES.....</b>	<b>123</b>
<b>REFERENCES.....</b>	<b>127</b>

## **List of tables**

<b>Table 1: List of PSA-based biomarkers and associated testing methods .....</b>	<b>24</b>
<b>Table 2: List of biomarkers identified through proteomic or genomic approaches.....</b>	<b>25</b>
<b>Table 3: Immune system-based biomarkers for prostate cancer .....</b>	<b>26</b>
<b>Table 4: List of prostate cancer driver mutations .....</b>	<b>31</b>

## List of figures

<b>Figure 1: Cartoon representation of the autophagy pathway .....</b>	<b>17</b>
<b>Figure 2: Schematic representation of ion channels present within the lysosomal membrane .....</b>	<b>40</b>
<b>Figure 3: Structure of TRPML channels.....</b>	<b>46</b>
<b>Figure 4: TRPML1 is overexpressed in PCa cell lines .....</b>	<b>65</b>
<b>Figure 5: TRPML1 inhibition causes a dose-dependent decrease in cell viability/proliferation.....</b>	<b>67</b>
<b>Figure 6: Loss of TRPML1 inhibits the proliferation of PCa cell lines .....</b>	<b>70</b>
<b>Figure 7: Generation of TRPML1 knockdowns and loss of TRPML1 channel functionality in PCa.....</b>	<b>74</b>
<b>Figure 8: Knockdown of TRPML1 decreases PCa cell proliferation .....</b>	<b>76</b>
<b>Figure 9: TRPML1 is a potential regulator of PCa cell proliferation as indicated by the increase in CFSE staining. ....</b>	<b>78</b>
<b>Figure 10: TRPML1 expression does apoptosis in prostate cancer or normal cell lines .....</b>	<b>83</b>
<b>Figure 11: TRPML1 knockdown arrests PCa cells in the G2/M phase of the cell cycle.....</b>	<b>86</b>
<b>Figure 12: Downregulation of TPRML1 induces cell cycle arrest due to the presence of DNA damage in PC3 cells.....</b>	<b>90</b>
<b>Figure 13: Accumulation of nitric oxide (NO) following TRPML1 knockdown in PC3 cells .....</b>	<b>93</b>
<b>Figure 14: Increased levels of reactive oxygen species (ROS) detected in TRPML1 KD PC3 cells .....</b>	<b>95</b>
<b>Figure 15: Increased lysosomal biogenesis is observed following knockdown of TRPML1.99</b>	<b>99</b>
<b>Figure 16: TRPML1 modulates cell proliferation via autophagy inhibition and activation of AKT .....</b>	<b>101</b>
<b>Figure 17: Correlation analysis between TRPML1 expression and prostate cancer patient overall survival, disease- free survival and Gleason sum.....</b>	<b>105</b>

**Figure 18: Association between TRPML1 gene modifications and overall PCa patient survival.....** 107

**Figure 19: TRPML1 co-expression with established and emerging PCa biomarkers .....** 109

**Figure 20: Schematic representation of the proposed mechanism for the involvement of TRPML1 in mediating PCa cell proliferation.....** 112

## **Abstract**

Prostate cancer (PCa) represents a multifactorial and complex disease affecting thousands of men each year. Although the prognosis of PCa is improving, limitations in early diagnosis pose a challenge for the effective treatment of patients with late stages of the disease. Research is now focusing on targeting ion channels as a means of delaying the progression of PCa in patients who do not respond to traditional therapies. One potential target is the ion channel TRPML1 whose function mediates cellular bioenergetics. Here, we demonstrate that TRPML1 is overexpressed in PCa cells and its downregulation decreases cell proliferation. At the molecular level, the loss of TRPML1 impairs autophagy resulting in the accumulation of free radicals, ultimately leading to DNA damage and cell cycle arrest. Our data suggests an important role for TRPML1 in the maintenance of PCa cell proliferation and its potential as a novel therapeutic target for the treatment of PCa.

## List of Abbreviations and Symbols Used

Abbreviation	Description
ADPR	Adenosine diphosphoribose
AJCC	American Joint Committee on Cancer
AR	Androgen receptor
Arf	ADP-ribosylation factor
ATCC	American Type Culture Collection
ATG	Autophagy- related genes
ATP	Adenosine triphosphate
Bcl-2	B-cell lymphoma 2
Bcl-XL	B-cell lymphoma extra large
BH	Bcl-2 homology domains
BK	Big conductance K <sup>+</sup>
CAT	Catalase
CCLE	Cancer Cell Line Encyclopedia
CFSE	5(6)-Carboxyfluorescein N-hydroxysuccinimidyl ester
CHD1	Chromodomain helicase DNA binding protein 1
CS	Cockayne syndrome
ct	Cycle time
DDR	DNA damage response
DNA-PKcs	DNA-dependent protein kinase
DR	Death receptors
DRE	Digital rectal exam
DSB	Double-strand DNA breaks
dsRNA	Double-stranded RNA
ER	Endoplasmic reticulum
ER	Endoplasmic reticulum
ERK	Extracellular signal regulated kinase
ETC	Electron transport chain
ETS	E26 transformation- specific transcription factors
ExoI	Exonuclease I
FA	Fanconi anemia
FasL	Fas ligand
FDA	Food and Drug Administration
FOXA1	Forkhead box A1
fPSA	Free PSA
FSC	Forward scatter
GG-NER	Global genome nucleotide excision repair
GPCR	G protein-coupled receptors
GPI-AP	Glycosylphosphatidylinositol- anchored proteins
GPS	Genomic prostate score
GPX	Glutathione peroxidases
hK2	Hk2
HR	Homologous recombination
JNK	C-Jun N-terminal kinase

KD	Knockdown
KDM6	Lysine-specific demethylase 6A
Lamp	Lysosomal-associated membrane proteins
LC3-I/II	Microtubule-associated protein light chain 3- I/II
LEL	Late endo-lysosome
LMP	Lysosome membrane permeabilization
LSD	Lysosomal storage disease
M6P	Mannose 6-phosphate
MAPK	Mitogen-activated protein kinase
MAPKKK	MAPK kinase kinase
MFI	Mean fluorescence intensity
MLIV	Mucolipidosis IV
MLL	Mixed-lineage leukemia
MMR	Mismatch repair
NER	Nucleotide excision repair
NHEJ	Nonhomologous end-joining
NO	Nitric oxide
NOS	Nitric oxide synthase
P2X4	P2X purinoceptor 4
PARP1	Poly(ADP-ribose) polymerase 1
PCa	Prostate cancer
PCA3	Prostate cancer antigen 3
PHI	Prostate health index
PHLPP1	PH domain and Leucine-rich repeat protein
PI	Propidium iodide
PI(3,5)P <sub>2</sub>	Phosphatidylinositol-3,5-bisphosphate
PI3K	Phosphoinositide 3-kinase
PIK3CA	Catalytic subunit of PI3K
PKB	Protein kinase B also known as AKT
PRX	Peroxiredoxins
PSA	Prostate-specific antigen
PTEN	Phosphatase and tensin homolog
Rad51	Recombination protein a
Raf	Rapidly accelerated fibrosarcoma
Ras	Rat sarcoma
RB	Retinoblastoma protein Rb
ROS	Reactive oxygen species
RTK	Receptor tyrosine kinases
SOD	Superoxide dismutase
SQSTM1	Sequestosome 1
SSC	Side scatter
ssDNA	Single-stranded DNA
TC-NER	Transcription-coupled nucleotide excision repair
TCGA	The Cancer Genome Atlas
TFEB	Transcription factor EB
TLR	Toll-like receptor

TLR9	Toll-like receptor 9
TM	Transmembrane
TMEM175	Transmembrane protein 175
TNBC	Triple negative breast cancer
TNF	Tumor necrosis factor
TP53	Tumor suppressor p53
TP53BP1	p53 binding protein 1
TPC	Two pore channel
tPSA	Total PSA
TRAIL	Tumor necrosis factor- related apoptosis- inducing ligand
TRP	Transient receptor potential
TRPML2lv	Transient receptor potential mucolipin 2 long variant
TRPML2sv	Transient receptor potential mucolipin 2 short variant
TTD	Trichothiodystrophy
ULK1	Unc- 51 like autophagy activating kinase 1
Va	Varitint waddler
VGCC	Voltage-gated calcium channel
WES	Whole exome sequencing
XPC	Xeroderma pigmentosum group C-complementing protein

## Acknowledgements

I would like to express my sincere gratitude to my supervisor, Dr. Yassine El Hiani for his support and guidance during my master's degree. His patience and knowledge have helped me grow as a researcher and made my graduate career a pleasant experience. I will always treasure the long talks, his encouragement and the time I spent in his lab. Thank you for letting me be a part of your lab.

To the Beatrice Hunter Research Institute (BHCRI), thank you. Your funding has opened the door to many opportunities that have shaped the researcher that I am today and for that I thank you.

I must also thank my parents, Elena and Stelian for their unconditional love and for supporting me every step of the way. Alina, thank you for all the late-night chats and for being an amazing sister. Lastly, Moamen, thank you for always being there and for all your constructive feedback, and help with this thesis.

# CHAPTER I: INTRODUCTION

## 1.1 Subchapter I: Cancer, A Historical Account and Current Knowledge

### 1.1.1 History of Cancer

The first recorded incidence of cancer dates back to Ancient Egypt around 3000 BC, a time when the disease was deemed incurable<sup>1</sup>. These early reports of cancer bearing patients were mainly describing cases of breast tumors that were removed by cauterization, a technique involving the use of fire to destroy the affected tissue<sup>2</sup>. Evidence of head and neck, and bone cancers was also found in human mummies and ancient writings. These abnormal growths inscribed by the Ancient Egyptians were later termed *carcinos* (*karkinos*) meaning “crab” by the Greek physician and “Father of Medicine”, Hippocrates (460-370 BC)<sup>1-3</sup>. The name of course, is derived from the physical appearance of tumors which is characterized by outward stretching projections, a feature that to the Greeks, resembled a crab and its legs. This term was later translated to *cancer*, the Latin word for “crab” by the Roman physician, Celsus (28- 50 BC)<sup>2,3</sup>. Adding to the expanding repertoire of terminologies used to described malignancies is *oncos*, the expression used by Greek physician Galen (130-200 BC) to account for the swelling often associated with tumor growth.

One of the main distinguishing features of cancer cells is their ability to proliferate uncontrollably and to invade distant tissues and organs through a process termed metastasis<sup>4</sup>. In normal cells, proliferation is a homeostatic process designed to maintain the balance between cell division and cell death; however, in cancer cells, this balance favors aberrant growth and the formation of tumors<sup>4</sup>. With the passage of time and expanding knowledge, several theories were

proposed in efforts to explain this seemingly paradoxical phenomenon where a cell's normal physiological state becomes the body's ultimate enemy. One such theory was proposed by Hippocrates who believed health was maintained by a steady state between the body's four humors: yellow bile, blood, phlegm and black bile<sup>5</sup>. Hippocrates's "Humoral theory" was based on the premises that disturbances in these body fluids caused disease, in particular, the excess of black bile which was believed to cause cancer<sup>6</sup>. A similar theory gained popularity in the 1700s when Stahl and Hoffman hypothesized that cancer arises from degenerating lymph<sup>7</sup>. Nonetheless, this theory was rejected around 1838 when German pathologist, Johannes Muller provided the first evidence that cancer is formed by cells and not lymph<sup>8</sup>. Shortly after this discovery, German surgeon Karl Thiersch demonstrated that cancer cells can metastasize and form secondary tumors in surrounding tissues<sup>8,9</sup>. Together, these ideas have laid the foundation for the developing field of cancer research which now includes over 100 cancer types<sup>10</sup>.

### **1.1.2 Current Knowledge and Challenges**

Today, cancer represents the second leading cause of death worldwide, partially due to its complexity and to difficulties in treating the disease. The most common cancers in men and women are prostate and breast cancer respectively, followed by lung cancer, while children are mostly affected by blood cancers<sup>4</sup>. The exact cause of cancer remains unknown and there are many confounding variables that contribute to the onset and progression of cancer. However, scientists have accumulated evidence suggesting that most cancers arise due to mutations in genes that affect the cell's machinery<sup>11</sup>. There are two types of mutations that occur in cancer cells: driver mutations and passenger mutations<sup>12</sup>. A driver mutation refers to an alteration in a gene that confers a growth advantage to the cell carrying it<sup>12</sup>. These mutations are implicated in

oncogenesis and have been selected for throughout the evolution of cancer<sup>12</sup>. As the name implies, the accumulation of these mutations is what drives the development of cancer. In contrast, passenger mutations are those that do not contribute to cancer development or offer a functional advantage to the cell<sup>13</sup>. In addition, passenger mutations are somatic mutations that co-occur with driver mutations during cell division. These mutations occur spontaneously but can also be caused by various factors including exposure to chemical compounds in the environment, smoking, radiation and aging, among others. For example, tobacco is a known carcinogen associated with a higher incidence of lung cancer while extensive exposure to sunlight can cause skin cancer<sup>14,15</sup>. Thus far, hundreds of compounds have been identified as potential carcinogens. In addition, cancers arising from spontaneous successive mutations make up approximately 95% of all cancers with the remaining 5% being attributed to inherited mutations (e.g. BRCA1 and BRCA2 mutations). Furthermore, certain bacteria (e.g. *Helicobacter pylori*) and viruses such as Hepatitis B or HPV have the potential of increasing an individual's risk of developing cancer<sup>16–19</sup>. Lastly, epigenetic changes including DNA methylation and histone modifications (methylation and deacetylation) have been demonstrated to play a critical role in the formation of tumors<sup>20</sup>. DNA methylation is a process through which a methyl group is added to cytosine residues of the DNA strand, often resulting in the suppression of gene expression<sup>21</sup>. Generally, cancer cells experience a reduction in DNA methylation (hypomethylation) in order to prevent the transcription of tumor suppressor genes, thus allowing cancer cells to grow uncontrollably<sup>22,23</sup>.

Over the last few decades, the scientific world has witnessed many advancements in molecular techniques and approaches which have led to the identification of genetic signatures of certain cancers and the development of biomarkers for early cancer diagnosis. Although the

prevalence of cancer appears to have increased over the years, this is partially due to the implementation of screening methods. In fact, the first screening test was developed by George Papanicolaou and it is still currently used for the detection of cervical cancer<sup>24</sup>. On the same premise, prostate exams are used in clinics as a routine procedure for individuals at risk (e.g. men over the age of 45) of developing prostate cancer. The introduction of screening procedures allowed for the early diagnosis of patients and as such, improved the efficacy of cancer treatments. However, despite major improvements made in early cancer detection and treatments, the path to a cure remains obscure. One of the main challenges in treating cancer patients is intra-tumor heterogeneity, a feature which is intimately linked with cancer progression, resistance to therapy and disease recurrence<sup>25-27</sup>. Intra-tumor heterogeneity refers to the presence of distinct morphological and molecular features amongst cells within the same tumor<sup>28</sup>. These distinct features arise due to the characteristic genomic instability of cancer cells which foster genetic diversity; thus, leading to intra-tumoral heterogeneity. Several sources are responsible for the observed intra-tumoral heterogeneity including cancer stem cells, phenotypic plasticity and clonal diversity<sup>29</sup>. It is believed that a small subset of tumor cells termed cancer stem cells harbor the potential to maintain and promote the growth of tumors due to their self-renewal and differentiation capabilities<sup>30</sup>. In addition, the idea of clonal evolution as a model of tumor progression presents a plausible explanation for the development of intra-tumor heterogeneity<sup>31</sup>. Initially proposed in 1976, the clonal evolution theory is based on the same premises as Darwin's models of evolution where organisms accumulate features that offer a selective advantage<sup>31</sup>. In tumors, cells acquire a plethora of mutations through cell division, but only those possessing genetic alterations that promote their growth and survival are selected; a concept that led to the identification of driver and passenger mutations<sup>32</sup>. There are also other

elements that contribute to the heterogeneity in tumors such as epigenetic modifications and differences in microenvironment<sup>33</sup>. Ultimately, these factors lead to the deregulation of various molecular pathways and processes resulting in the “Hallmarks of cancer”. These hallmarks are essential for the development and progression of cancer.

### **1.1.3 The Molecular Mechanisms of Cancer and the Basis for the Famous “Hallmarks of Cancer”**

In the year 2000, Douglas Hanahan and Robert A. Weinberg published their seminal review “The Hallmarks of Cancer” which summarized the complexity of cancer biology into six hallmarks that have become a staple for cancer research<sup>34</sup>. The hallmarks include self-sufficiency in growth signals, insensitivity to anti-growth signals, tissue invasion and metastasis, limitless replicative potential, sustained angiogenesis and apoptosis evasion<sup>34</sup>. While these hallmarks encompass the main features of cancer cells, they do not account for tumor heterogeneity, a concept that gave rise to Hanahan and Weinberg’s 2011 “The Hallmarks of Cancer: The Next Generation”<sup>35</sup>. The new extended version included two “emerging hallmarks”: avoiding immune destruction and deregulating cellular energetics<sup>35</sup>. At the basis of these hallmarks are what the authors referred to as “enabling characteristics” in the form of genome instability and tumor-promoting inflammation. Enhanced genomic instability increases the rate of genetic alterations per cell division; thus, increasing the rate of malignant transformation. Cancer cells also evade immune system surveillance and manipulate the cell’s metabolism to sustain their exacerbated growth<sup>35</sup>. In essence, the principle behind these hallmarks was to encompass and categorize the various molecular mechanisms that allow cancer cells to grow and invade the body’s tissues. The

following few paragraphs will discuss fundamental pathways that make up the basis for the hallmarks of cancer as well as those relevant to this dissertation.

### **1.1.3.1 PI3K/AKT/mTOR Pathway**

The PI3K/AKT/mTOR pathway is an important signaling cascade responsible for regulating cell cycle and survival; thus, disruptions within this pathway have been linked to various pathological states including cancer<sup>36,37</sup>. With increased expression, copy number alterations and epigenetic changes, the PI3K/AKT pathway is often dysregulated in cancer cells and contributes to tumorigenesis<sup>36</sup>. Since the discovery that the PI3K/AKT/mTOR pathway plays a significant role in promoting cancer growth and progression, the pathway has become a major target for the development of anticancer drugs<sup>38,39</sup>. Moreover, clinical trials using drugs selectively targeting mTOR have shown to be efficacious when treating lung cancer patients<sup>40</sup>.

AKT is a serine/threonine-specific protein also known as protein kinase B (PKB) which acts as the primary effector of phosphoinositide 3- kinase (PI3K) and as such, PI3K is required for AKT activation<sup>41</sup>. However, AKT can also be directly activated in a PI3K-independent manner. Studies have shown that AKT is activated by inflammation, reactive oxygen species (ROS) and DNA damage<sup>42</sup>. Nonetheless, upon activation of PI3K, AKT becomes phosphorylated and translocates from the cytosol to nucleus in its active form where it controls many of the cell's functions through the transcription of antiapoptotic and pro-survival genes<sup>43</sup>. In addition, cytosolic AKT phosphorylates and subsequently activates the mammalian target of rapamycin (mTOR) which in turn blocks the process of autophagy<sup>44</sup>. The PI3K/AKT/mTOR pathway is negatively regulated by the phosphatase and tensin homolog (PTEN) whereby PTEN can inhibit

AKT activation<sup>45,46</sup>. Not surprisingly, PTEN is found mutated or deleted in various cancers which prompts aberrant activation of downstream effectors of the PI3K/AKT/mTOR pathway<sup>47</sup>.

### 1.1.3.2 JNK Signaling Pathway

The c-Jun N-terminal kinase (JNK) pathway is one of the major members of the mitogen-activated protein kinase (MAPK) family and it is involved in inflammation, metabolism and apoptosis. The JNK pathway is activated by MAPK kinase kinases (MAPKKKs) as well as through G protein-coupled receptors (GPCRs) in response to harmful stimuli such as radiation, ROS or inflammatory cytokines<sup>48–51</sup>. Once activated, JNK can induce cell death by phosphorylating downstream effectors such as c-Jun which is present in the nucleus<sup>52</sup>. The JNK pathway is highly complex and its regulation depends on many MAPKKKs; however, despite its complex nature, this pathway holds tremendous anticancer properties<sup>53</sup>. For example, a paper published by Ashenden *et al.* showed that inhibition of the JNK pathway enhances the efficacy of chemotherapy in triple negative breast cancer (TNBC) while hyperactivation of the pathway was associated with poor patient outcome<sup>54</sup>. Furthermore, the same study presented novel evidence suggesting that the level of activation of the JNK pathway could act as a potential biomarker of response to therapy<sup>54</sup>. Similar results were found in a rodent model of ovarian cancer where JNK activation resulted in resistance to therapy<sup>55</sup>. However, the role of JNK signaling in cancer remains controversial with evidence suggesting that depending on the activating signal, or the type of cancer, JNK can either have a pro-tumorigenic or inhibitory role<sup>56–60</sup>.

### **1.1.3.3 ERK Pathway**

Similar to the JNK signaling pathway, the extracellular signal regulated kinase (ERK) is also part of the MAPK family<sup>61</sup>. As the name implies, the ERK pathway is activated by extracellular signals such as hormones and growth factors, and it is involved in regulating meiosis, mitosis, proliferation, differentiation and other cellular functions<sup>62,63</sup>. Cancer cells have evolved mechanisms to hijack this pathway in order to sustain their high proliferative rate and as such, inappropriate ERK activation is often observed in cancer cells<sup>64</sup>.

The ERK pathway is initiated through the stimulation of membrane receptors including GPCRs, receptor tyrosine kinases (RTKs) and ion channels<sup>65</sup>. The signal sent through these receptors results in the activation of Rat Sarcoma (Ras), a GTPase found at the plasma membrane<sup>65</sup>. Active RAS binds the Rapidly Accelerated Fibrosarcoma (Raf) kinase which in turn activates a series of MAPKs<sup>65,66</sup>. These kinases phosphorylate and subsequently activate MEK1/2, ultimately leading to the activation of ERK<sup>65</sup>. Upon its activation, ERK acts on different downstream effectors to modulate various cellular functions. One of the ways through which cancer cells are able to manipulate the ERK pathway to support their needs is via Ras mutations<sup>67</sup>. When Ras is mutated it becomes a constitutively active oncogene that can maintain ERK activation to induce proliferation.

### **1.1.3.4 Autophagy**

Autophagy is an evolutionary conserved cellular degradation process necessary for the maintenance of cell homeostasis. The main purpose of this process is the breakdown of cytoplasmic material such as aggregated proteins, damaged/old organelles and foreign bodies in

order to prevent the buildup of toxic material and disruption of the cell's steady state<sup>68,69</sup>. Autophagy becomes especially important during nutrient starvation when the cell begins to recycle cellular components to generate energy for survival. Thus, autophagy represents an attractive target for cancer cells<sup>70</sup>. However, autophagy acts as a double-edged sword in cancer cells where a basal level of autophagy is beneficial and can provide enough energy to promote cell division, but too much autophagy can lead to cell death<sup>71,72</sup>.

The autophagy pathway can be initiated by the inhibition of mTOR which allows for the activation of Unc-51 like autophagy activating kinase 1 (ULK1) (Fig. 1)<sup>73</sup>. During autophagy, the cellular components destined for degradation are isolated from the rest of the cell through the formation of a phagophore. The phagophore engulfs the material resulting in the formation of a double membrane compartment known as the autophagosome (Fig. 1)<sup>74,75</sup>. The formation of the autophagosome is controlled by autophagy-related genes (ATGs), in particular ATG5, 12 and 16 which are responsible for autophagosome elongation and maturation (Fig. 1)<sup>76</sup>. While the autophagosome is up-taking the cytoplasmic material, microtubule-associated protein light chain 3-I (LC3-I, an ATG8 homologue) is converted to LC3-II which is then recruited to the autophagosome membrane where it binds with p62, a ubiquitinated protein also known as sequestosome 1 (SQSTM1)(Fig. 1)<sup>77,78</sup>. Upon fusion of the autophagosome with the lysosome, LC3-II and p62 are degraded<sup>79,80</sup>. Once the fusion event occurs, the sequestered material is degraded with the help of lysosomal enzymes.

#### **1.1.3.5 Generation of Reactive Oxygen and Nitrogen Species**

ROS generation exists as a delicate balance between homeostasis and stress<sup>81</sup>. On one hand, low amounts of ROS can act as signaling molecules that participate in various cellular

processes<sup>81</sup>. These ROS are tightly regulated by the cell's antioxidant system which can remove excess ROS via catalase (CAT) activity, peroxiredoxins (PRXs) and glutathione peroxidases (GPXs) by converting them to H<sub>2</sub>O<sup>82</sup>. On the other hand, accumulation of ROS can be detrimental to the cell, often resulting in the development of various pathologies including cancer<sup>83,84</sup>. While the build-up of ROS can favor certain pathological conditions, sustained ROS-induced damage ultimately leads to mitochondrial damage and the subsequent death of the cell<sup>85</sup>. Of note, the exact role of ROS in the pathophysiology of cancer remains a question for debate as some studies have shown that ROS can promote cancer cell proliferation and angiogenesis while others claim that increased anti-oxidant levels worsen carcinogenesis suggesting that too little ROS can also enhance cancer growth<sup>86</sup>. ROS generation can occur in the cytosol, peroxisomes and the endoplasmic reticulum (ER); however, the major source of ROS in the cell is the mitochondria, commonly known as the “powerhouse of the cell”<sup>87,88</sup>. The production of ROS is mediated by the electron transport chain (ETC) located inside the inner membranes of the mitochondria<sup>89</sup>. The ETC consists of four complexes, each transferring electrons from donors to acceptors across the mitochondrial inner membrane<sup>89</sup>. This creates a proton gradient which drives adenosine triphosphate (ATP) production. However, electrons leaking from complexes I and III during ATP synthesis react with oxygen to form superoxide which is in turn converted to hydrogen peroxide (ROS) by superoxide dismutase 1 and 2 (SOD1 and 2) in the mitochondrial matrix<sup>89</sup>. Accumulation of ROS in the mitochondria resulting in the release of ROS into the cytosol where it can react quickly with DNA leading to DNA damage<sup>90,91</sup>. Furthermore, when the cell is under energetic stress (e.g. nutrient starvation) it increases its ATP demand and prompts the mitochondria to produce more ATP subsequently leading to the overproduction of ROS.

Nitric oxide (NO) is a free radical that can be formed through enzymatic and non-enzymatic pathways with the enzymatic reaction being the most common<sup>92</sup>. The enzymatic NO formation occurs through the degradation of L-arginine to L-citrulline and NO by nitric oxide synthase (NOS)<sup>93</sup>. In contrast, the non- enzymatic pathway of NO production involves the conversion of nitrite to NO<sup>94</sup>. Similar to ROS, NO has physiological and pathological roles. Some of the physiological roles of NO include vasodilatation, synaptic plasticity, immunity and maintenance of the cellular redox state<sup>92</sup>. In addition, the involvement of NO in the mechanism of cancer is controversial<sup>95,96</sup>. Current literature suggests that low levels of NO promotes angiogenesis; thus, stimulating tumor progression<sup>97</sup>. However, studies have also shown that overproduction of NO leads to DNA damage, impairment of oxidative DNA damage repair and induction of apoptosis in some cancers including prostate cancer<sup>98</sup>. Conversely, in endometrial cancer, increased NO levels were demonstrated to promote cancer cell growth.

#### **1.1.3.6 DNA Damage and Repair**

The integrity of our DNA is highly susceptible to damage due to exposure to environmental agents such as ionizing radiation, mechanical stress and genotoxic chemicals that can disrupt its structure<sup>99</sup>. DNA damage can also arise from errors during DNA replication and metabolism. To compensate for this, cells have developed repair mechanisms to manage the different types of DNA damage occurring on a daily basis. If left unrepaired, DNA damage can accumulate and generate mutations that can lead to disease and cell death; hence, the cell must maintain a balance between the amount of DNA damage and appropriate repair system activation<sup>100,101</sup>. The upcoming paragraphs will present a brief description of the five DNA repair

systems found in human cells: homologous recombination, mismatch repair, nucleotide excision repair, double strand crosslink repair and nonhomologous end-joining.

#### **1.1.3.6.1 Homologous Recombination**

Homologous recombination (HR) is a double-stranded DNA (dsDNA) break, single-strand DNA (ssDNA) gaps and interstrand crosslinks repair system whose mechanism relies on homology search and DNA strand invasion<sup>102</sup>. HR consists of three steps: pre-synapsis, synapsis and post-synapsis, all of which are mediated by Recombination Protein A (Rad51)<sup>103</sup>. In the pre-synapsis step of homologous recombination, Rad51 binds to single-stranded DNA and forms a Rad51-ssDNA filament (pre-synaptic filament)<sup>104</sup>. During synapsis, Rad51 facilitates the formation of heteroduplex DNA (D-loop) by allowing the physical contact between the invading strand and the homologous duplex DNA template<sup>102</sup>. Lastly, during the post- synapsis phase of HR, Rad51 dissociates from double- stranded DNA to allow for DNA synthesis<sup>102</sup>. Interestingly, cancer cells deficient in HR are susceptible to poly(ADP-ribose) polymerase 1 (PARP1) inhibition<sup>105</sup>. PARP1 is an important protein involved in DNA repair that has been shown to induce cell death in various cancers upon its downregulation<sup>106-108</sup>.

#### **1.1.3.6.2 Mismatch Repair**

The DNA mismatch repair (MMR) is a highly conserved system responsible for replacing mismatched base pairs<sup>109</sup>. DNA base pair mismatching normally occurs due to replication errors but could also arise from other biological processes<sup>109</sup>. Importantly, disturbances in MMR have been linked to the development of sporadic and hereditary cancers<sup>110</sup>. The molecular mechanism of MMR involves recognition of the daughter strand DNA mismatch through MutS<sub>2</sub> which binds

to the mutated DNA followed by the exonuclease I (ExoI)-mediated mismatch excision and DNA re-synthesis<sup>111–114</sup>. The gap created at the excision site is sealed by DNA ligase and methylated with the help of DNA methylase.

#### **1.1.3.6.3 Nucleotide Excision Repair**

DNA damage acquired through exposure to UV light, some chemotherapeutics and environmental mutagens is generally corrected through the nucleotide excision repair (NER) system<sup>115</sup>. NER consists of two pathways operating through different sets of proteins: global genome NER (GG-NER) and transcription-coupled NER (TC-NER), each responsible for the repair of bulky DNA damage at different sites<sup>116</sup>. GG-NER can repair DNA damage anywhere in the genome<sup>116</sup>. In contrast, TC-NER can only repair DNA strand lesions of transcriptionally active genes<sup>116</sup>. In GG-NER, DNA damage is recognized by Xeroderma pigmentosum group C-complementing protein (XPC)-RAD23B<sup>115</sup>. The reaction is initiated when XPC-RAD23B binds to a non-damaged region of the DNA strand opposite to the damaged strand and opens the two DNA strands with the help of its XPB subunit<sup>117</sup>. An incision is made by a protein complex and the damaged region is removed<sup>118</sup>. TC-NER differs from GG-NER only in the DNA recognition step whereby TC-NER is initiated when RNA polymerase stops transcribing the DNA strand upon reaching the damaged site<sup>119</sup>.

#### **1.1.3.6.4 DNA Strand Crosslink Repair**

The induction of DNA strand crosslinks represents the foundation of many chemotherapeutic drugs<sup>120,121</sup>. DNA strand crosslinks are highly cytotoxic due to their ability to prevent DNA replication and transcription, two processes necessary for cellular homeostasis and

survival<sup>120</sup>. In order to repair DNA strand crosslinks that have occurred in the G0/G1 phase of the cell cycle, the DNA must undergo two rounds of NER since both strands are affected<sup>122,123</sup>. However, repair becomes more complicated when the damage occurs during the S phase of the cycle. Here, the damage is repaired through HR<sup>124</sup>. Failure to repair DNA strand crosslinks can result in the development of several hereditary pathologies including Cockayne syndrome (CS), Fanconi anemia (FA) and Trichothiodystrophy (TTD)<sup>125</sup>.

#### **1.1.3.6.5 Nonhomologous End-Joining**

Nonhomologous end-joining (NHEJ) is a pathway responsible for repairing dsDNA breaks (DSBs) where the ends are directly ligated; thus, eliminating the need for homology-directed repair<sup>126</sup>. This type of damage can result in telomere fusion or the loss of large portions of a chromosome if left unrepaired and can lead to the development of cancer<sup>126</sup>. One of the main causes of DSBs is the accumulation of ROS, but they can also occur from exposure to ionizing radiation or failures of type II topoisomerases<sup>127,128</sup>. The initiation of NHEJ depends on the binding of the Ku protein to the damaged ends of the DNA helix<sup>129</sup>. Ku acts to provide structural support for the DNA molecule prior to the binding of the catalytic subunit of DNA-dependent protein kinase (DNA-PKcs)<sup>129</sup>. DNA-PKcs then phosphorylates and binds to the Artemis protein resulting in the cleavage of the DNA overhangs<sup>129</sup>. The two ends of the DNA are joined together by DNA ligase IV<sup>129</sup>.

#### **1.1.3.7 Apoptosis**

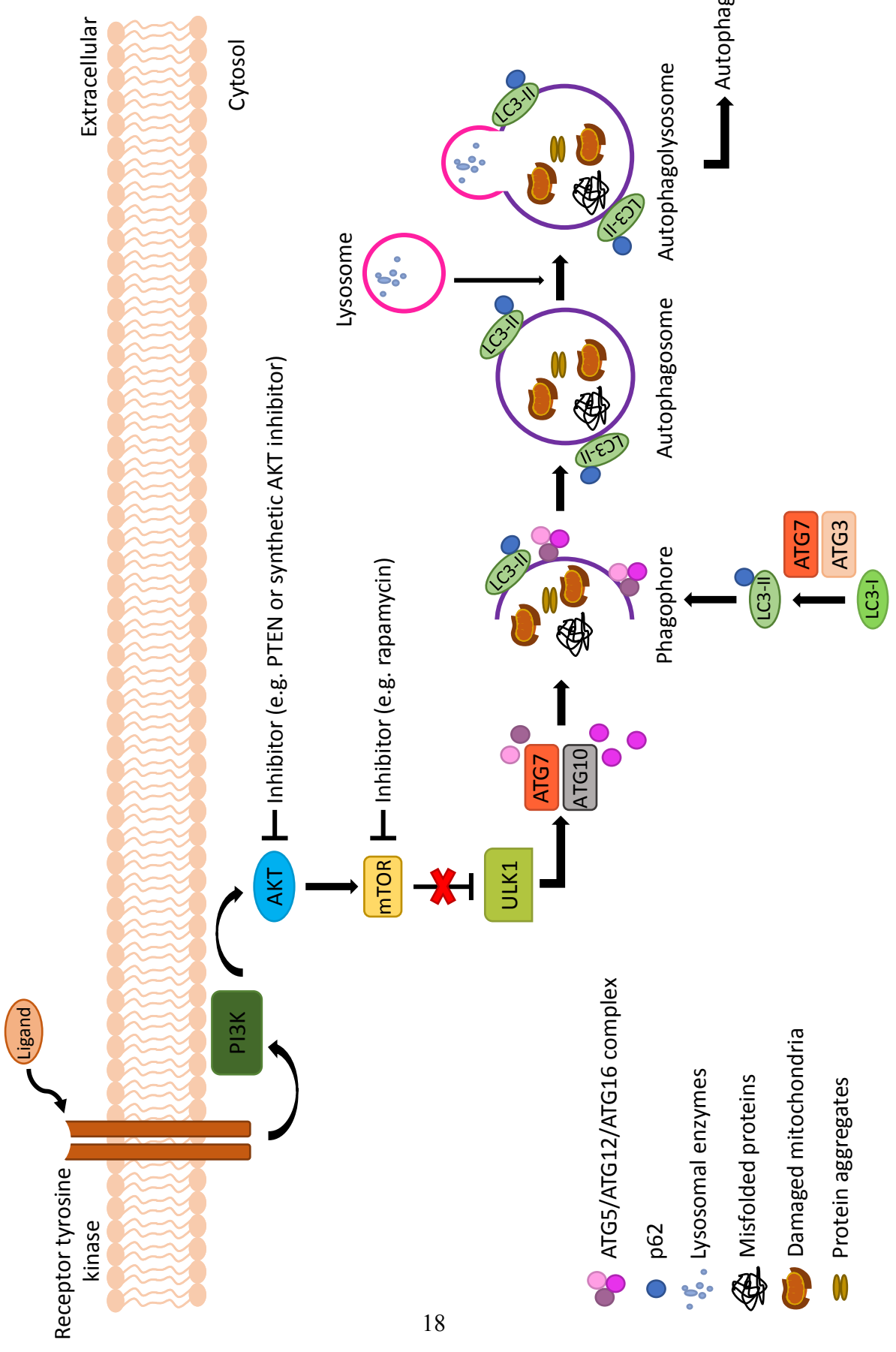
Apoptosis is a regulatory process involved in the removal of cells from living tissues during tissue remodeling and cell turnover<sup>130</sup>. This physiological process includes a series of

events that ultimately result in the formation of apoptotic bodies which are then cleared by phagocytic cells<sup>130</sup>. Naturally, once apoptosis is initiated it cannot be stopped and as such, apoptosis is a highly regulated process. Interestingly, cancer cells have evolved ways of bypassing the cell's apoptosis- related pathways making apoptosis a suitable target for anticancer therapies.

Commonly known as programmed cell death, apoptosis can be initiated via two mechanisms, the intrinsic and extrinsic pathways depending on the activating signal<sup>131</sup>. The intrinsic pathway is mediated by the mitochondria during periods of cell stress such as the presence of DNA damage or oxidative stress (e.g. increased ROS)<sup>132</sup>. Once activated, the intrinsic pathway results in the release of cytochrome c into the cytoplasm where it initiates the formation of an apoptosome<sup>133</sup>. This complex cleaves caspase 9 which then activates caspases 3, ultimately resulting in cell death<sup>134</sup>. This pathway is regulated by the presence of B-cell lymphoma 2 (Bcl-2) proteins within the mitochondrial membrane. These proteins are characterized by the presence of specific sequence motifs known as Bcl-2 homology domains (BH)<sup>135</sup>. The Bcl-2 proteins are subdivided into three groups, each containing at least one BH motif: anti-apoptotic (Bcl-2 and Bcl-extra large (XL)), pro-apoptotic (BAX and BAK) and Bcl-2 homology 3 only family members (BH3-only → BIM, BID, PUMA, BAD)<sup>136,137</sup>. The pro-apoptotic proteins are activated by BH3-only proteins which affects the permeability of the mitochondrial membrane and triggers the release of cytochrome c. In contrast, the anti-apoptotic proteins prevent the release of cytochrome c, a mechanism that has been exploited in cancer cells allowing them to evade cell death<sup>138</sup>. Cancer cells arise more often from failures of the intrinsic pathway than the extrinsic pathway. In contrast to the intrinsic pathway, the extrinsic pathway involves the activation of death receptors (DR), namely DR4 and DR5 which are activated by

Fas ligand (FasL) and the tumor necrosis factor (TNF)-related apoptosis-inducing ligand (TRAIL), respectively<sup>139</sup>. Activation of these receptors mediates the cleavage of procaspase 8; thus, leading to the activation of caspase 3<sup>134</sup>. Similar to the intrinsic pathway, caspase 3 then initiates apoptosis.

**Figure 1: Cartoon representation of the autophagy pathway.** The autophagy pathway is initiated through the activation of ULK1 which is normally inhibited by mTOR. mTOR is in turn activated by phosphorylated AKT; therefore, inhibition of AKT (e.g. indirectly by PTEN or with a synthetic AKT inhibitor) or mTOR (e.g. rapamycin) prevents the inhibition of ULK1 and allows for autophagy to occur. Once ULK1 is activated, the cell starts recruiting ATG proteins which trigger the sequestration of unwanted cellular material (e.g. damaged mitochondria, protein aggregates, misfolded proteins, etc.) into a phagophore. The ATG5/12/16 complex is important in the elongation and maturation of the phagophore into an autophagosome which engulfs the cellular components destined for degradation. LC3 I is then converted to LC3 II by ATG7 and ATG3, and recruited to the autophagosome membrane where it binds p62. LC3 II and p62 facilitate the fusion of the autophagosome with the lysosome. The enzymes present within the lysosome begin the degradation of the contents of the autophagosome along with LC3 II and p62.



## **1.2 Subchapter II: A Comprehensive Description of Prostate Cancer**

### **1.2.1 Physiology of the Prostate Gland**

Prostate development occurs during the tenth week of gestation when the gland begins forming from invaginations of the posterior urogenital sinus<sup>140</sup>. This process requires the presence of 5α-dihydrotestosterone which stimulates and maintains the growth and function of the prostate<sup>141</sup>. The prostate is a walnut sized gland surrounding the prostatic urethra and located beneath the bladder<sup>140</sup>. Enclosed by an elastic pseudocapsule (not a true capsule), the structure of the prostate gland is divided into the upper part known as the base and the lower portion called the apex<sup>142</sup>. These sections are further subdivided into four zones (outermost to innermost) making up the entirety of the prostate: the anterior fibromuscular zone, peripheral zone, central zone and transition zone<sup>143</sup>. As the name implies, the anterior fibromuscular zone is composed of smooth muscle fibers and fibrous connective tissue making it the thickest part of the prostate<sup>142</sup>. This zone surrounds the apex of the prostate and does not contain any glands. Interestingly, cancer rarely develops in this zone. In contrast, the peripheral zone which makes up most of the prostate and is the most common area for cancer development with 75% of PCa occurring in this zone<sup>144</sup>. Furthermore, the peripheral zone contains most of the prostatic glandular tissue which is easily examined by a physician during digital rectal exams (DRE)<sup>142</sup>. The central zone of the prostate surrounds the ejaculatory ducts and it is an area of relatively low risk for cancer development; however, cancers that arise within this zone are believed to display an aggressive phenotype with high possibility of metastasis<sup>145</sup>. Lastly, the transition zone surrounds the urethra and makes up approximately 5% of the glandular issue in the prostate<sup>142</sup>. About 25% of benign prostate cancers are found in the transition zone<sup>142</sup>.

The function of the prostate is to produce and secrete a slightly alkaline fluid which contains an abundance of proteins, minerals and enzymes necessary for the nourishment and protection of sperm cells<sup>146</sup>. In combination with sperm cells, the prostatic fluid is collectively termed as semen. In addition, the prostate specific antigen (PSA) is a protease found in prostatic fluid whose main function is to breakdown larger proteins present in the seminal coagulum into peptides of smaller molecular weight to make the prostatic fluid less viscous for the purposes of increasing the likelihood of fertilization during sexual intercourse<sup>147,148</sup>. The muscles in the prostate contract and release the semen into the urethra followed by expulsion during ejaculation<sup>149</sup>. Interestingly, the composition of the prostatic fluid is different in PCa patients. Normally, prostatic fluid contains high levels of zinc and citrate, but PCa patients appear to have decreased levels of zinc and citrate, a feature that may be exploited as a potential diagnostic screening tool for PCa<sup>150,151</sup>.

### **1.2.2 Prostate Cancer Epidemiology**

Prostate cancer (PCa) is the third most lethal form of cancer in Canada, affecting approximately 21,600 men with 4,000 dying each year<sup>152</sup>. Statistically, one in eight men will develop PCa at some point during their life time, making it the most common cancer in men<sup>152</sup>. PCa is a growing global concern as more than 1.1 million patients were diagnosed worldwide in 2012 and 307,000 lost the battle with this devastating disease<sup>153</sup>. The incidence of PCa is highly variable across the globe and this is primarily due to PCa being a multifactorial disease as genetics, access to care, and environmental factors have been demonstrated to affect the diagnosis, clinical presentation, and progression of PCa<sup>154</sup>. Interestingly, the incidence and mortality of PCa is lower in East Asian countries than in Western countries with Martinique,

France and Norway having the highest rates of PCa<sup>155,156</sup>. This phenomenon is largely a consequence of the differences in medical expenditure and management as well as differences in life style<sup>157</sup>.

### **1.2.3 Diagnosis**

Although the five-year survival rate for PCa patients is favorable, the likelihood of survival drops significantly in late stages of the disease<sup>158</sup>. Unfortunately, most patients present with advanced stage cancer at which point the disease is no longer responsive to therapies. Efforts are being made towards the development of more accurate early diagnosis methods to prolong patient survival and enhance quality of life. Currently, the most common tests for the detection of PCa are the PSA blood test and the digital rectal exam (DRE)<sup>159</sup>. The rectal exam is a normal routine procedure in men over 45 years of age where the physician examines the prostate for the presence of any abnormalities that may be indicative of cancer or pre-cancerous lesions. The PSA test is usually performed in men without symptoms of PCa as a precautionary method, but it is also one of the first tests done in men who have symptoms of PCa<sup>160</sup>. PSA is a protein produced by normal and malignant cells of the prostate gland<sup>161</sup>. The test is designed to measure the level of PSA in the blood where 4 nanograms per milliliter or less is reflective of the absence of cancer whereas levels higher than 5 nanograms per milliliter are considered a strong indicator of PCa<sup>160</sup>. However, recent studies have shown that some men with PSA levels under 4 nanograms do develop cancer while those with high levels do not<sup>162</sup>. In addition, the levels of PSA in the blood can fluctuate due to various factors such as urinary tract infections, trauma, benign hyperplasia and prostatitis<sup>163,164,165,166</sup>. Furthermore, the sensitivity of PSA testing is 21% for any cancer and 51% for high-grade cancers<sup>164</sup>. Nonetheless, the higher the level of PSA, the

more likely the individual is to develop PCa. A continuous rise in the levels of PSA over time is also associated with the presence of malignant cells<sup>164</sup>. If high levels are detected, the patients will undergo a series of tests which can include transrectal ultrasounds, X-rays, cystoscopy, prostate biopsies and biomarker testing (refer to section 1.2.4 Biomarkers).

#### **1.2.4 Biomarkers**

Despite the unsettling statistics surrounding PCa, advances have been made towards early detection and personalized approaches. The latter was made more possible with the implementation of prognostic biomarkers. Generally, prognostic biomarkers are indicative of tumor progression and as such, can be used to predict patient outcome and the potential for disease recurrence<sup>167</sup>. Additionally, prognostic biomarkers often guide and support the choice of therapy for a given patient (advanced disease = more aggressive treatment)<sup>168</sup>. This section will review current (Table 1) as well as emerging PCa biomarkers (Table 2 and 3).

##### **1.2.4.1 PSA Testing**

As previously mentioned, PSA testing is a widely used method for prostate cancer screening where patients with elevated PSA ( $> 4$  ng/mL) are considered at risk<sup>169,170</sup>. The decision to perform a prostate biopsy is usually based on the respective PSA levels, often leading to unnecessary invasive procedures due to the inaccuracy of PSA. Although improvements to PSA testing have been made through the development of additional measurements of PSA derivatives such as PSA velocity and density, these efforts were met with little success in terms of better prognostic value<sup>171,172</sup>. Nonetheless, the attempts to enhance the efficacy of PSA continued and resulted in the identification of PSA isoforms and the establishment of the prostate

health index (PHI). PHI is a mathematical formula designed to distinguish between benign and malignant PCa in older patients ( $> 50$  years old) by measuring the levels of the three PSA isoforms: proPSA, fPSA (free PSA) and benign PSA<sup>173–175</sup>. The test was approved by the Food and Drug Administration (FDA) in 2012. Another prognostic marker is the 4K Score which employs a similar method of combining several biomarkers to estimate the probability of having aggressive PCa<sup>176</sup>. This score compiles the levels of four kallikrein proteins (produced by prostatic epithelial cells): tPSA (total PSA), fPSA, intact PSA and kallikrein-related peptide 2 (hK2)<sup>177,178</sup>. This test has shown to be successful at predicting aggressive disease, but it is not yet approved by the FDA.

**Table 1: List of PSA-based biomarkers and associated testing methods**

Biomarker	Description
Prostate specific antigen (PSA)	Protein produced in the normal prostate. Most commonly used biomarker for PCa.
Free PSA (fPSA)	Unbound form of PSA tested for in the Prostate Health Index (PHI) and 4K Score test.
proPSA	Single chain form of PSA. Used in the Prostate Health Index (PHI) and 4K Score test.
Prostate Health Index (PHI)	Tests for proPSA, fPSA and PSA using the (proPSA/fPSA) x PSA <sup>1/2</sup> formula to identify benign and malignant tumors.
4K Score	Test for the presence of four kallikrein proteins. Gives the probability of having aggressive PCa
Prostate cancer antigen 3 (PCA3)	Protein found in the prostate that can be detected using the Progensa test. Determines whether the patient should have a repeat biopsy.

**Table 2: List of biomarkers identified through proteomic or genomic approaches**

Biomarker	Description
Oncotype DX	Test analyzing the expression of 17 genes involved in different cellular processes to predict the severity of the disease.
Prostarix	Test for urine metabolites. Useful when deciding to do a repeat biopsy.
Mi-Prostate Score	Urine test specific for TMPRSS2:ERG, PCA3 and PSA. Identifies aggressive disease.
Androgen receptor splice variant 7 (AR-V7)*	Detected in cancer cells in men with castration-resistant prostate cancer (CRPC). Useful for treatment selection.
Polaris score*	Analysis of 46 cell cycle and housekeeping genes to identify the likelihood of relapse and metastatic potential of the PCa.
Circulating cancer cells (ECAM-positive and CD45-negative)*	The number of cells present in peripheral blood correlates with overall survival.

\*Biomarkers listed with an asterisk have not been addressed in the main text. Information obtained from Gaudreau *et al.* 2016<sup>158</sup>.

**Table 3: Immune system-based biomarkers for prostate cancer**

Biomarker	Description
Interleukin 8 (IL-8)	Elevated levels of IL-8 post-treatment predict poor survival in patients with advanced stages of PCa.
Toll-like receptor 9 (TLR9)	High levels of TLR9 found in high grade PCa
CD276 (B7-H3)	Immune checkpoint protein. Elevated levels indicate poor overall survival.
Autoantibodies	Antibodies targeted at tumor-specific antigens present on the surface of PCa cells. Can be detected in the blood.
C-reactive protein (CRP)*	Usually involved in inflammation and necrosis. Its prognostic potential depends on the stage of the disease.
Neutrophil to lymphocyte ratio*	Relative number of neutrophil and lymphocytes useful in predicting the outcome with PCa patients undergoing enzalutamide treatment.

\*Biomarkers listed with an asterisk have not been addressed in the main text. Information obtained from Gaudreau *et al.* 2016<sup>158</sup>.

#### **1.2.4.2 Emerging “omics”-Related Biomarkers**

Over the last decade, cancer research has entered the era of big data as high-throughput proteomic and genomic approaches have enabled the identification of many genes and proteins with biomarker potential. One such example is Prostate Cancer Antigen 3 (PCA3) which is present in prostate tissue and its expression correlates with malignant disease<sup>179</sup>. The Prognos assay was designed to measure the concentration of PCA3 and PSA RNA in urine specimens<sup>180</sup>. A ratio of PCA3 to PSA RNA of more than 25 was indicative of increased likelihood of having PCa and poorer overall prognosis<sup>181,182</sup>. This test is useful for clinicians when deciding whether or not to repeat a biopsy on a patient who presented with elevated PSA but had a negative biopsy. Similar to the PCA3 test, another applicable test is the Prostarix Risk Score which analyzes the levels of sarcosine, alanine, glycine and glutamate in urine samples. Studies have shown that the Prostarix Risk Score holds therapeutic potential as a prognostic tool for PCa and may decrease the use of unnecessary secondary biopsies<sup>183,184</sup>.

Other PCa prognostic strategies include the combination of multiple biomarkers to predict outcome as well as to improve PSA performance. For example, the Mi-Prostate Score urine test detects the fusion event between TMPRSS2 and ERG, and measures the levels of PCA3 and PSA<sup>185</sup>. The corresponding score is representative of high grade PCa on biopsy<sup>186</sup>. Despite its initial success, the Mi-Prostate Score urine test has not yet been approved by the FDA. Following the same strategy, the Oncotype DX assay quantifies the expression of 12 cancer-related genes (e.g. FAM13C, GSTM2, TPX2, etc.) and 5 reference genes (e.g. ARF1, CLTC, PGK1, etc.) in prostate biopsies, and generates a Genomic Prostate Score (GPS) ranging from 0 to 100<sup>187,188</sup>. The score is adjusted for PSA, Gleason score and clinical stage, and acts as

an indicator of the patient's pathological state<sup>187</sup>. Each 20-point increase in GPS represents an increase in the risk of having high grade and/or non-organ confined PCa (e.g. potential for metastasis)<sup>187</sup>.

#### **1.2.4.3 Immune System-Based Biomarkers**

Aside from the biomarkers identified through the “omics” techniques, various cytokines and other immune system-associated proteins also harbor the potential to serve as prognostic biomarkers for PCa. For example, high expression of interleukin-8 (IL-8) correlated with poor overall survival in PCa patients while overexpression of Toll-like receptor 9 (TLR9) was associated with high grade tumors and poor prognosis<sup>189–191</sup>. Additionally, CD276 (B7-H3), an immune checkpoint protein is upregulated in PCa and has been shown to correspond with disease spread, and poor patient outcome<sup>192,193</sup>. Furthermore, autoantibody signatures can also be used to distinguish between healthy individuals and those with PCa. This test originated from the idea that PCa cells produce peptides that are not normally found in healthy cells leading to the development of autoantibodies. The autoantibodies in cancer patients can be identified through the application of protein microarrays and used as a prognostic markers<sup>194,195</sup>.

With the turn of the 21<sup>st</sup> century, the field of biomarker research has experienced a surge in the availability of high-throughput genomic and proteomic data which led to a growing body of information about potential novel biomarkers. Progress is currently being made in the use of PSA in conjunction with other biomarkers such as PCA3 and TMPRSS2:ERG as well as other specific metabolites. Whether it is improving the sensitivity and selectivity of current prognostic biomarkers, or the development of brand new biomarkers, the future holds great promise for PCa patients.

## **1.2.5 Tumor Biopsy Analysis**

### **1.2.5.1 Grading**

Although PSA testing does not constitute the most reliable measure of the probability of an individual to develop or have PCa, it is currently the best biomarker for PCa. Often, patients who are thought to have PCa are sent for a biopsy where samples of the prostate tissue are extracted and delivered to a pathologist. The pathologist will grade the tissue biopsy based on the Gleason scoring system<sup>196</sup>. The Gleason system uses numbers from 1 to 5 based on the degree of resemblance between the cancerous cells and the surrounding normal cells. Usually, prostate cancer biopsies are graded 3 or higher<sup>196</sup>. However, because prostate tumors consist of areas with different grades, two areas making up most of the cancerous tissue are graded. These two grades are then added up giving a final Gleason score called the Gleason sum. The maximum score that a tumor biopsy can receive is 10. A score of 6 is indicative of a well differentiated or low-grade tumor while a score between 9 and 10 is considered poorly differentiated or high-grade meaning that these cells are likely to grow and spread more quickly<sup>197</sup>.

### **1.2.5.2 Staging**

The most widely used staging system for cancer biopsies is the American Joint Committee on Cancer (AJCC) TNM system<sup>198</sup>. The TNM system is based on five factors: the extent and size of the primary tumor (T), whether the cancer has spread to nearby lymph nodes (N) or distant tissues and organs (M), the PSA level at the time of diagnosis and the Gleason score. Once the T, N and M categories are determined, the information is grouped into Stage I (least advanced), II, III and IV (most advanced) to give the overall stage of the cancer. This

staging method helps determine which treatment strategy is best suited for a particular patient and the chances of survival.

### **1.2.6 Driver Mutations**

Genomic characterization of PCa has revealed a high level of mutational heterogeneity which may be implicated in the variability seen in patient outcome. The mutational landscape of PCa cells was uncovered using various techniques including whole exome sequencing (WES), transcriptome sequencing and copy number analysis<sup>199</sup>. These high throughput analysis techniques have identified numerous pathways that are commonly altered in different cancers, but also molecular changes which are specific to PCa. Below is a brief description of the pathways and driver mutations that contribute to prostate carcinogenesis (Table 4).

#### **1.2.6.1 Genes Alterations in PCa and Other Cancers**

As mentioned in section 1.1.3.1, the PI3K pathway is one of the most commonly dysregulated pathways in many cancers, including 25-70% of prostate cancers<sup>199</sup>. In PCa, this pathway is affected due to heterozygous and homozygous (less common) deletions at the *PTEN* locus, the gene encoding the PTEN protein responsible for inhibiting PI3K signaling<sup>200</sup>. These mutations occur in approximately 40% of prostate cancers<sup>201</sup>. Interestingly, PCa cells harboring *PTEN* inactivation mutations also possess *PHLPP1* gene deletions<sup>202</sup>. *PHLPP1* is translated into the PH domain and Leucine- rich repeat protein (PHLPP1) which dephosphorylates AKT; thus, inactivating the PI3K pathway<sup>203</sup>. Furthermore, a catalytic subunit of PI3K, *PIK3CA* was found amplified in 25% of PCa<sup>204,205</sup>. Activating mutations in *PIK3CA* were also identified in 5% of the prostate cancers analyzed<sup>204</sup>.

**Table 4: List of prostate cancer driver mutations**

Driver mutation	Pathway/Function	Specific to PCa?
Phosphatase and tensin homolog (PTEN)	PI3K signaling pathway, cell cycle and survival	No
PH domain and Leucine-rich repeat protein (PHLPP1)		
Catalytic subunit of PI3K (PIK3CA)		
Tumor suppressor p53 (TP53)	DNA repair, cell cycle, apoptosis	
Retinoblastoma protein Rb (RB1)	Tumor suppressor, cell cycle	
Androgen receptor (AR)		
Forkhead box A1 (FOXA1)	Tumor suppressor	
TMPRSS2:ERG	Promotes cancer cell invasion, cell cycle	Yes
Mixed-lineage leukemia 2 (MLL2)	Tumor suppressor, cell differentiation, development	
Mixed-lineage leukemia 3 (MLL3)	Transcription	
Lysine-specific demethylase 6A (KDM6A)	Histone demethylase, cell cycle	
Chromodomain helicase DNA binding protein 1 (CHD1)	Maintenance of stem cell function, transcription, DNA repair	

Mutations in the tumor suppressor p53 (*TP53*) are some of the most well-known changes that occur in cancer cells. The p53 protein is important in many cellular functions including DNA repair, cell cycle and apoptosis<sup>206</sup>. Therefore, it is to no surprise that deletions in the *TP53* locus are present in 25- 40% of PCa cells while point mutations are found in approximately 5-40% of patients<sup>207,208</sup>. Another classic tumor suppressor with functions similar to those of p53 that is often mutated in cancer cells is the retinoblastoma protein Rb (RB encoded by *RBI*)<sup>202,207</sup>. In 45% of PCa cases, *RBI* was found inactive<sup>202</sup>.

#### **1.2.6.3 Mutations Specific to PCa**

Although many of the mutations present in the genomes of PCa cells are found in other cancers, the genetic makeup of these cells also includes PCa specific gene alterations. Most of these PCa specific mutations occur along the androgen receptor signaling axis including alterations within the androgen receptor (*AR*) gene. Genomic analysis revealed that *AR* undergoes a series of changes such as amplifications, simple deletions and point mutations in PCa. Interestingly, *AR* gene amplifications appear to exist only in metastatic tumors, but not in localized PCa or primary tumors<sup>209</sup>. Moreover, one of the consequences of point mutations and simple deletions within the *AR* gene are premature stop codons which result in the translation of a truncated AR protein with limited function<sup>210</sup>. These mutations can also change the affinity of AR to ligands and cause AR to interact differently with its co-factors. In addition, point mutation in Forkhead box A1 (*FOXA1*) whose protein product interacts with androgen receptors were also found in metastatic PCa and primary tumors<sup>205</sup>. Nonetheless, aside from simple deletions and point mutations in *AR* or *AR*-associated genes, numerous fusion events occurring between *AR*-related genes and E26 transformation-specific (ETS) transcription factors were identified<sup>211</sup>.

Aberrant activation of ETS transcription factors has been described in many cancers and demonstrated to enhance tumorigenesis<sup>211</sup>. As outlined in the biomarker section, the fusion event between *TMPRSS2* and *ERG* (member of the ETS transcription factor family) is currently investigated as a potential biomarker for PCa and this is due to its prevalence in PCa<sup>211,212</sup>.

In addition to mutations in the androgen signaling pathway, a number of other PCa specific alterations have also been identified. For example, mutations affecting chromatin integrity such as mixed-lineage leukemia (*MLL*) 2, *MLL3* and lysine-specific demethylase 6A (*KDM6A*) were found to disrupt the methylation of histone variant H3 in PCa<sup>209</sup>. Following the same theme of histone modification, the gene encoding the chromodomain helicase DNA binding protein 1, *CHD1* has been implicated in 10-25% of PCa<sup>213</sup>.

### **1.3 Subchapter III: Prostate Cancer Therapies and Patient Care**

Prostate cancer can arise in different cell types within the prostate. Based on its origin, PCa can be categorized as follows: acinar adenocarcinoma (most common), ductal adenocarcinoma, transitional cell (or urothelial) cancer, squamous cell cancer and small cell prostate cancer. Other rare prostate cancers include carcinoid and sarcomas<sup>214</sup>. Furthermore, PCa is also further subdivided into androgen-sensitive and androgen-resistant PCa depending on their response to therapy. During the early stages of tumor growth, PCa cells are dependent on androgens for growth and regulation of their cellular processes<sup>215</sup>. Androgen suppression therapy is an effective treatment strategy for androgen- dependent PCa; however, this therapy does not kill androgen- independent cancer cells which are often characteristic of highly metastatic PCa<sup>216</sup>. Androgen-independent PCa can arise through various mechanisms such as increased

expression of steroid-generating enzymes and AR gene amplifications (extensively covered by Saraon *et al.* 2014)<sup>214</sup>.

### **1.3.1 Current Treatments**

Patient survival and quality of life are arguably the most important indicators of the effectiveness of anticancer drugs and also, the overall end goal of therapy. The type of treatment given to a prostate cancer patient depends on their health condition as well as the stage and/or grade of the tumor<sup>217</sup>. Men diagnosed with late stage PCa usually receive more aggressive treatment than those who have early stage or low grade PCa<sup>218,219</sup>. Currently, the treatment options available include active surveillance, surgery, radiation therapy, hormonal therapy, chemotherapy, high-intensity focused ultrasound, bone-directed treatment and vaccine treatment<sup>159</sup>. Radical prostatectomy is the most common strategy used to treat patients with PCa but can only be performed in patients whose cancer has not spread outside of the prostate gland. For patients presenting with metastatic cancer, radiation therapy is often administered in combination with either hormone therapy or chemotherapy<sup>159</sup>. However, in addition to severe side effects, these therapies are often unsuccessful at treating patients with advanced stages of the disease. In these cases, patients can opt to participate in clinical trial studies which test new ways to prevent, detect, treat or manage cancer.

### **1.3.2 Emerging Therapies**

Emerging therapies for cancer are now focusing on targeting ion channels to prevent cancer growth and metastasis. Ion channels are proteins that form pores in the membranes of cells and organelles to facilitate the flow of ions between the extracellular environment and the

cytosol, and between various intracellular compartments. Ion channels play a pivotal role in maintaining the cell's physiology and often mediate different cellular functions such as metabolism and proliferation. Due to their importance in orchestrating various processes within the cell, it is to no surprise that researchers have started exploring the potential role of ion channels in cancer cells, including PCa cells. Specific examples relevant to this dissertation will be discussed in the following sections.

### **1.3.2.1 TRP Ion Channel-Based Therapies for Cancer**

The last two decades have witnessed a rise in our knowledge of Transient Receptor Potential (TRP) channels and their role in the underlying mechanisms of carcinogenesis. Thus far, several TRP channels have been implicated in various aspects of oncology. For instance, studies have found that expression of TRPC3 is upregulated in breast and ovarian tumors while knock down of this channel leads to decreased ovarian tumor formation *in vivo*<sup>220,221</sup>. Additionally, TRPC6 is overexpressed in breast, liver and stomach cancer, and inhibition of this channel reduces proliferation in esophageal and breast cancer cell lines<sup>221–223</sup>. Furthermore, TRP channels have been demonstrated to not only act as key proteins in the pathophysiology of cancer, but also as potential biomarkers<sup>224</sup>. A positive correlation between TRPM7 and breast cancer metastasis was recently described where increased expression of TRPM7 was associated with poorer prognosis<sup>225,226</sup>. Lastly, TRP channels have the potential to influence therapy outcome and effectiveness. For example, TRPC5 and 6 have been demonstrated to enhance the efficacy of chemotherapy in breast and colorectal cancer cell lines<sup>227–229</sup>.

### **1.3.2.2 TRP Ion Channel-Based Therapies for Prostate Cancer**

One could argue that TRP channels are part of a new era of oncogenes, but at the very least, TRP channels harbor the potential to serve as new therapeutic targets for cancer, in particular prostate cancer. An article published in 2001 by Tsavaler and colleagues provided compelling evidence showing that the expression of TRPM8 was elevated in prostate cancer, but not in normal tissue<sup>230</sup>. Later papers investigating the role of TRPM8 in metastasis revealed that PSA is able to reduce PCa cell motility through activation of the TRPM8<sup>231</sup>. Furthermore, TRPM8 inhibition was shown to reduce PCa survival<sup>232</sup>. Given its tissue specificity and anticancer properties, TRPM8 entered Phase I clinical trials to determine the efficacy of D-3263 (small molecules able to target TRPM8) at triggering cell death in patients with tumors displaying high TRPM8 expression<sup>233,234</sup>. Other channels that have been implicated in PCa include TRPV6 and TRPM4 whose expression positively correlates with high grade tumors, TRPV2 which is upregulated in metastatic PCa and TRPV1 that has been demonstrated to be functionally active in PCa cell lines and human tissues<sup>235–238</sup>. In addition, a recent paper published in 2018 revealed that TRPM4 regulates PCa cell proliferation through the modulation of AKT and β-catenin signalling<sup>238,239</sup>.

## **1.4 Subchapter IV: Lysosomal TRP Channels and Their Role in Carcinogenesis**

### **1.4.1 Lysosome Physiology**

Before diving into a discussion about the different TRP channels present within the lysosomal membrane, this dissertation will offer a brief description of the lysosomal physiology and how ion channels play a pivotal role in maintaining its function. Although the concept of

enzymes being compartmentalized within organelles was only demonstrated in the 1950s, lysosomes have since paved the way to major scientific breakthroughs, from uncovering the molecular mechanisms of metabolic diseases to understanding the basic physiology of the cell<sup>240</sup>. Lysosomes are now regarded as major cellular signalling hubs critical for the regulation of various processes within the cell.

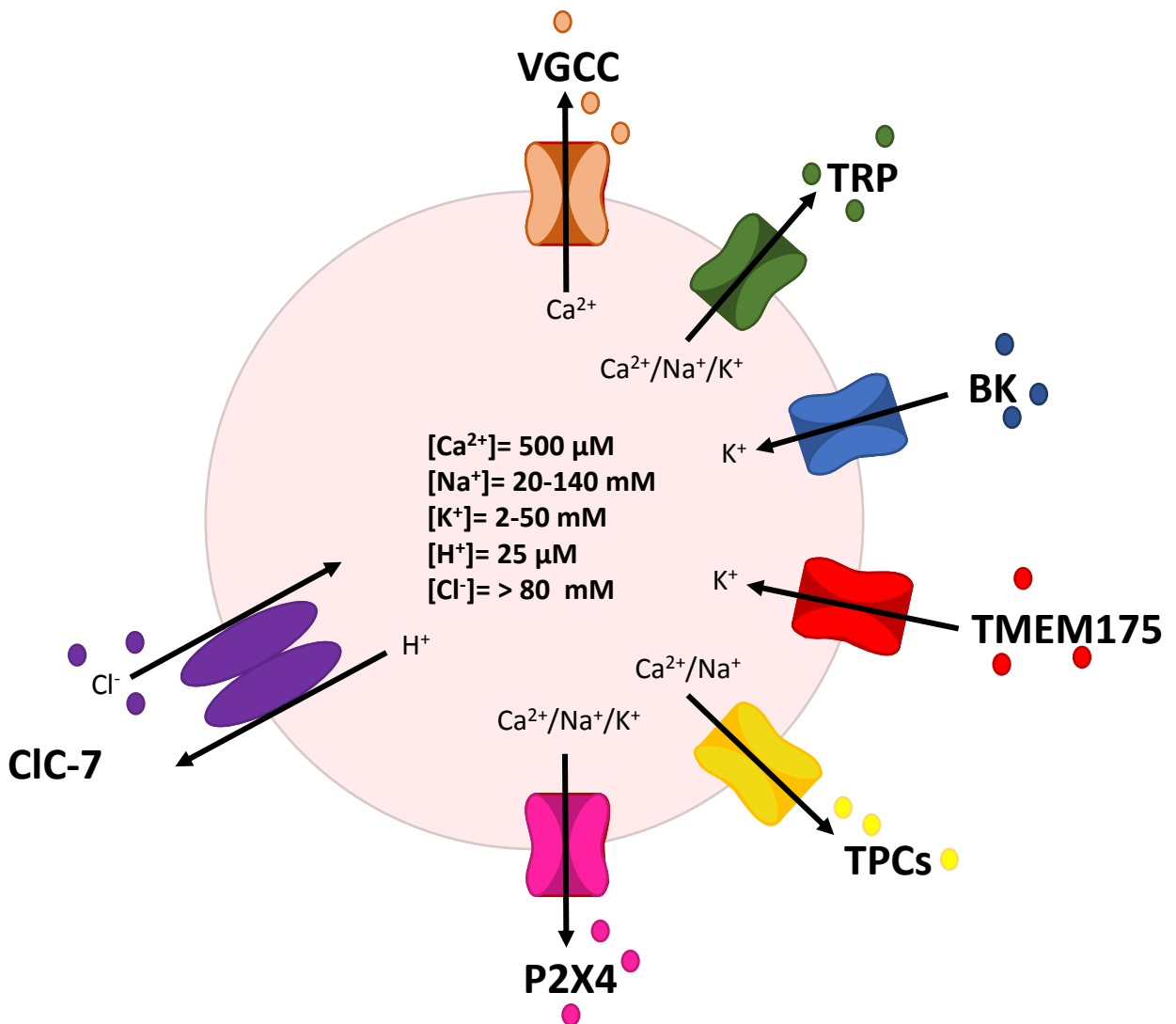
Lysosomes are complex, membrane-bound organelles that contain a plethora of enzymes involved in breaking down biological material including carbohydrates, proteins, nucleic acids and lipids. With over 60 types of acidic hydrolases (e.g. nucleases, lipases, phosphatases, proteases, etc.), lysosomes are often described as the “trash cans” of the cell responsible for the clearance of unwanted cellular components<sup>241–243</sup>. The enzymes are specifically targeted to the lysosomal compartment via the presence of mannose 6-phosphate (M6P) residues which directs their transport from the rough endoplasmic reticulum to the lysosome<sup>244</sup>. In addition, due to the presence of these acidic enzymes, the pH of the lysosome is approximately 4.6-5 to ensure the proper functioning of the enzymes and subsequently, the degradative function of the organelle<sup>245</sup>. Vacuolar ATPases are responsible for maintaining the acidic pH of the lysosome by driving the movement of protons across the membrane through the generation of a voltage gradient<sup>245,246</sup>. Furthermore, aside from the multitude of enzymes present inside the lysosomal lumen, these organelles are also known for their abundance of membrane proteins. Some of these proteins are the lysosome-associated membrane proteins (Lamps) which play a protective role by preventing the self-digestion of the lysosome<sup>245,247,248</sup>. Furthermore, Lamp1 and Lamp2 make up 50% of the proteins associated with the lysosomal membrane and their function is to maintain the pH and integrity of the lysosomes<sup>249</sup>. Hence, due to their integral role within the lysosomes, these Lamps are commonly used as markers for the detection of lysosomes within a cell or protein lysate.

As mentioned in previous sections, lysosomes are important in mediating the breakdown of cellular material during autophagy, a process which is under the regulation of PI3K/AKT/mTOR signalling. However, lysosomal function is also dependent on the presence and proper functioning of ion channels. The ion channel families present within the lysosomal membrane include the TRP channels (TRPMLs and TRPM2), big conductance K<sup>+</sup> (BK) channels, two pore channels (TPC1 and TPC2), the transmembrane protein 175 (TMEM175), voltage-gated calcium channels (VGCC), P2X purinoceptor 4 (P2X4) and the transporter, ClC-7 (Fig. 2)<sup>250</sup>. These ion channels have different ion sensitivities and are responsible for the conductance of Cl<sup>-</sup>, K<sup>+</sup>, Ca<sup>2+</sup>, Na<sup>+</sup>, H<sup>+</sup> and K<sup>+</sup> across the lysosomal membrane<sup>250</sup>. The ion concentration within the lysosomal lumen is highly variable across different cell types; however, the estimated concentration of Ca<sup>2+</sup>, Na<sup>+</sup>, K<sup>+</sup>, H<sup>+</sup>, and Cl<sup>-</sup> are 500 μM, 20-140 mM, 2-50 mM, 25 μM and > 80 mM, respectively<sup>251</sup>. Each ion passing through these channels has been shown to affect various aspects of lysosomal function. For example, upon activation of TRP channels such as TRPML1 (see section 1.4.2.1), Ca<sup>2+</sup> is released from the lysosome into the cytosol where it binds calcineurin which then translocates to the nucleus and activates the transcription factor EB (TFEB), subsequently triggering the transcription of autophagy genes<sup>252-254</sup>. The activation of TFEB is also responsible for inducing lysosomal biogenesis and facilitating the exocytosis of degraded material<sup>255,256</sup>. To further showcase the importance of proper ion homeostasis, studies have demonstrated that a decrease in the lysosomal concentration of Cl<sup>-</sup> alters the luminal pH resulting in a reduction in the degradative capacity of the lysosome<sup>257,258</sup>.

The last few decades have witnessed major breakthroughs in our knowledge of the functional and genetic aspects of the lysosome. These advancements have made it possible to uncover the underlying mechanisms of certain diseases that were unknown prior to the discovery

of the lysosome. Although very rare, lysosomal storage diseases (LSD) are a group of diseases associate with the accumulation of waste products within the lysosome due to defects or lack of hydrolases, hydrolase activators or transporters<sup>259</sup>. The clinical presentation of LSD is highly variable, but most patients present with some degree of neurodegeneration<sup>260</sup>. Additionally, the severity of LSDs is mainly determined by the type of waste product accumulated in the lysosome<sup>259</sup>. Some of LSDs are caused by defects in the structure or function of specific ion channels. One such example is Mucolipidosis IV (MLIV), an inherited disorder characterized by psychomotor delay and visual impairment<sup>261</sup>. This disease is the consequence of mutations within the *MCOLN1* gene whose protein product is TRPML1, a lysosomal TRP channel<sup>262</sup>. The most common mutation that occurs in MLIV patients results in the introduction of a premature stop codon leading to the production of a truncated, non-functional protein lacking the ion conducting pore and, in some cases, the protein is completely absent<sup>263–265</sup>. The loss of TRPML1 functionality results in improper Ca<sup>2+</sup> from the lysosome which in turn affects Ca<sup>2+</sup> dependent pathways such as autophagy<sup>266,267</sup>. This further emphasizes the intimate relationship between the lysosome and its constituent ion channels.

**Figure 2: Schematic representation of ion channels present within the lysosomal membrane.** Lysosomal ion channels mediate the function of the lysosome through the maintenance of ion homeostasis. The ion channels found in the lysosomal membrane are TRP channels (TRPMLs and TRPM2), BK channels, TPC 1 and 2, TMEM175, VGCC, P2X4 and the transporter, CLC-7. These ion channels are responsible for the inflow of  $\text{Cl}^-$  and  $\text{K}^+$ , and the outflow of  $\text{Ca}^{2+}$ ,  $\text{Na}^+$ ,  $\text{H}^+$  and  $\text{K}^+$ . The estimated concentrations of  $\text{Ca}^{2+}$ ,  $\text{Na}^+$ ,  $\text{K}^+$ ,  $\text{H}^+$ , and  $\text{Cl}^-$  within the lysosomal lumen are 500  $\mu\text{M}$ , 20-140 mM, 2-50 mM, 25  $\mu\text{M}$  and > 80 mM, respectively.



## 1.4.2 TRP Channels

The first TRP channel was described in a mutant strain of *Drosophila melanogaster* in 1969 by Cosens and Manning, but it was only characterized as an ion channel in 1992<sup>268,269</sup>. Since this initial discovery, 28 structurally similar TRP channels have been identified and subsequently divided into six groups depending on their individual function: TRPM (Melastatin), TRPV (Vanilloid), TRPP (Polycystin), TRPC (Canonical), TRPML (Mucolipin) and TRPA (Ankyrin)<sup>270,271</sup>. TRP channels are widely expressed across species including mice, zebrafish, worms, flies and humans where they are involved in an array of physiological functions necessary for the maintenance of cellular homeostasis<sup>272</sup>. However, one of the main functions of the TRP channels is to sense and regulate changes in the cytosolic levels of Ca<sup>2+</sup><sup>273</sup>. The TRP ion channel family members are considered to be non-selective to cations, thus facilitating the passage of positively charged ions. These channels are located within the plasma membrane and/or the membranes of various organelles. However, for the purposes of this dissertation, only the lysosomal TRPML1 channel will be discussed in detail.

### 1.4.2.1 TRPML1

TRPML1, an ion channel located in the membranes of lysosomes and late endosomes, is one of the three members of the Mucolipin subfamily. The three TRPML channels (TRPML1, 2 and 3) share a similar structural architecture, each possessing six transmembrane (TM) domains, a large luminal histidine-rich loop located between TM1 and TM2, short cytosolic tails making up the N and C termini of the channel and two helices forming the channel pore in between TM5 and TM6<sup>274</sup>. However, the complete structure of TRPML1 was only identified in 2017 when Schmiege and colleagues used cryo-electron microscopy to determine the exact amino acid

structure of TRPML1<sup>275</sup>. The group studied the channel in its open conformation at a pH of 6 and in closed conformation at pH 7<sup>275</sup>. The full length human TRPML1 was determined to consist of 580 residues and have a molecular weight of approximately 65 kDa<sup>275</sup>. Furthermore, this study revealed that the synthetic TRPML1 activator, ML-SA1, binds in an aromatic pocket created by two TRPML1 subunits, thus releasing the restriction on the lower gate of the channel and allowing the opening of the selectivity filter<sup>275</sup>. Interestingly, the binding of ML-SA1 is different from that of the endogenous activator of TRPML1, the lysosome-specific phosphatidylinositol-3,5-bisphosphate (PI(3,5)P<sub>2</sub>) which binds to specific basic amino acid cluster in the N terminus of the channel<sup>262,276–279,275</sup>. Additionally, other modes of TRPML1 activation have been proposed, but the exact mechanism behind these interactions remains elusive. For example, some studies have provided evidence that TRPML1 is regulated by pH and Ca<sup>2+</sup> where acidic and low concentration of Ca<sup>2+</sup> activate the channel. It is believed that H<sup>+</sup> and Ca<sup>2+</sup> interact with the luminal pore to modulate TRPML1 activity<sup>280</sup>. Li *et al.* demonstrated that aspartate residues present within the luminal loop of TRPML1 can modulate the conductance of Ca<sup>2+</sup> through the channel<sup>280</sup>. The study provided compelling evidence showing that depending on the pH, the aspartate residues can either retain their negative charge (pH= 7.4) or become protonated (pH= 4.6) which in turn blocks or promotes Ca<sup>2+</sup> conductance, respectively<sup>280</sup>. Moreover, mutational analysis provided insight into the gating mechanism of TRPML1 showing that a gain-of-function mutation, V432P maintains the channel in its open conformation<sup>281</sup>.

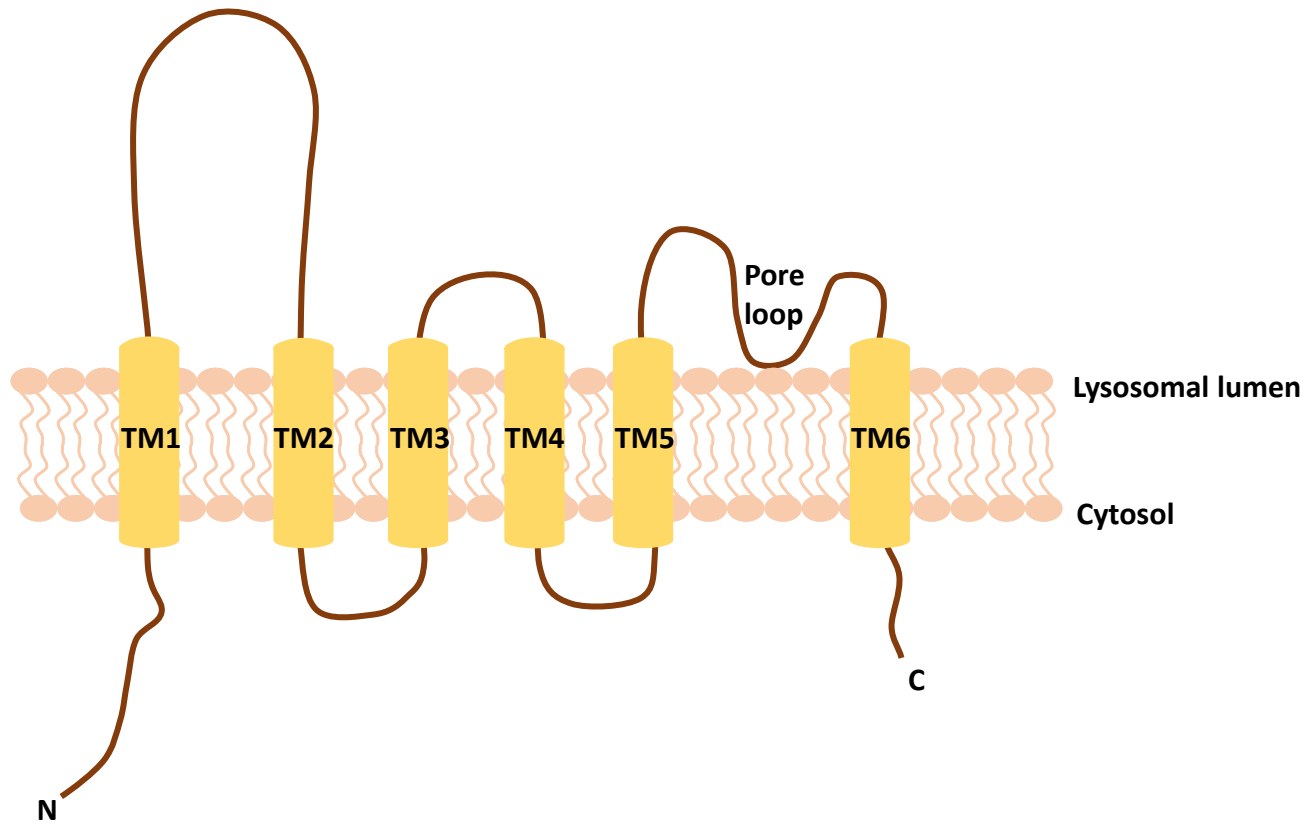
Aside providing insight into the architectural design and gating mechanism of TRPML1, structure-function studies have identified many aspects of the function and selectivity of this channel. As mentioned previously, TRPML1 localizes to the membranes of lysosomes and late endosomes, a tightly regulated process facilitated by two di-leucine motifs found in the N and C

termini of the channel<sup>282</sup>. The N terminus di-leucine facilitates the direct transport of TRPML1 to the lysosome whereas the C terminus motif is responsible for the internalization of the channel from the plasma membrane<sup>282,283</sup>. Of note, an alanine substitution in both of these motifs promotes the trafficking of TRPML1 to the plasma membrane<sup>282,283</sup>. Once embedded within the lysosomal membrane, TRPML1 associates with Lamp1 and functions as an inward rectifying channel responsible for maintaining ion homeostasis and subsequently, the function of the lysosome<sup>284-286</sup>. TRPML1 is permeable to  $\text{Ca}^{2+}$ ,  $\text{Na}^+$ ,  $\text{Fe}^{2+}$ ,  $\text{Mg}^{2+}$ , and  $\text{K}^+$  and mediates the release of these ions from the lysosomal lumen upon its activation<sup>287,288,281</sup>. Although TRPML1 requires the binding of specific molecules in order to become activated, various studies have provided evidence suggesting that TRPML1 can also be activated during nutrient starvation. When a cell is depleted of nutrients it activates its autophagy machinery in order to provide itself with an internal source of energy to sustain survival. As mentioned in section 1.4.1, release of  $\text{Ca}^{2+}$  from TRPML1 triggers the dephosphorylation of TFEB and the transcription of autophagy-related genes which initiates the process of autophagy and therefore, the cell survival<sup>255,289,290</sup>. Once the degradation process is complete, the lysosome experiences a decrease in pH and becomes acidified, a condition that can alter the efficacy of its enzymes<sup>246</sup>. However, as previously mentioned, TRPML1 can be activated by acidic pH, thus, one could argue that TRPML1 acts as a pH sensor which allows the channel to maintain the optimal pH of the lysosome through the release of  $\text{H}^+$ . In addition, cells lacking TRPML1 contain lysosomes with a lower luminal pH than cells with normal TRPML1 expression<sup>291</sup>. Hence, TRPML1 is necessary for lysosomal adaptation during nutrient deprivation and subsequently, cell survival.

Given the importance of TRPML1 as a regulator of major physiological processes, mutations affecting the structural integrity and function of this channel have been linked to

numerous disease pathologies including the development of Mucolipidosis IV and the progression of Alzheimer's disease<sup>292,293</sup>. However, unlike the other lysosomal ion channels (e.g. TPCs in breast cancer) or members of the TRP channel family, TRPML1 has yet to be described in a cancer model. However, a paper published in 2008 by Fehrenbacher *et al.* demonstrated that Lamp proteins are associated with chemotherapy resistance<sup>294</sup>. In a series of clever experiments, Fehrenbacher and colleagues showed that the downregulation of Lamps can sensitise cancer cells to chemotherapeutics through the induction of lysosome membrane permeabilization (LMP)<sup>294</sup>. LMP is a process triggered by various factors (e.g. TNF, osmotic stress, etc.) that compromise the integrity of the lysosomal membrane resulting in the release of enzymes into the cytosol and the initiation of lysosomal apoptotic pathways<sup>295</sup>. One could speculate that the loss of lysosomal TRPML1 (e.g. sequestration within the Golgi or translocation to the plasma membrane) could potentially decrease the expression of Lamps and promote cancer cell death through the activation of LMP following treatment with anticancer drugs. Thus, the possibility of the Mucolipin family existing as potential players in the development and treatment of cancer is not unfeasible.

**Figure 3: Structure of TRPML channels.** The members of the Mucolipin family share a similar architecture with 6 transmembrane domains, a large loop and N and C termini facing the cytosol. The large loop of the TRPML channels is found between TM1 and TM2 while the channel pore is located in between TM5 and TM6.



## **1.5 Subchapter V: Project Rationale and Objectives**

### **1.5.1 Rationale and Hypothesis**

The importance of ion channels as potential oncogenes has been demonstrated in various cancer models and while many have been described as key regulators of cancer growth and progression, others have yet to take the center stage in our quest for a cancer cure. One such channel is TRPML1, a member of the TRP family which has not been characterized in the pathology of cancer. Various members of the TRP ion channel family have already shown great promise as therapeutic targets for the treatment of cancer, observations which set in motion the work behind this dissertation. As mentioned in previous sections, aberrant cell proliferation is a defining feature of cancer cells and one of the mechanisms often deregulated to support this increased growth rate is autophagy. The process of autophagy is heavily dependent on the proper functioning of lysosomes and since TRPML1 plays a vital role in maintaining the lysosomal function, we hypothesize that TRPML1 is involved in sustaining PCa cell proliferation. Furthermore, as mentioned in the introduction section, TRPML1 is ubiquitously expressed whereas TRPML2 is present mainly in immune cells and its function revolves around mediating various immune processes such as B cell development and defence against viruses and bacteria<sup>296–298</sup>. On the same premise, TRPML3 is primarily found in the cells of the inner ear where knockdown of TRPML3 results in deafness and circling behaviour in mice<sup>274,277,299–301</sup>. TRPML3 is also found in somatosensory neurons and melanocytes<sup>244</sup>. Thus, TRPML2 and 3 are unlikely candidates as potential regulators of PCa cell proliferation. Hence, the expression profiles and distinct functional properties of the TRPML channels were part of the rationale

behind choosing to study TRPML1 in PCa and not the other two members of the Mucolipin family.

As mentioned in previous paragraphs, the prognosis for PCa patients is relatively good if the disease is detected early, but the likelihood of survival decreases drastically when patients present with advanced PCa. In addition, although progress is currently being made in the identification of novel biomarkers for PCa, the reliability and sensitivity of most PCa biomarkers is rather low which highlights the need for new therapeutic and diagnostic targets to improve overall PCa patient survival. For these reasons, we chose PCa as our model to study the effects of TRPML1 on cancer cell proliferation. Furthermore, TRP channels, namely TRPC6, TRPV6, TRPV2 and TRPM8 have already been demonstrated to play important roles in PCa; thus, it is possible that TRPML1, a member of the TRP channel family could be of significance in the pathophysiology of PCa cells<sup>302</sup>.

### **1.5.2 Objectives**

1. Identify the role of TRPML1 in PCa cell proliferation and survival.
2. Identify the mechanism of action behind the effect of TRPML1 on PCa cell proliferation.
3. To determine the potential of TRPML1 as a biomarker for PCa.

## CHAPTER II: MATERIALS AND METHODS

### 2.1 Cell Lines

The cell lines used throughout the experiments presented in this dissertation are as follows: HEK293 (epithelial human embryonic kidney cells), RWPE-1 (normal epithelial cells from the peripheral zone of the prostate), PC3 (prostate adenocarcinoma cells), DU145 (prostate carcinoma cells), PC-TU1 (prostate adenocarcinoma cells) and PC-LC (prostate adenocarcinoma cells). HEK293 (CRL- 1573), RWPE-1 (CRL- 11609), PC3 (CRL-1435) and DU145 (HTB- 81) were purchased from the American Type Culture Collection (ATCC; Manassas, Virginia, USA) while PC-TU1 and PC-LC were received as a gift from Dr. David Waisman at Dalhousie University (Halifax, Nova Scotia, Canada). RWPE-1, PC3, DU145, HEK293, PC-TU1 and PC-LC were cultured in Keratinocyte SFM (1X), RPMI Medium 1640 (1X), MEM (Minimum Essential Medium) (1X) and DMEM (Dulbecco Modified Eagle Medium) (1X), respectively. All cell lines with the exception of RWPE-1 were cultured in medium supplemented with 10% fetal bovine serum (FBS) and 1% Pen Strep (10,000 units/mL Penicillin and 10,000 µg/mL Streptomycin). RWPE-1 cells were grown in medium enriched with human recombinant epidermal growth factor 1- 53 (EGF 1- 53), bovine pituitary extract (BPE) and 1% Pen Strep. All experiments were performed with cells cultured in 10% FBS enriched media, with the exception of RWPE-1 cells which do not required FBS for growth.

### 2.2 Reagents

Culture media, EGF 1-53, BPE, 1X HBSS (Hank's Balanced Salt Solution), 1X Phosphate Buffered Saline (PBS), FBS and Pen Strep were purchased from Gibco by Life

Technologies (Thermo Fisher Scientific; Waltham, Massachusetts, USA). The Mucolipin-specific inhibitor (ML-SI) was received from Dr. Haoxing Xu's laboratory at Michigan University (Ann Arbor, Michigan, USA) while the TRPML agonist (ML-SA1) was acquired from Sigma-Aldrich (CAS 332382-54-4; St. Louis, Missouri, USA). TRPML1 shRNA plasmids were purchased from Dharmacon (Lafayette, Colorado, USA). All dyes used for flow cytometry and calcium imaging experiments were obtained from: Thermo Fisher Scientific (Fura-2 AM, DAF-FM and CM-H<sub>2</sub>DCFDA), Invitrogen (Alexa 488- Annexin V; Burlington, Ontario, Canada), BioLegend (7AAD; San Diego, California, USA) and Abcam (5(6)-Carboxyfluorescein N-hydroxysuccinimidyl ester, CFSE; Cambridge, United Kingdom). The PureLink RNA Mini Kit used for RNA extraction was procured from Ambion by Life Technologies (Thermo Fisher Scientific). Superscript II is available from Invitrogen. SsoAdvanced™ Universal SYBR® Green Supermix used for RT-qPCR and the 4X Laemmli sample buffer and the Dual Color Precision Plus Protein™ Prestained Protein Standards used for western blotting were received from BIO-RAD (Hercules, California, USA). Primers were manufactured and received from Invitrogen. Antibodies used for western blotting and confocal microscopy were purchased from: Cell Signalling (Danvers, Massachusetts, USA) and Santa Cruz Biotechnology (Dallas, Texas, USA). The Pierce™ Protease Inhibitor and Phosphatase Inhibitor Mini Tables were acquired from Thermo Fischer Scientific. Doxorubicin, Polyethylenimine (PEI), Polybrene, Puromycin and chemicals used for the preparation of buffers/solutions were provided by Sigma- Aldrich.

### **2.3 Mucolipin-Specific Inhibitor (ML-SI) Treatment**

Cells were seeded at the respective confluencies and allowed to incubate for 24 hrs prior to the addition of ML-SI. The concentrations of inhibitor used were 5, 10, 15, 20 and 25 µM.

Once cells were treated with the inhibitor, they were incubated for an additional 24, 48 or 72 hrs depending on the experiment. Media were not changed in between timepoints.

## **2.4 TRPML1 Knockdown**

The TRPML1 stable knockdown was generated using the 3<sup>rd</sup> generation lentiviral packaging system<sup>303</sup>. For the purposes of producing lentivirus particles, 500,000 HEK293 cells were seeded in 6 cm plates and incubated for 24 hours. When cells reached 50-60% confluence, HEK293 cells were co-transfected with pPAX (6 µg), MD2G (3 µg) and PLKO-LV-shTRPML1 (6 µg) plasmids with the PEI transfection reagent. At 24 and 48 hrs post-transfection, the lentivirus was collected, filtered and stored at -80 °C until use. For transduction, 150,000 cells were cultured in 6-well plates and allowed to incubate for 24 hrs or until 70% confluent. A total of 500 µL of lentivirus was then added in the presence of 8 µg/mL of Polybrene. Cells were incubated with the lentivirus for 48 hrs followed by selection with Puromycin at a concentration of 1 µg/mL. The efficiency of the knockdown was determined using RT-qPCR. Knockdown cells were used until passage 10 at which point a new cell stock from the original knockdown was thawed, selected with puromycin and analyzed with RT-qPCR to ensure that the cells retained the knockdown prior to use in experiments.

## **2.5 RT-qPCR**

Total RNA was extracted from normal and cancerous prostate cells using the standard TRIzol procedure and diluted to a final concentration of 2 µg. The RNA was then used for the synthesis of complementary DNA (cDNA) using the Superscript II First-Strand Synthesis system. Sections of the cDNA were amplified and quantified using specific primers (see section

2.5.1), the SsoAdvanced™ Universal SYBR® Green Supermix and the CFX96 Deep Well Real-Time PCR Detection System. Data and primer efficiencies were recorded using the CFX Manager Software (BIO-RAD). The mRNA expression cycle time (ct) values for each gene was calculated relative to the 3-phosphate dehydrogenase (GAPDH) reference gene using the Livak and Schmittgen's  $2^{-\Delta\Delta CT}$  method previously described<sup>304</sup>. For knockdown experiments, the fold change was first normalized to GAPDH then compared against the scrambled controls of the respective cell line. In ML-SI experiment, the fold change was calculated relative to the non-treatment (NT) group. All data was plotted using the GraphPad Prism software.

### **2.5.1 Primer Sequence Table**

<b>Gene name</b>	<b>Gene symbol</b>	<b>Sequence (5' to 3')</b>
3-phosphate dehydrogenase	GAPDH	Forward: TTTCCTGGTATGACAACGAATTGG
	GAPDH	Reverse: TTATTGATGGTACATGACAAGGTGC
Transient receptor potential Mucolipin 1	TRPML1	Forward: TCTTCCAGCACGGAGACAAC
	TRPML1	Reverse: GCCACATGAACCCCCACAAAC
H2A Histone Family Member X	H2AX	Forward: CGACAACAAGAACGCGAA
	H2AX	Reverse: GGGCCCTCTTAGTACTCCTG
Tumor Protein P53 Binding Protein 1	TP53BP1	Forward: GAGTTTGTGAGCCCCTGTGA
	TP53BP1	Reverse: GGTTGTGCCATGGTAAGGA

### **2.6 Western Blot**

Protein was extracted using 1X RIPA lysis buffer (1% Triton-X100, 5 mM EDTA, 5mM EGTA, 0.1% SDS and 150 mM NaCl with 2X protease and phosphatase inhibitors). After the addition of the lysis buffer, cells were scrapped using a cell scraper and lysates were then transferred to Eppendorf tubes and incubated on ice for 10 minutes followed by a 10 minute

centrifugation at 15,000xg at 4 °C. The protein-containing supernatant was placed in a clean microcentrifuge tube and stored at -80 °C until use. Protein samples were quantified using the Bradford reagent where protein lysates were incubated with 1 mL of the Bradford reagent for 10 minutes at room temperature (RT). The protein concentration was determined at wavelength of 595 nm using a spectrophotometer. SDS/PAGE electrophoresis was carried out using 8 and 12% acrylamide resolving gels with a 4% stacking gel and 1X Running buffer (35 mM SDS, 250 mM Tris, 192 mM glycine and 1 L of water). Electrophoresis was allowed to proceed for approximately 1 hr. A total of 7 µL of the dual color protein ladder was added to one lane of each gel prior to the loading of the protein samples. Samples were prepared with 1X Laemmli sample buffer and loaded at a concentration of 40 µg unless otherwise specified in the figure legends. Protein samples were then transferred onto 0.22 µm nitrocellulose membranes for 1 hr and 10 minutes in 1X Transfer buffer (25 mM Tris, 192 mM glycine, 800 mL of water and 200 mL of 100% Methanol). Prior to the overnight incubation at 4 °C with primary antibodies, membranes were blocked with 5% milk powder dissolved in 1X TBST (137 mM NaCl, 2.7 mM KCl, 19 mM Tris-base, 0.1% TWEEN 20) for 45 minutes at RT. Secondary antibodies were prepared in 1X TBST and incubated with the membranes for 2 hours at RT on the shaker. Membranes were imaged using the LI-COR Odyssey 9120 Infrared Imaging System. Protein bands were quantified with the Odyssey software by subtracting the background density from the protein band density. β-Actin was used as the reference protein for all western blots. All samples were first normalized to β-Actin (e.g. sample band density divided by β-Actin band density) and fold change was calculated relative to the scrambled control of each blot (e.g. knockdown value divided by the scrambled value). The antibodies used in western blot experiments were as follows: anti-Lamp (Cell Signalling; 15665S), anti-Cyclin B1 (Cell Signalling; 4138S), anti-JNK

(Cell Signalling; 9252), anti-p-JNK (Cell Signalling; 4668), anti-AKT (Santa Cruz Biotechnology; SC-46915), anti-p-AKT (Cell Signalling; 9271), anti-p62 (Cell Signalling; 8025S), anti-LC3A/B (Cell Signalling; 12741S), anti-PARP (Cell Signalling; 9532), and anti- $\beta$ -Actin (Santa Cruz Biotechnology; SC-8432).

## 2.7 Flow Cytometry

The following paragraphs contain descriptions of the flow cytometry-based staining procedures used to acquire data presented in this dissertation. Flow cytometry data acquired throughout experiments was quantified using the Flowing software (developed by Perttu Terho at the Turku Centre for Biotechnology) and plotted as mean fluorescence intensity (MFI) or percentage of positive cells using GraphPad Prism, unless otherwise specified in the materials and methods section of the particular staining procedure or in the figure legends.

### 2.7.1 CFSE (5(6)-Carboxyfluorescein N-Hydroxysuccinimidyl Ester) Staining

Cell proliferation was assessed using CFSE, a fluorescent cell permeant dye. CFSE forms stable, covalent bonds with intracellular residues such as lysines which prevents the dye from leaking out of the cells. In addition, due to the bond formation between the succinimidyl group of the CFSE dye and the cellular residues, only half of the daughter cells will have CFSE; therefore, the amount of CFSE is inversely proportional to the rate of cell proliferation. First, cells were centrifuged at 1,7000 rpm for 5 minutes and resuspended in 1 mL of 1X PBS. A total of 100  $\mu$ L of 2.5  $\mu$ M CFSE was added to each sample and vortex briefly to ensure proper mixing of the cells with the CFSE dye. Cells were incubated with the dye for 5 minutes at 37 °C and 5% CO<sub>2</sub>. Scrambled and knockdown cells were then seeded at a confluence of 20,000 cells/well in 12-well

plates (or 30,000 PC3, DU145, PC-TU1 and PC-LC wildtype cells for ML-SI experiments) and incubated at 37 °C and 5% CO<sub>2</sub> for 3 days. Following the 3 days incubation, cells were washed with 1X PBS and centrifuged at 500xg for 5 minutes at 4 °C. Samples were resuspended in 500 µL of 1X PBS following the centrifugation step and processed using the 488 nm blue Argon laser (FL1: 515-545 nm detection range) of the Calibur cytometer at Dalhousie university.

## **2.7.2 Propidium Iodide (PI) Staining**

Propidium Iodide was used to quantify the amount of DNA present during each of the cell cycle stages within the normal and cancerous prostate cells. Cells (100,000 cells/well) were cultured in complete medium in 6-well plates and allowed to incubate for 4 days at 37 °C and 5% CO<sub>2</sub>. On day 4, cells were washed twice with 1X PBS, trypsinized and re-suspended in 4 mL of 1X PBS. Cells were then centrifuged at 2,000 rpm for 6 minutes at 22 °C. The supernatant was removed following centrifugation and 200 µL of 1X PBS was added to each sample. Then, a total of 3 mL of ice cold 70% ethanol (EtOH) were added drop by drop to each sample while vortexing to avoid the formation of aggregates. Samples were stored at 4 °C overnight. After the overnight incubation, samples were centrifuged at 3,000 rpm for 10 minutes at 4 °C. Cells were then washed twice with 3 mL of 1X PBS to remove the EtOH and centrifuged as before. Cells were stained with 1 mL of the PI solution ([PI]= 10 mg/mL, [RNase A]= 20 mg/mL and 1X PBS up to 1 mL/reaction) and incubated at RT for 1 hr. Samples were run on the cytometer subsequent to the incubation without removing the excess dye. The 488 nm blue Argon laser (FL2: 564-606 nm detection range) of the cytometer was used to process the samples. Data was analyzed using the ModFIT LT software. Histograms and percentage of cells were generated using the same software.

### **2.7.3 DAF-FM and H<sub>2</sub>DCFDA Staining**

For the purposes of quantifying the amount of intracellular nitric oxide (NO) and reactive oxygen species (ROS) present within cells, DAF-FM diacetate (4-Amino-5-Methylamino-2', 7'-Difluorofluorescein Diacetate) and H<sub>2</sub>DCFDA (General Oxidative Stress Indicator, a chloromethyl derivative of H<sub>2</sub>DCFDA) were used, respectively. A total of 60,000 cells/well were seeded in 12-well plates and incubated for 48 hrs. H<sub>2</sub>O<sub>2</sub> (0.015%) was used as a positive control for ROS production where H<sub>2</sub>O<sub>2</sub> was added 15 minutes prior to the staining procedure. Following the addition of H<sub>2</sub>O<sub>2</sub>, cells were incubated at 37 °C and 5% CO<sub>2</sub> for 15 minutes. Samples were trypsinized, re-suspended in 2 mL of FACS buffer (1X PBS with 1% FBS and 1% 0.5 mM EDTA) and centrifuged at 500xg for 5 minutes at 4 °C. Cells were then washed twice with 1X PBS and centrifuged as before prior to staining with 5 µM of DAF-FM and/or 5 µM of H<sub>2</sub>DCFDA for 45 minutes at 37 °C and 5% CO<sub>2</sub>. The dyes were prepared in 1X PBS and 100 µL of each dye was added to the respective samples. Excess dye was washed off with 2 mL of 1X PBS after the incubation followed by centrifugation at 500xg for 5 minutes. Samples were re-suspended in 500 µL of 1X PBS and processed on the cytometer using the 488 nm blue Argon laser (FL1: 515- 545 detection range).

### **2.7.4 Annexin V/7AAD Staining**

Cell death, specifically apoptosis and necrosis were assessed using Annexin V and 7AAD, respectively. For these experiments, cells were seeded at a confluence of 50,000 cells/well in 6-well plates and allowed to incubate for 24 days prior to the addition of the positive controls. The positive controls used were 60 nM and 100 nM Doxorubicin (apoptosis control) and 50% EtOH (necrosis control). Cells were incubated for an additional 3 days. After the 3 day

incubation period, the supernatant and adherent cells were collected, and centrifuged at 500xg for 5 minutes at 4 °C. Cells were then washed once with double distilled water (ddH<sub>2</sub>O) and once with 1X Annexin buffer (0.1M HEPES, 1.4M NaCl, 25mM CaCl<sub>2</sub> and ddH<sub>2</sub>O at a pH of 7.4) and centrifuged as before. Samples were then labelled with 2 µL of Annexin V for 10 minutes followed by staining with 1 µL of 7AAD for an additional 5 minutes in the dark at RT. Following the incubation with the two dyes, 100 µL of 1X Annexin buffer was added to each sample. Finally, samples were processed on the cytometer immediately after the staining procedure using the 488 nm blue Argon laser (FL1: 515-545 nm and FL2: 564-606 nm detection range for Annexin V and 7AAD, respectively).

## **2.8 MTS Assay**

This assay was implemented to assess and quantify cell viability. 3,000 (or 5,000 for inhibitor experiments) cells/well were seeded in 96-well plates and incubated for 24, 48 and 72 hrs. The media was not replenished in between timepoints. At each timepoint, 5 mg/ml of 3-(4,5-Dimethyl-2-thiazolyl)-2,5-diphenyl-2H-tetrazolium dissolved in 200 µL of 1X PBS were added to each well and incubated for 3 hrs at 37 °C and 5% CO<sub>2</sub>. A volume of 100 µL of dimethyl sulfoxide (DMSO) was then added to individual wells to dissolve the formazan crystals. Cells were incubated with DMSO for 30 minutes at 37 °C and 30 minutes at RT on the shaker. Absorbance was read at 570 nm using a spectrophotometer. Data was calculated relative to the scrambled control (or non-treated control (NT) for inhibitor experiments) of the respective cell line at each timepoint and plotted using the GraphPad Prism software, either as percentage of viable cells or as OD570.

## **2.9 Confocal Microscopy**

To quantify the number of lysosomes, normal and cancerous cells were stained and analyzed using confocal microscopy. Cells grown on coverslips were washed twice with 1X PBS and fixed with 4% paraformaldehyde for 15 minutes at RT. Coverslips were then washed three times with 1X PBS for 5 minutes/wash. Fixed cells were permeabilized with 0.1% Triton X-100 in 1X PBS for 5 minutes then washed three times with 1X PBS for 5 minutes/wash. Following the wash step, cells were blocked with 3% bovine serum albumin (BSA) in 1X PBS for 1 hour at RT then washed three more times as before. Cells were incubated with the primary antibody (1:250 dilution for  $\alpha$ -Lamp1) prepared in 3% BSA at 4 °C overnight. Samples were washed three times with 1X PBST (1X PBS with 0.1% Tween 20) and incubated with the appropriate secondary antibody for 45 minutes at RT in the dark. Lastly, coverslips were washed three times with 1X PBST for 15 minutes and processed with a confocal microscope. Images were acquired using the LSM510 Zeiss confocal microscope with a 63X oil-immersion objective lens and captured using the ZEN22012 software. The number of lysosomes was calculated using the ImageJ software and plotted as a bubble graph in GraphPad Prism.

## **2.10 Calcium Imaging**

Calcium imaging was used to assess the functionality of the TRPML1 channel through the quantification of cytoplasmic calcium changes following TRPML1 activation. 200,000 cells were cultured in cell imaging dishes and incubated for 24 hrs. Cells were washed twice with 1X HBSS and incubated with 3  $\mu$ g/mL of Fura-2 AM in 1X HBSS for 1 hr in the dark at RT. Prior to imaging, cells were washed twice with 1 mL of bath solution (140 mM NaCl, 2 mM MgCl<sub>2</sub>, 5 mM KCl, 2 mM CaCl<sub>2</sub>, 10 mM D-glucose, 10 mM HEPES and 1 mM EGTA, adjusted to pH

7.2-7.4). The cell imaging dishes were placed in a chamber on a Zeiss microscope equipped with a camera for fluorescence imaging. Fura-2 fluorescence was excited to 340 and 380 nm using monochro-mator (Lambda-DG4, Sutter Instruments). Fluorescence was captured by an Andor-DV2 camera (Photometrics). Cells were continuously perfused with the bath solution. The flow rate of the cell imaging dish perfusion system was set to 2 mL per minute. Calcium recording began while cells were in 1 mL of bath solution for ~ 200 seconds at which time ML-SA1 (TRPML1 activator) was gradually (5mL) perfused into the bath solution. The recording continued until ~ 900 seconds when usually a steady plateau of cytoplasmic calcium is reached. Metafluor software (Version 7) was used for data analysis. The intracellular calcium concentration time course was plotted as a ratio of fluorescence 340/380 using Excel while the quantification bar graph was generated using GraphPad Prism software.

## **2.11 Bioinformatics Analysis**

The following is a description of the bioinformatics analysis used to generate some of the results presented in this dissertation. All curves were plotted using the GraphPad Prism software and data downloaded from cBioPortal, an open access website administered by the the Genomic Data Commons (GDC) from the NIH (National institute of Health). cBioPortal compiles datasets from published literature, each dataset used for the analysis in this dissertation is listed in the figure legends of each corresponding figure. In addition, The Cancer Genome Atlas (TCGA) is a major contributor to the GDC cBioPortal genomic data. Some TCGA datasets have been previously published while others are considered provisional as raw data is curated from the TCGA data centre and are updated every few months. Of note, provisional datasets are curated from the TCGA data centre and updated every few months.

### **2.11.1 Kaplan Meier Survival Analysis**

Survival analysis was performed on the provisional TCGA prostate cancer cohort. Raw expression values of TRPML1 along with survival time (time to last-follow-up) and survival status (e.g. alive or deceased) were all downloaded via cBioPortal and analysed using the well-established Kaplan-Meier method<sup>305–307</sup>. The patients were separated into low and high expression groups of TRPML1 based on a median cut-off. To plot the Kaplan Meier survival curve, patients were assigned a value of 0 (living or disease-free) or 1 (deceased or progressive disease) depending on the status of the patient. Overall survival was measured as the time elapsed between diagnosis and the time of last follow-up or death. Disease-free survival was determined as the duration between treatment completion and the return and/or progression of disease at the time of last follow-up. Statistical significance was determined using the Log-rank (Mantel-Cox test) test in GraphPad.

### **2.11.2 CCLE Gene Expression**

TRPML1 Z-scores in PCa cell lines from the Cancer Cell Line Encyclopedia (CCLE) were accessed through cBioPortal<sup>306,307</sup>. A z-score for a sample indicates the number of standard deviations away from the mean of expression in a reference set of samples. The reference samples are often from within the same dataset and are not disclosed through the portal. All z-scores were plotted using GraphPad software.

### **2.11.3 Co-Expression Analysis**

Raw expression values were downloaded from cBioPortal as RNA Seq V2 RSEM gene expression data. The RNA Seq V2 RSEM represents a sequencing platform (RNA sequencing)

offered by Illumina which is capable of measuring expression of almost all genes. RSEM represents a software-build normalization method that corrects for other variables. Values were entered into GraphPad Prism where Pearson correlation coefficients and statistical significance were calculated.

## 2.12 Statistics

Statistical analysis was performed using the GraphPad Prism software. For comparisons between multiple (more than two) groups, a One-way ANOVA statistical test was used while Student's *t* tests were implemented to determine significance between two groups. The corresponding statistical significance for each condition is represented by the asterisks above each bar ( $**** = p \leq 0.0001$ ,  $*** = p \leq 0.0005$ ,  $** = p \leq 0.001$ ,  $* = p \leq 0.01$ , n.s =  $p > 0.05$ ). All experiments were conducted at least three times; however, only one representative run is shown in each figure.

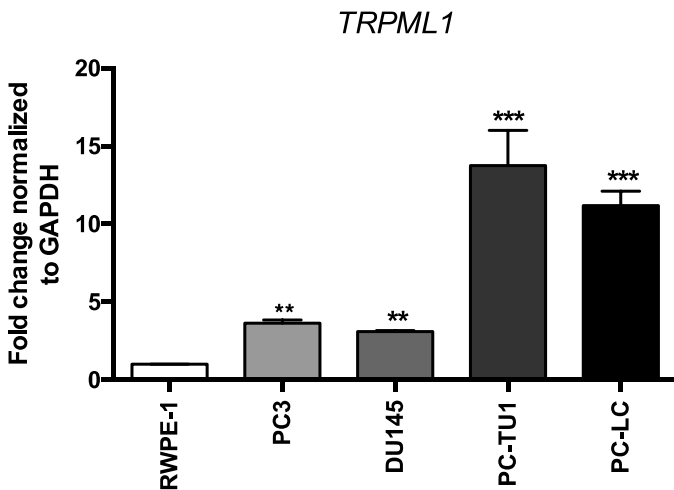
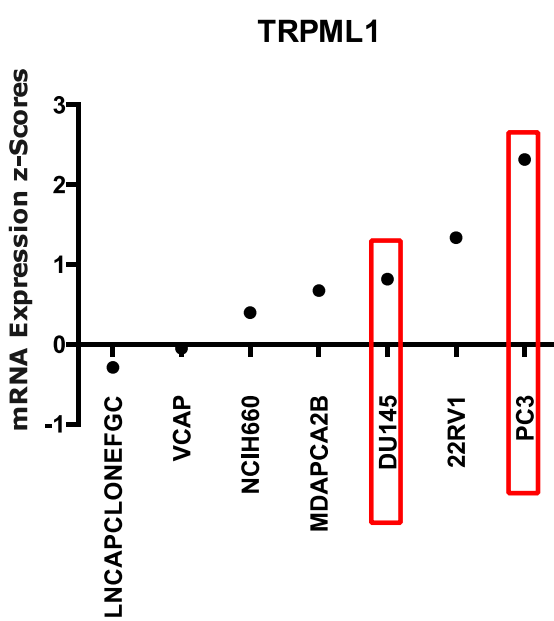
## CHAPTER III: RESULTS

### 3.1 The Loss of TRPML1 Decreases Cell Proliferation in PCa Cell Lines in a Dose-Dependent Manner

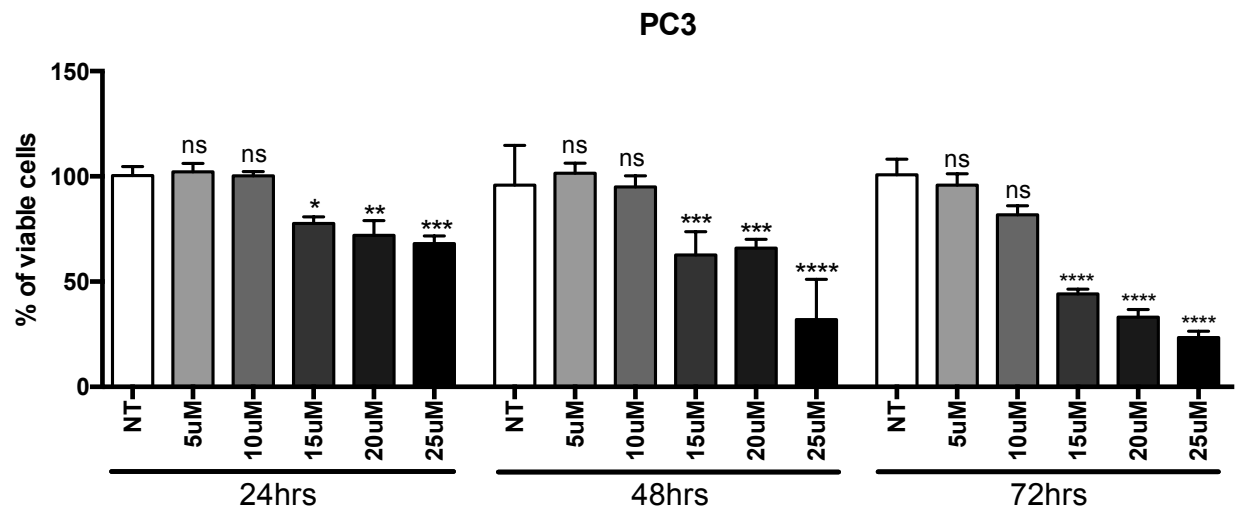
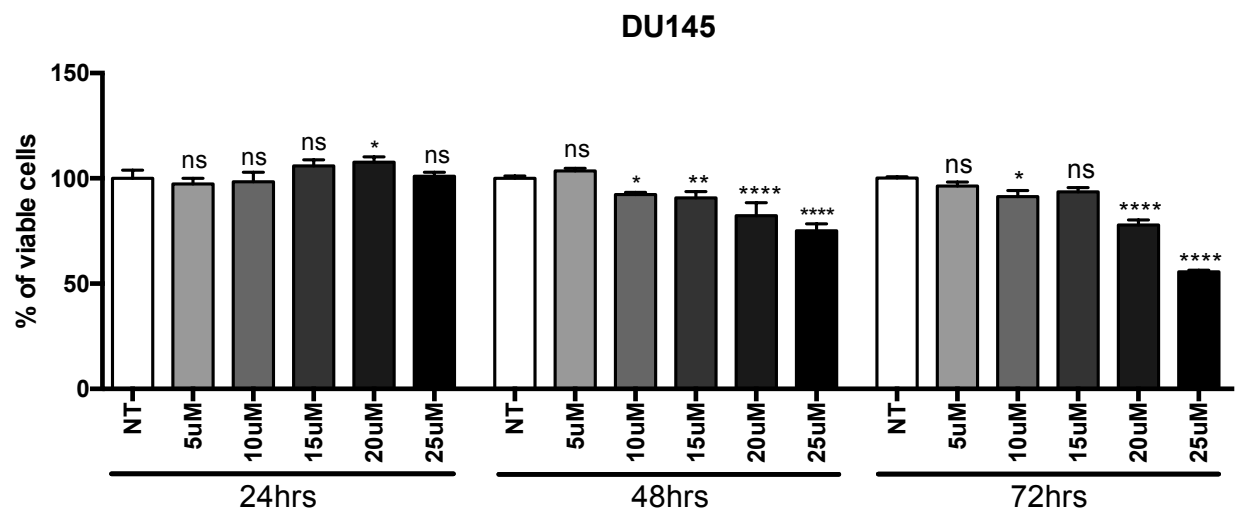
To determine the role of TRPML1 in prostate cancer cell proliferation, we first assessed whether PCa cells differentially express this channel in comparison to normal prostate cells. We utilized RT-qPCR to compare TRPML1 expression in a panel of five prostate cell lines: RWPE-1 (normal), PC3, DU145, PC-TU1 and PC-LC using RT-qPCR. As shown in Fig. 4A, TRPML1 is overexpressed in all PCa cell lines as compared to the normal, RWPE-1 cells. We further confirmed our results using the Cancer Cell Line Encyclopedia (CCLE) data set available online which showed the upregulation of TRPML1 in PC3 and DU145 cell lines (Fig. 4B). Having established the enhanced expression of TRPML1 in PCa cells, we then examined the effect of ML-SI, a TRPML inhibitor on PCa viability and proliferation using the tetrazolium-based MTS assay. Interestingly, inhibitor treatment decreased the viability of all PCa (PC3, DU145, PC-TU1 and PC-LC) in a dose-dependent manner over the course of 72 hrs with the highest significance observed at 72 hrs and a concentration of 25  $\mu$ M (Fig. 5A-D). To confirm our MTS results, we used CFSE staining where the amount of dye present within a cell population is inversely proportional to cell proliferation and as such, increased CFSE fluorescence represents a decrease in proliferation. In accordance with our MTS data, CFSE staining and flow cytometric analysis of PCa cells treated with ML-SI displayed a significant decrease in proliferation after 72 hrs; thus, suggesting that TRPML1 is a potential regulator of PCa cell growth and proliferation (Fig. 6C-J).

Although ML-SI has been shown to inhibit TRPML1, its specificity is rather low<sup>308</sup>. To account for the off-target effects of the inhibitor and to demonstrate the role of TRPML1 as a key player in PCa cell proliferation, we generated TRPML1 knockdown (KD#1 and KD#3) cells using the lentivirus and specific shRNA system. Knockdown efficiency was determined using RT-qPCR (Fig. 7A-E). To ensure the main function of TRPML1 in calcium release from the lysosome was also hampered by the KD, we performed calcium imaging to quantify the amount of intracellular Ca<sup>2+</sup> following channel activation with 100 µM of ML-SA1 (Fig. 7F and G). As indicated in Fig. 5F, the TRPML1 KD decreased the release of Ca<sup>2+</sup> through TRPML1 from the lysosome. We then hypothesized that TRPML1 KD would likely decrease PCa cell proliferation but have no effect on normal cells. In accordance with our previous results, KD PCa cells showed a decreased rate of proliferation in the MTS assay while RWPE-1 cells remained unaffected by the loss of TRPML1 over the course of 72 hrs (Fig. 8A-E). These results were confirmed with flow cytometry as indicated by the rightward shift in CFSE staining (Fig. 9A-J). Collectively, these data suggest that TRPML1 is important in PCa proliferation and loss of channel functionality results in decreased growth.

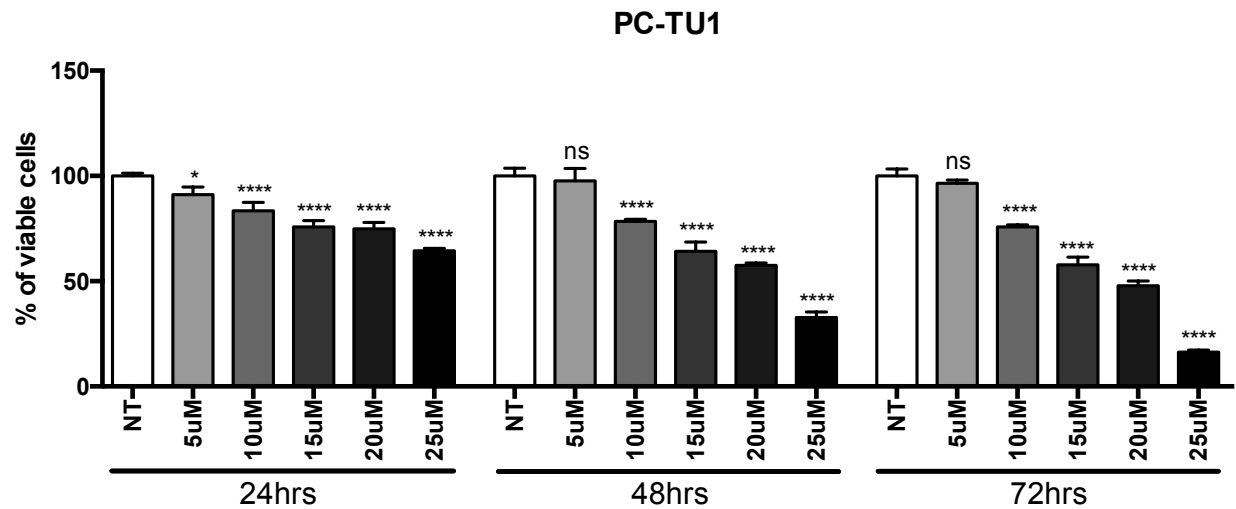
**Figure 4: TRPML1 is overexpressed in PCa cell lines.** A) The mRNA expression level of TRPML1 was assessed using RT-qPCR in the prostate cancer cell lines PC3, DU145, PC-TU1 and PC-LC. RT-qPCR cycle time (ct) values were first normalized against GAPDH followed by a comparison between the PCa cell lines against the normal prostate cell line, RWPE-1. TRPML1 was found to be upregulated in the PCa cell lines when compared to the normal prostate cells. B) The overexpression of TRPML1 was confirmed using the CCLE dataset where the z score values for PC3 and DU145 were elevated as highlighted by the red boxes. Of note, the z scores for other PCa cell lines (LNCAP, VCAP, NCIH660, MDAPCA2B and 22RV1) included in the data set acquired from CCLE were also plotted as a comparison for the level of TRPML1 expression across different PCa cell lines. Description of CCLE data analysis is provided in the Materials and Methods. Statistical significance for the RT-qPCR results was calculated using a One-way ANOVA. Asterisks above each bar represents the significance of results and corresponds to the following p values: \*\*\*\* =  $p \leq 0.0001$ , \*\*\* =  $p \leq 0.0005$ , \*\* =  $p \leq 0.001$ , \* =  $p \leq 0.01$ , n.s =  $p > 0.05$ . Three ( $n= 3$ ) independent RT-qPCR experiments (RNA extraction, synthesis and RT-qPCR) were performed to validate the overexpression of TRPML1 in PCa cell lines, but only one set of results is represented in this figure.

**A****B**

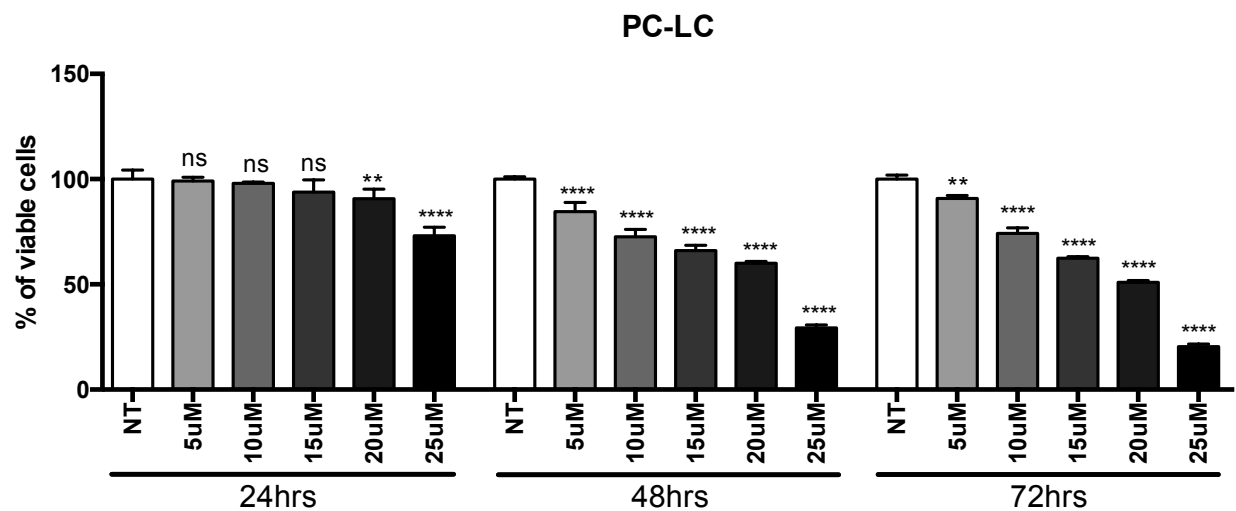
**Figure 5: TRPML1 inhibition causes a dose-dependent decrease in cell viability/proliferation.** A-D) PCa cell lines, PC3, DU145, PC-TU1 and PC-LC were treated with 5, 10, 15, 20 and 25  $\mu$ M of ML-SI and incubated for 24, 48 and 72 hrs. The absorbance of the soluble formazan compound formed after the addition of the MTS reagent was measured at each time point at a wavelength of 570 nm. OD570 values were converted and plotted as percentage of cell viability. All PCa cell lines showed a decrease in cell viability/proliferation upon treatment with ML-SI; however, the most statistically significant difference between the scrambled control and TRPML1 KD of each cell line was at 72 hrs with 25  $\mu$ M while 5  $\mu$ M of ML-SI showed the least significant reduction in viability/cell proliferation. One-way ANOVA tests were used to determine the statistical significance at each concentration (e.g. NT vs. 5  $\mu$ M) and timepoint for the four PCa cell lines. Significance was represented with asterisks placed about each bar ( $**** = p \leq 0.0001$ ,  $*** = p \leq 0.0005$ ,  $** = p \leq 0.001$ ,  $* = p \leq 0.01$ , n.s =  $p > 0.05$ ). MTS experiments were performed three times ( $n= 3$ ) in quintuplicates; however, only one representative run is depicted in this figure.

**A****B**

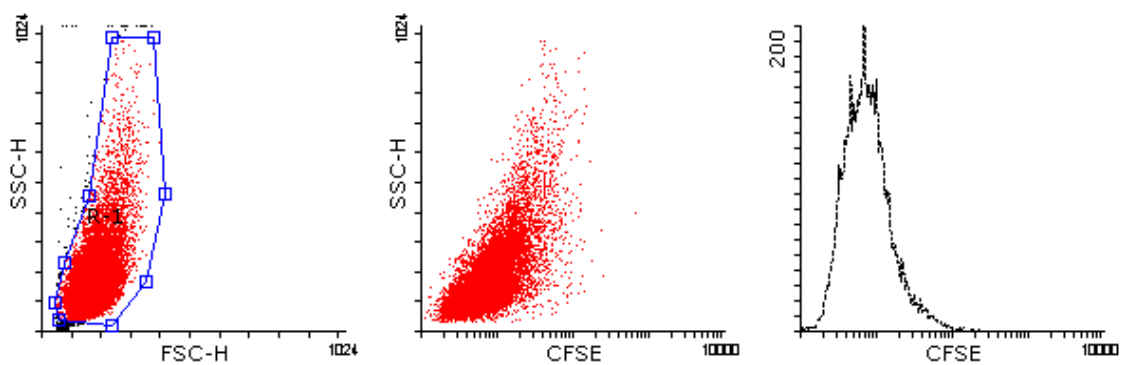
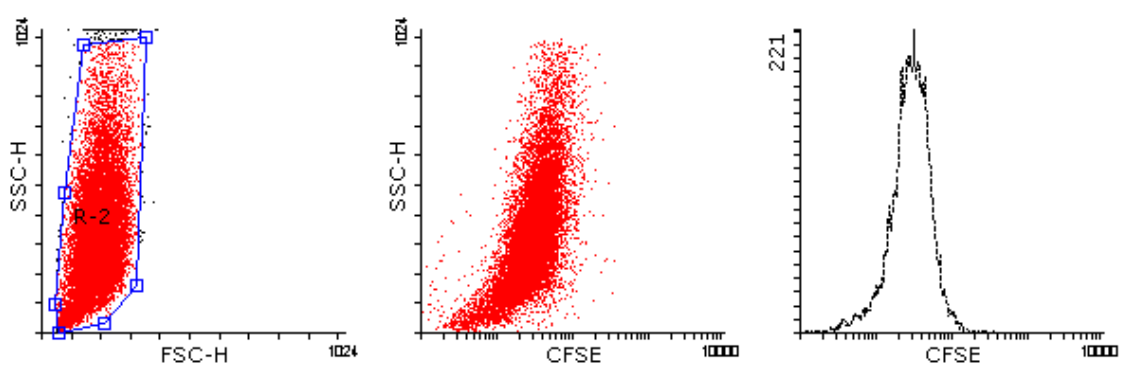
C

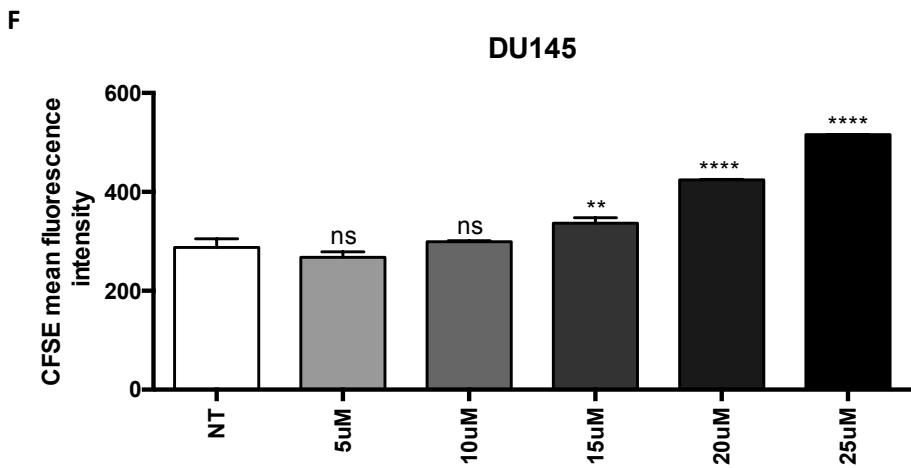
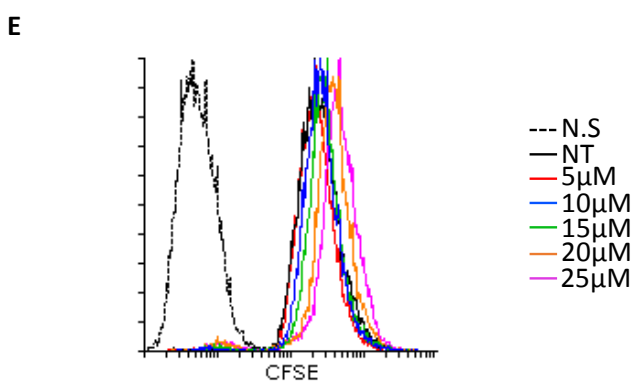
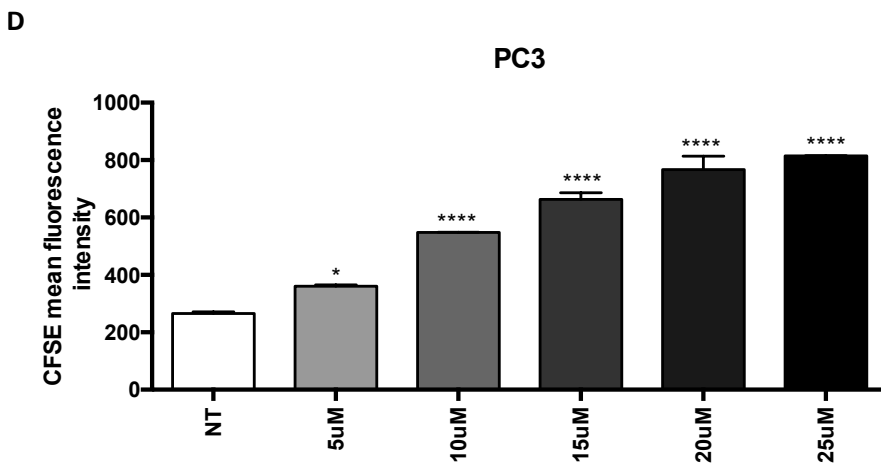
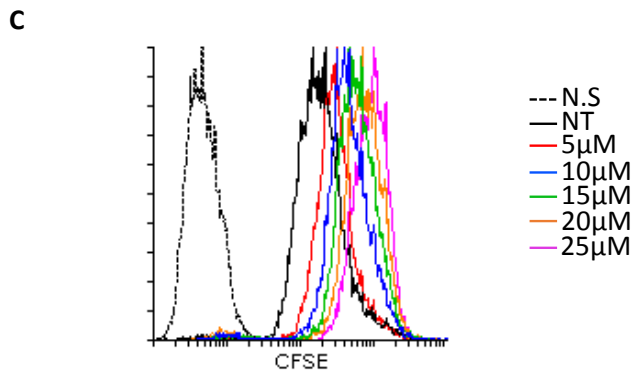


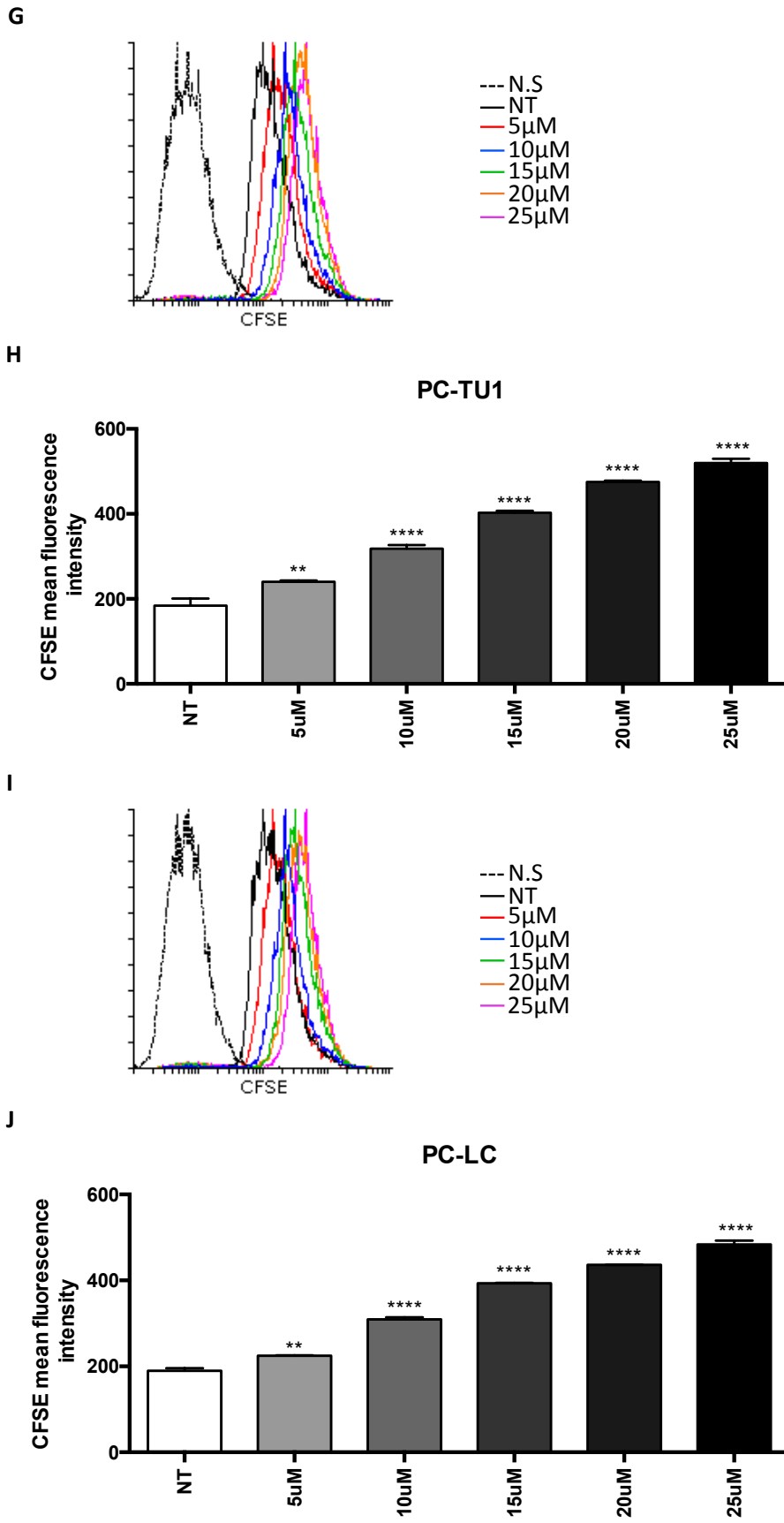
D



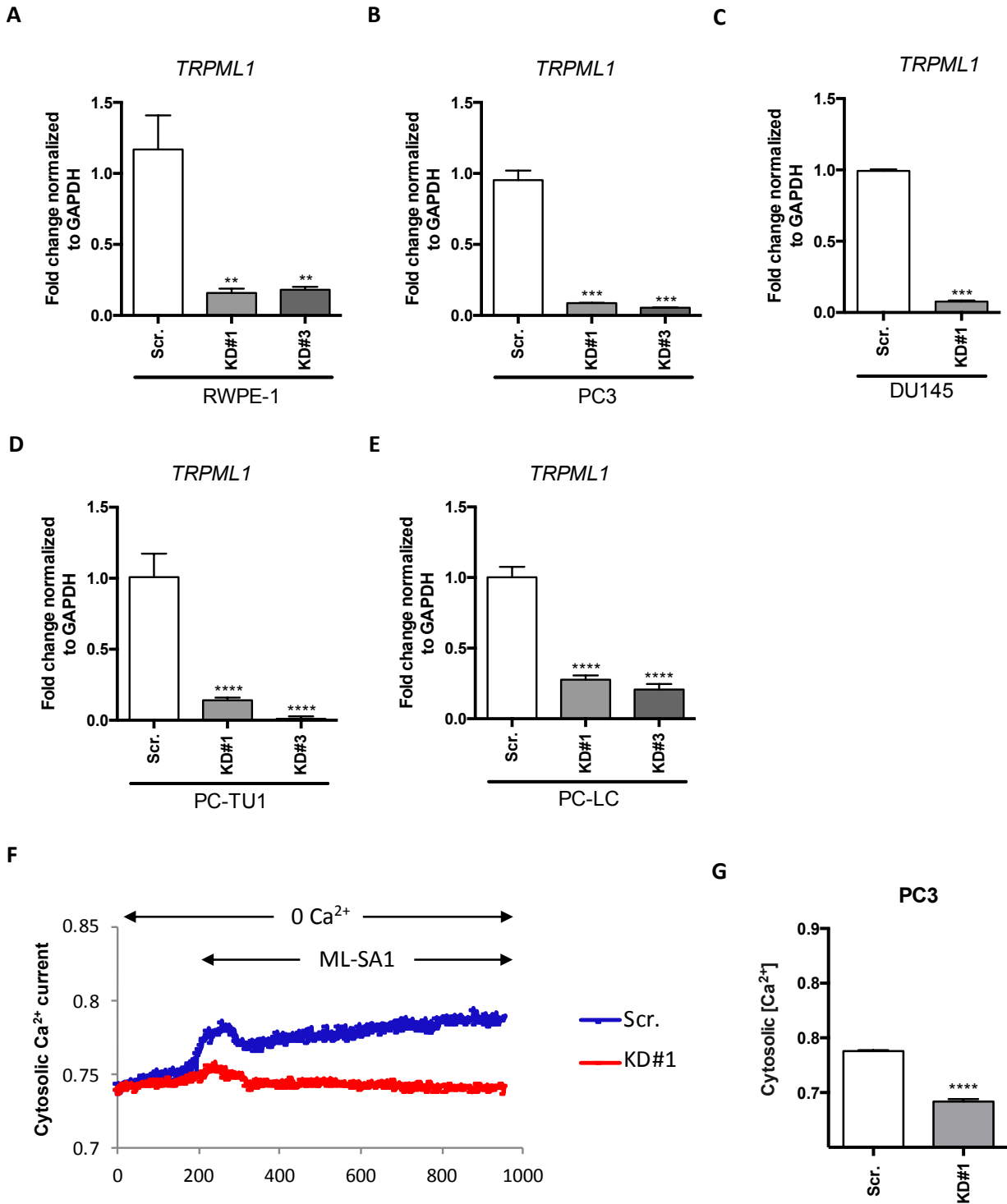
**Figure 6: Loss of TRPML1 inhibits the proliferation of PCa cell lines.** Gating strategy for the analysis of A) non-stained and B) stained flow cytometry data. Cells stained with CFSE and processed on a flow cytometer were first gated on the forward (FSC) and side scatter (SSC). Cells within the gate were then represented in a histogram as mean fluorescent intensity (MFI) to quantify the amount of CFSE staining in scrambled control cells and TRPML1 KD cells. Cells were treated with ML-SI (5, 10, 15, 20 and 25  $\mu$ M) 24 hrs after CFSE staining and allowed to incubate for an additional 72 hrs. C, E, G and I) An overlay histogram was generated for each of the four PCa cell lines (PC3, DU145, PC-TU1 and PC-LC) to evaluate and visualize the difference in staining between the, non-stained (NS), non-treated (NT) and treated groups where a rightward shift in CFSE staining is indicative of decrease proliferation. Each condition (NS, NT and treated) was represented using a different color as indicated by the legend to the right of each overlay histogram. D, F, H and J) Quantitative bar graph of CFSE MFI for each of the presented overlay histograms showing an increase in CFSE staining in treated samples which corresponds to a dose- dependent decrease in cell proliferation. To determine the statistical significance of these results, One-way ANOVA tests were performed. The asterisks above each bar correspond to specific p values ( $**** = p \leq 0.0001$ ,  $*** = p \leq 0.0005$ ,  $** = p \leq 0.001$ ,  $* = p \leq 0.01$ , n.s =  $p > 0.05$ ). These experiments were performed three times (n=3) in triplicates, but only one representative run for each cell line is presented in this figure.

**A****B**

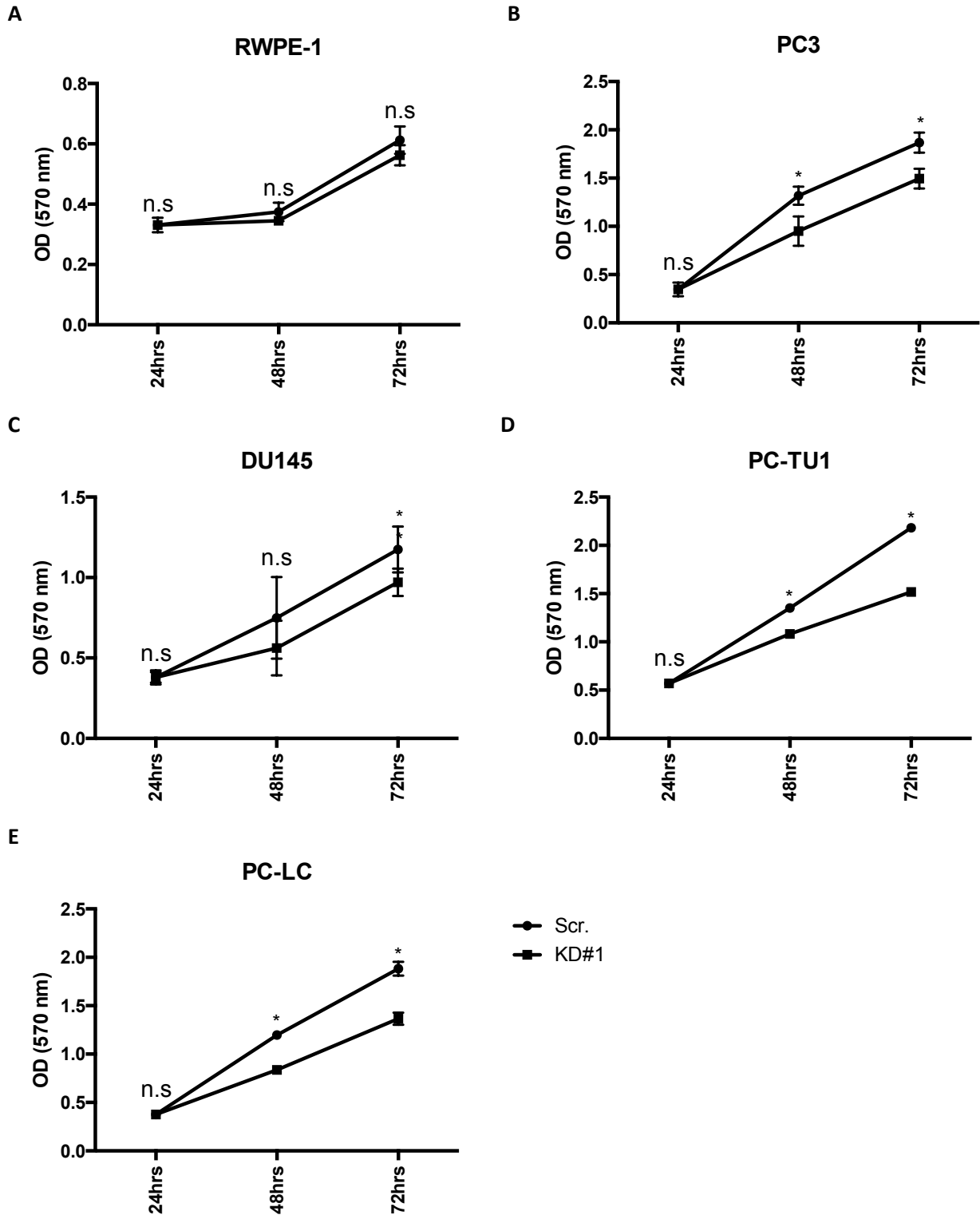




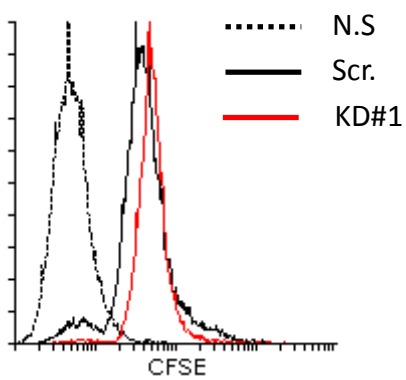
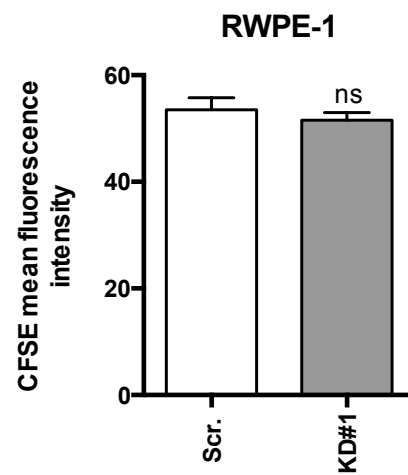
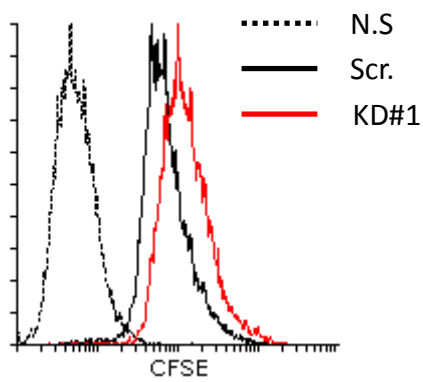
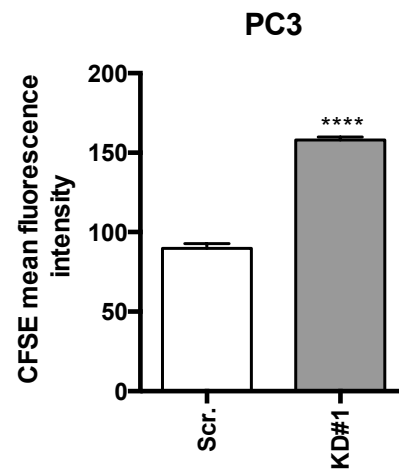
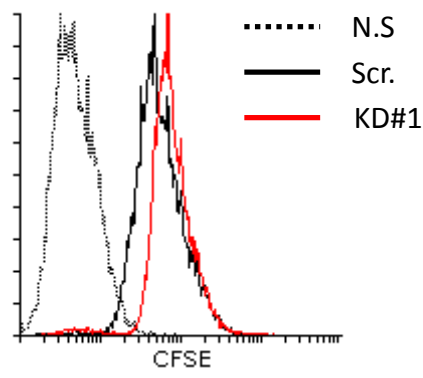
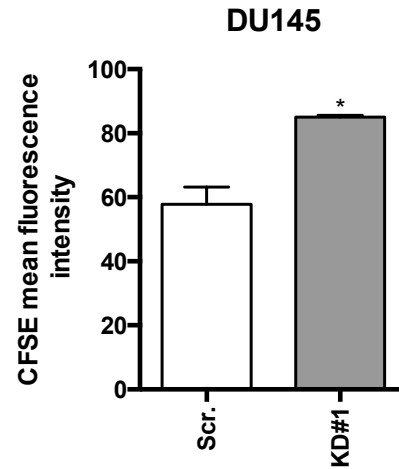
**Figure 7: Generation of TRPML1 knockdowns and loss of TRPML1 channel functionality in PCa.** A-E) RT-qPCR analysis of TRPML1 knockdown efficiency in normal (RWPE-1) and prostate cancer cell lines (PC3, DU145, PC-TU1 and PC-LC). KD cells showed a significantly lower mRNA level of TRPML1 indicating that the KD was successful. Ct values were first normalized against the reference gene, GAPDH and then against the scrambled control sample of each individual cell line (e.g. RWPE-1 TRPML1 KD#1 vs. RWPE-1 scr.). F) Intracellular calcium recording (~ 900 seconds) from scrambled (scr.) and TRPML1 knockdown (KD#1) PC3 cells following activation of the TRPML1 ion channel with ML-SA1 (added at ~200 seconds from the start of recording). G) Quantification bar graph of the intracellular  $\text{Ca}^{2+}$  concentration recorded using calcium imaging showing a decrease in cytosolic  $\text{Ca}^{2+}$  in KD cells. Statistical significance for RT-qPCR results for RWPE-1, PC3, PC-TU1 and PC-LC was calculated using One-way ANOVA tests while knockdown efficiency for DU145 cells was determined with a Student's *t* test. In addition, the significance of calcium imaging results was confirmed with a Student's *t* test. Asterisks above each bar represents the statistical significance of the respective result which corresponds to the following p values: \*\*\*\* =  $p \leq 0.0001$ , \*\*\* =  $p \leq 0.0005$ , \*\* =  $p \leq 0.001$ , \* =  $p \leq 0.01$ , n.s =  $p > 0.05$ . KD efficiency was quantified at least three times (see Materials and Methods section for TRPML1 knockdown) while calcium imaging was performed three times ( $n=3$ ). Only one experiment is presented in this figure.

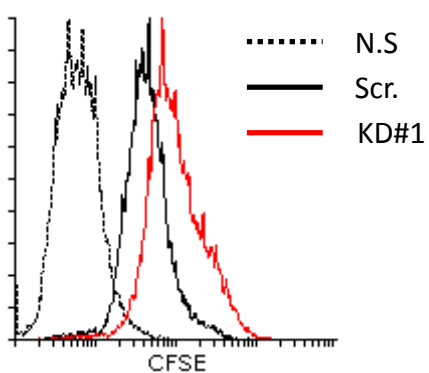
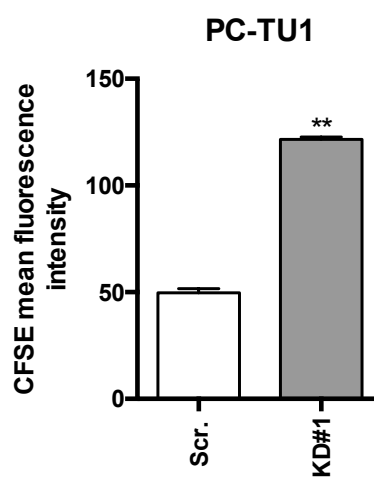
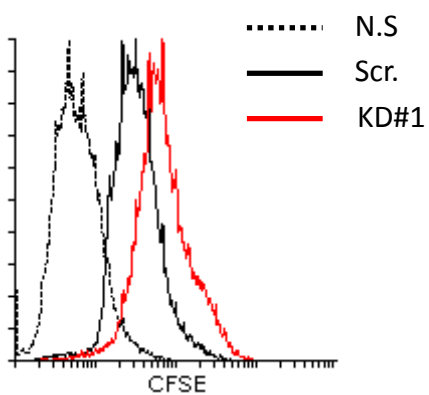
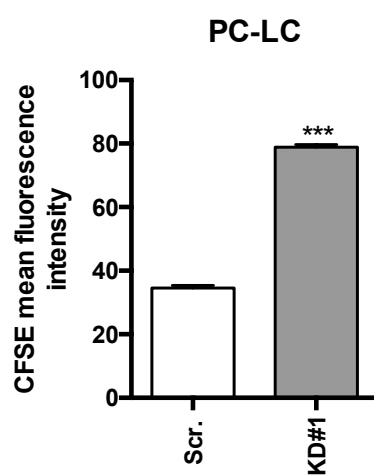


**Figure 8: Knockdown of TRPML1 decreases PCa cell proliferation.** A-E) The proliferative capacity of normal (RWPE-1) and PCa (PC3, DU145, PC-TU1 and PC-LC) cells following the loss of TRPML1 was assessed using the MTS assay over the course of 72 hrs. At the indicated time points, the absorbance was measured at 570 nm (OD (570 nm)) and plotted relative to the scrambled control of each cell line at each timepoint. RWPE-1 showed a non-significant change in proliferation following TRPML1 KD; however, the proliferation rate of PCa cell lines decreased after the loss of TRPML1 as indicated by the lower slope of the TRPML1 KD cells. Multiple *t* tests were used to evaluate the significance at each timepoint. Statistical significance was represented as asterisks placed above each timepoint node (black circle for Scr. and black square for KD#1). The p values associated with each asterisk correspond to \*\*\* =  $p \leq 0.0001$ , \*\*\* =  $p \leq 0.0005$ , \*\* =  $p \leq 0.001$ , \* =  $p \leq 0.01$ , n.s =  $p > 0.05$ . Of note, the error bars for the PC-TU1 and PC-LC graphs are not visible (with the exception of PC-LC at 72 hrs.) due to small standard deviations. This experiment was repeated three times ( $n=3$ ) with one representative run shown in this figure.



**Figure 9: TRPML1 is a potential regulator of PCa cell proliferation as indicated by the increase in CFSE staining.** Normal (RWPE-1) and PCa cells (PC3, DU145, PC-TU1 and PC-LC) were stained with CFSE and incubated for three days. Samples were analyzed using a flow cytometer on Day 3. A, C, E, G and I) CFSE positive scrambled (black line) and KD cells (red line) were gated and represented in overlay histograms as previously described (Fig. 6). B, D, F, H and I). The MFI of each cell line was plotted as a bar graph showing a significant increase in CFSE staining which is indicative of decreased proliferation. The statistical significance of the difference between scrambled control and KD cells of each cell line was calculated using the Student's *t* test and represented with an asterisk above each bar. The asterisk corresponds to the following \*\*\* =  $p \leq 0.0001$ , \*\* =  $p \leq 0.0005$ , \* =  $p \leq 0.001$ , \* =  $p \leq 0.01$ , n.s =  $p > 0.05$ . All experiments were performed three times ( $n=3$ ) with three or more replicates per experiment. A single representative experiment is shown here.

**A****B****C****D****E****F**

**G****H****I****J**

### **3.2 Knockdown of TRPML1 in PCa Leads to G2/M Cell Cycle Arrest due to DNA Damage**

Our next objective was to determine the underlying mechanism behind the observed decrease in proliferation of PCa cells upon TRPML1 knockdown and/or pharmacological inhibition. Normally, cell growth is dependent on the delicate balance between cell division and death, a process tightly regulated through the cell cycle. As such, there are two possibilities that can explain why TRPML1 KD can inhibit cell proliferation: cell cycle arrest or induction of apoptosis. To address whether TRPML1 KD affected cellular apoptosis, PCa cells were stained with Annexin V and 7AAD to evaluate the percentage of apoptotic and necrotic cells, respectively. As illustrated in Fig. 10, TRPML1 KD does not induce apoptosis in normal cells or PCa as indicated by the percentage of Annexin V<sup>+</sup> cells. The percentage of Annexin V<sup>+</sup> cell was not significantly different in KD cells as compared to scramble control cells of RWPE-1, PC3 and PC-LC cells. Of note, although statistically significant, the apparent increase of approximately 1% in 7AAD<sup>+</sup> and Annexin V<sup>+</sup>7AAD<sup>+</sup> in PC3 and PC-LC cells, respectively is likely not physiologically relevant and it will not be considered further. To conclude, these results show that the loss of TRPML1 does not promote apoptosis or necrosis in these cells.

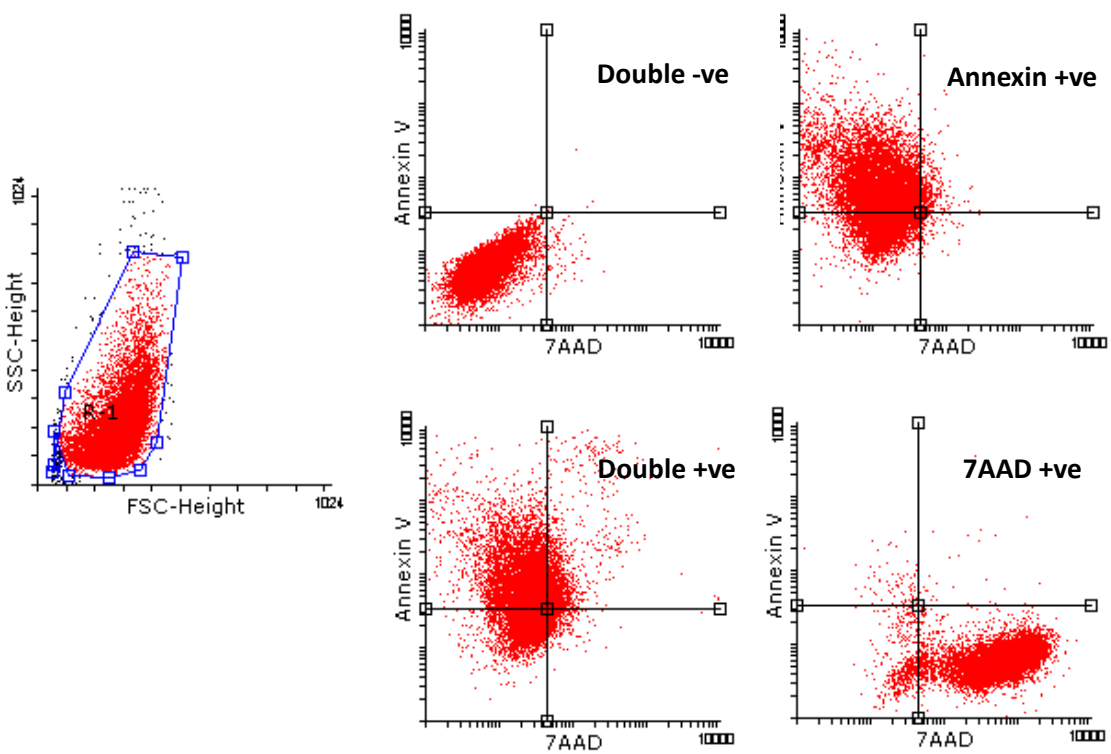
In order to assess whether the KD of TRPML1 had an effect on the cell cycle control of PCa cells, we used propidium iodide (PI) to quantify the amount of DNA present within each stage of the cell cycle: G0/G1, S and G2/M. Interestingly, the loss of TRPML1 resulted in the accumulation of PCa cells in the G2/M phase; however, normal cells were not arrested in either of the cycle phases (Fig. 11A-F). The G2/M phase is driven by cyclins, in particular Cyclin B1 which is required for the progression into the M (Mitotic) phase. Given the association between

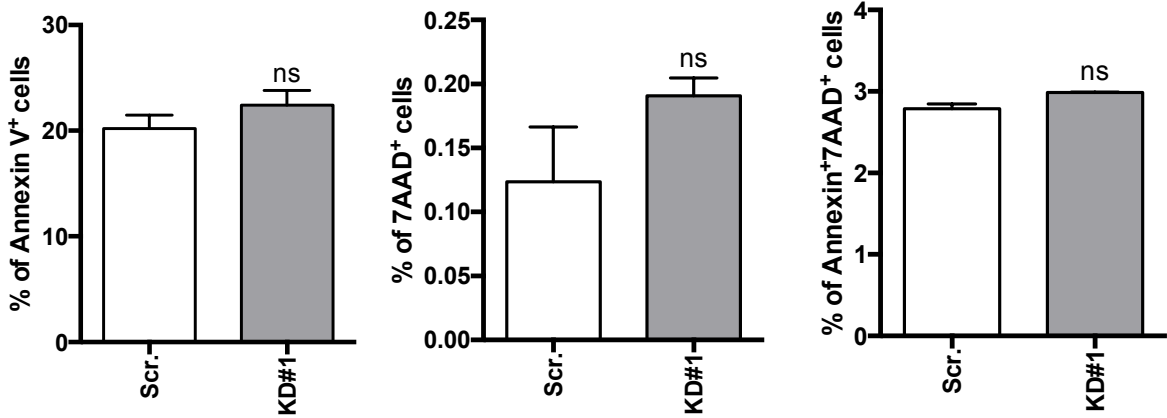
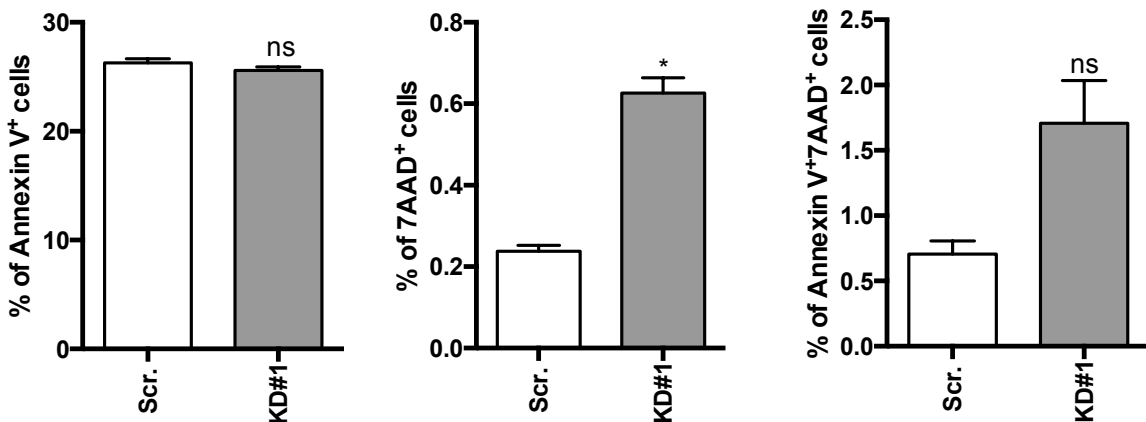
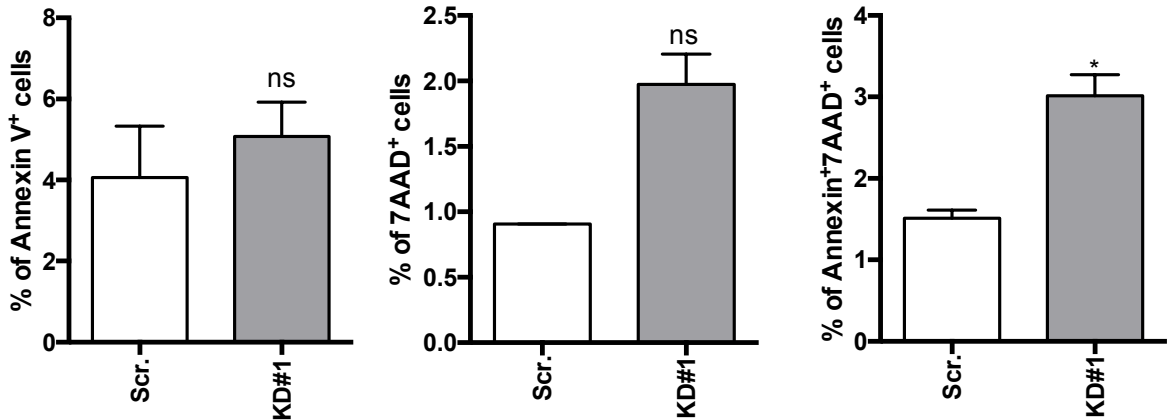
Cyclin B1 and the cell cycle, we speculated that KD cells will express less Cyclin B1 than their scrambled counterpart. Indeed, KD of TRPML1 decreased the protein level of Cyclin B1 in PC3 cells which further confirms our PI cell cycle results (Fig.12A).

The G2/M checkpoint is an important control mechanism that ensures the integrity of the DNA prior to the initiation of mitosis<sup>309</sup>. Arrest in this phase prevents cells that possess DNA damage from entering the mitotic phase before repairing their genetic material. Thus, our next experiment aimed to determine whether DNA damage is present within the KD cells and as such, we used the previously established marker for DNA damage, H2AX<sup>310</sup>. As expected, KD cells showed an increase in the mRNA expression level of H2AX (Fig. 12B). We also assessed the levels of the DNA damage response (DDR) protein, TP53BP1 (p53 binding protein 1). RT-qPCR analysis revealed an increase in TP53B1 in KD cells which is an indication of active DNA damage repair in PC3 cells (Fig. 12C). In addition, we found a very modest increase in PARP protein expression, a known DNA repair system marker which indicates that the loss of TRPML1 does not hamper the DNA damage repair system of the PC3 cells (Fig. 12D). To summarize, KD of TRPML1 induced a G2/M cell cycle arrest in PCa cells as indicated by the presence of DNA damage and an enhanced DNA damage response.

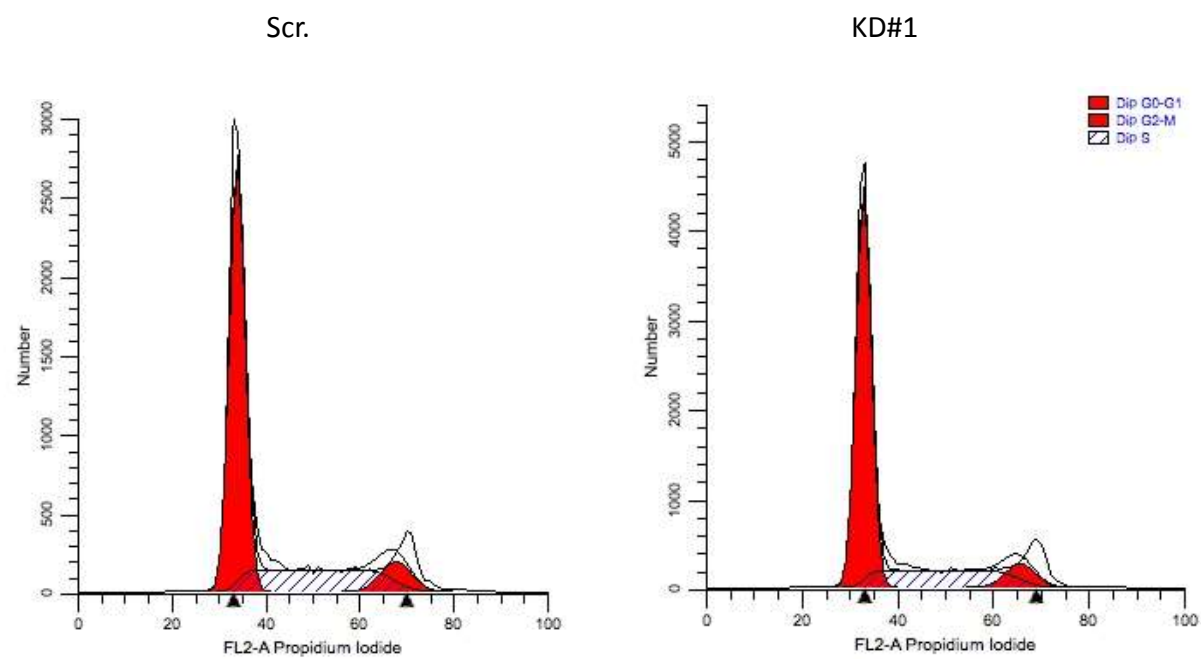
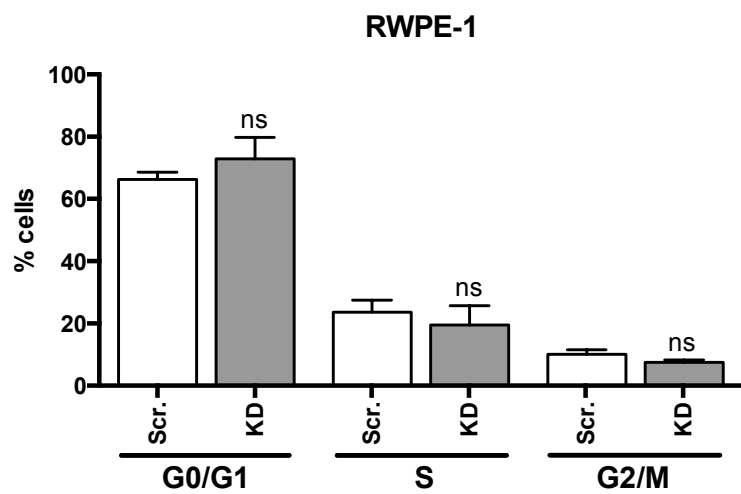
**Figure 10: TRPML1 expression does apoptosis in prostate cancer or normal cell lines.** A) Sample gating strategy for the analysis of Annexin V/7AAD staining used for the quantification of apoptosis and necrosis in scrambled and TRPML1 KD normal (RWPE-1) and PCa cell lines (PC3 and PC-LC). Cells were incubated for three days prior to Annexin V and 7AAD staining. Samples were first gated on the SSC and FSC, then further gated on Annexin and 7AAD. Cells within the bottom left quadrant represent the double negative (Annexin V<sup>-</sup> 7AAD<sup>-</sup>) population, those in the top left quadrant are designated as the Annexin V positive cells (Annexin V<sup>+</sup>) followed by the double positive (Annexin V<sup>+</sup> 7AAD<sup>+</sup>) population in the top right quadrant and the 7AAD positive (7AAD<sup>+</sup>) in the bottom right quadrant. B-D) The percentage of cells within each quadrant (except the double negative) was quantified using the Flowing software and plotted as individual bar graphs. Statistical significance was determined using *t* tests and represented with asterisks corresponding to \*\*\* =  $p \leq 0.0001$ , \*\* =  $p \leq 0.0005$ , \* =  $p \leq 0.001$ , \* =  $p \leq 0.01$ , n.s =  $p > 0.05$ . One of three independent experiments ( $n = 3$ ) performed in triplicates is shown in this figure.

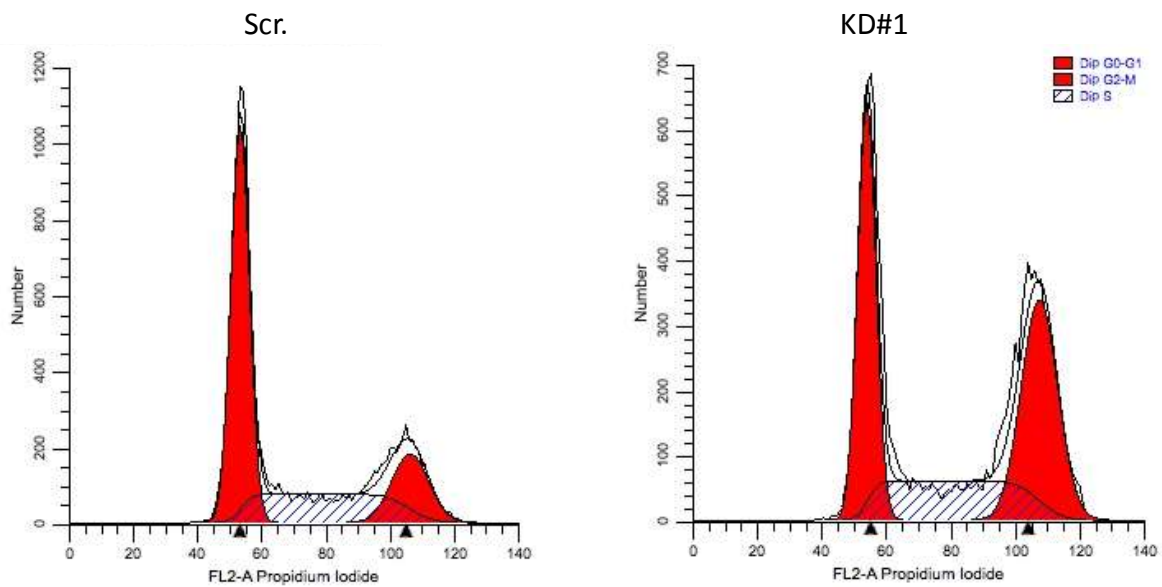
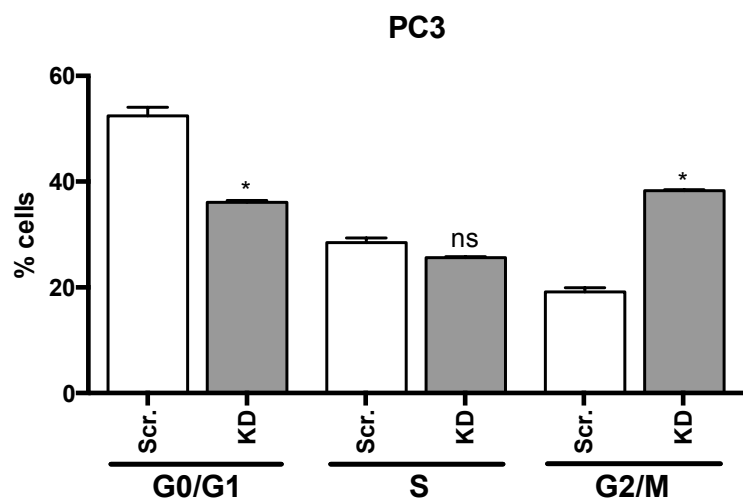
**A**



**B****RWPE-1****C****PC3****D****PC-LC**

**Figure 11: TRPML1 knockdown arrests PCa cells in the G2/M phase of the cell cycle.** To assess the possibility of cell cycle arrest, cells were incubated for four days followed by staining with PI and flow cytometry analysis. A, C and E) Samples were processed with a flow cytometer and histograms were generated with the ModFIT LT software to represent the amount of DNA within each phase of the cell cycle in RWPE-1, PC3 and PC-LC cells. The height of the peak is representative of an accumulation of cells within the respective phase which indicates that cell cycle arrest has occurred. B, D and F) The percentage of cells generated by the ModFIT LT software were plotted as bar graphs for each histogram showing that TRPML1 PCa cells (PC3 and PC-LC) were arrested in the G2/M phase whereas the normal, RWPE-1 cells remained unaffected by the KD. One-way ANOVA tests were performed to determine the significance of these results. Asterisks above each bar represent the statistical significance of the difference between the scrambled control and KD cells. Each asterisk corresponds to \*\*\* =  $p \leq 0.0001$ , \*\* =  $p \leq 0.0005$ , \* =  $p \leq 0.001$ , \* =  $p \leq 0.01$ , n.s =  $p > 0.05$ . The cell cycle experiment was performed three times ( $n= 3$ ) in duplicates with one representative run presented in this figure.

**A****B**

**C****D**

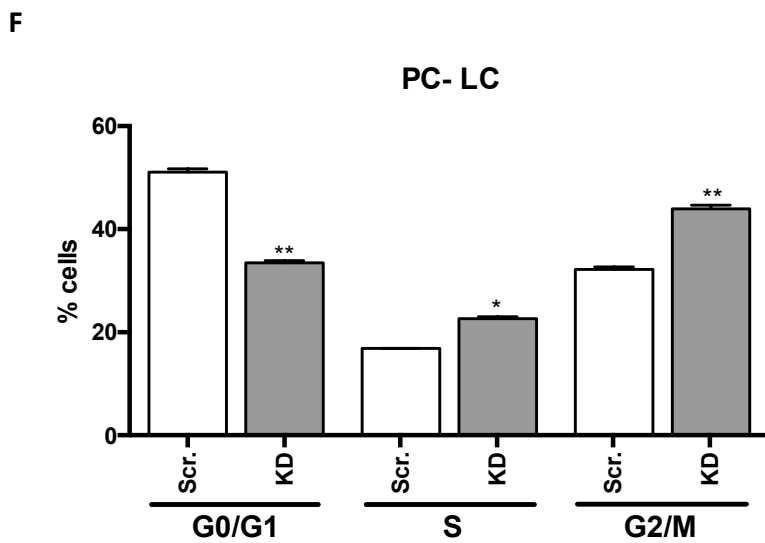
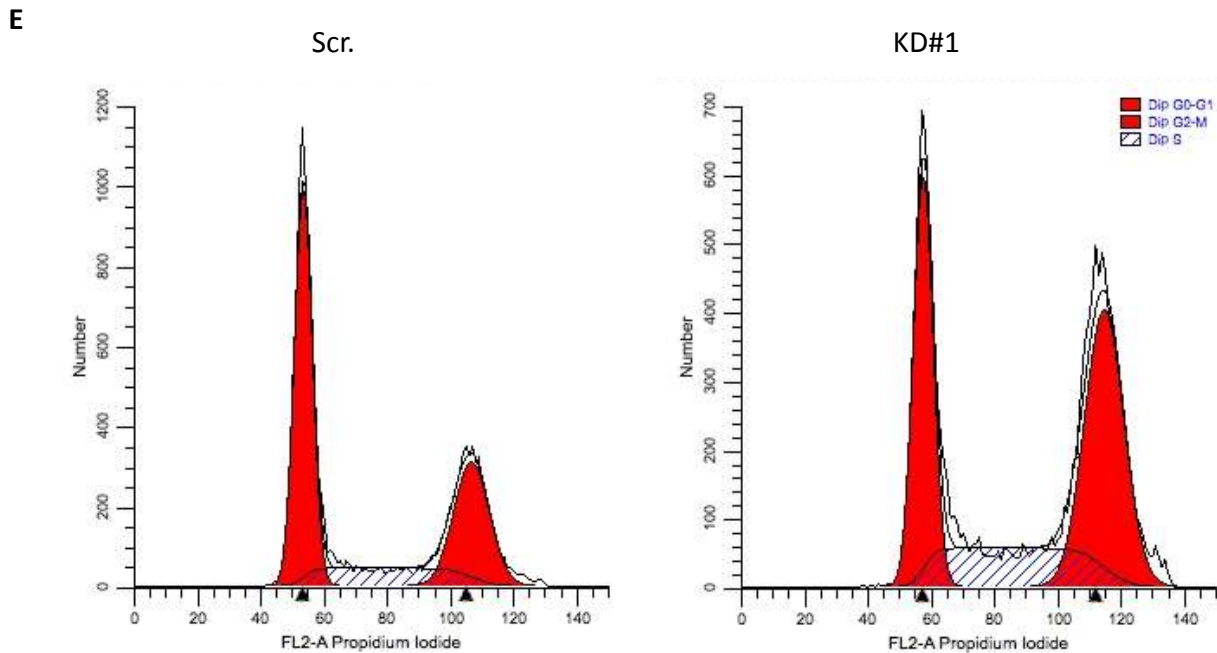
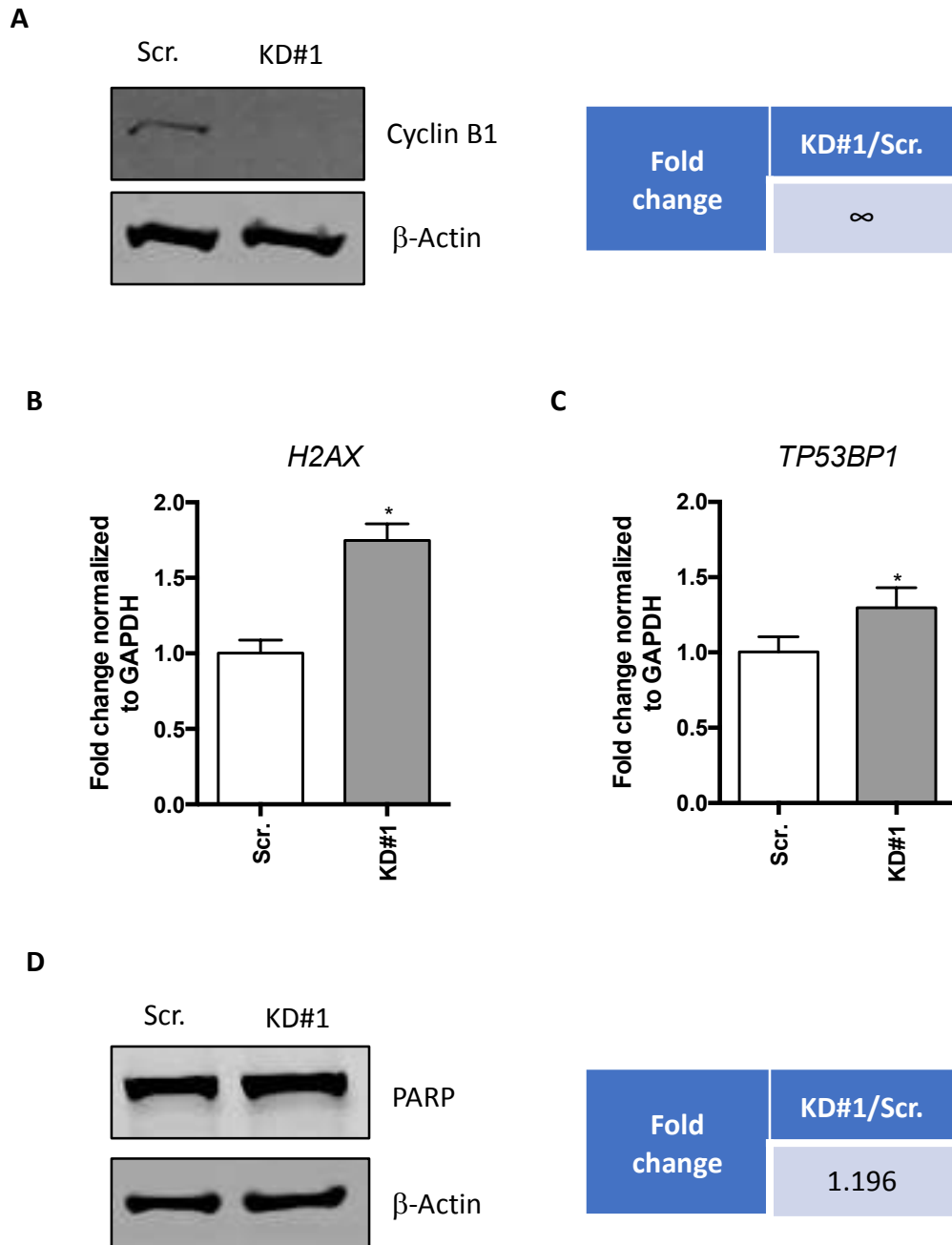


**Figure 12: Downregulation of TPRML1 induces cell cycle arrest due to the presence of DNA damage in PC3 cells.** A) Western blot analysis of the protein level of Cyclin B1 in scrambled and TRPML1 KD PC3 cells. The Cyclin B1 band was absent in the KD sample; therefore, fold change was not calculated and designated as the infinity symbol. B) mRNA expression of H2AX and C) TP53BP1 in PC3 cells as revealed through RT-qPCR analysis showing a modest increase in both genes. mRNA fold change was first normalized to GAPDH then to the corresponding scrambled control. D) Western blot image showing the protein expression level of DNA damage repair protein, PARP with the fold change represented in the table adjacent to the blot image. Fold change was calculated relative to  $\beta$ -Actin and the scrambled control. Significance was determined using *t* tests. Asterisks placed above the bars are indicative of the following p values: \*\*\*\* =  $p \leq 0.0001$ , \*\*\* =  $p \leq 0.0005$ , \*\* =  $p \leq 0.001$ , \* =  $p \leq 0.01$ , n.s =  $p > 0.05$ . RT-qPCR experiments were performed three times ( $n= 3$ ) in triplicates while each western blot experiment ( $n= 3$ ) was carried out with one replicate. One representative experiment is shown here.

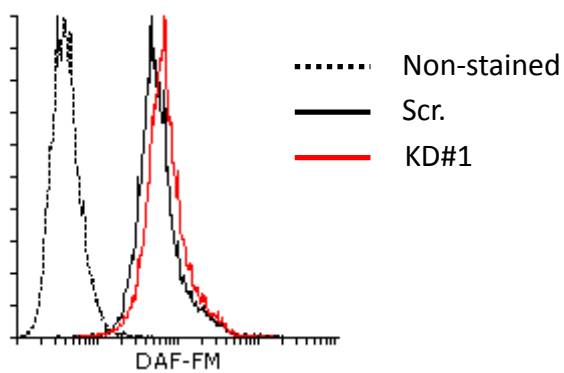
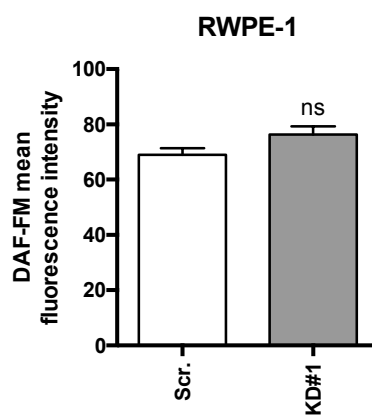
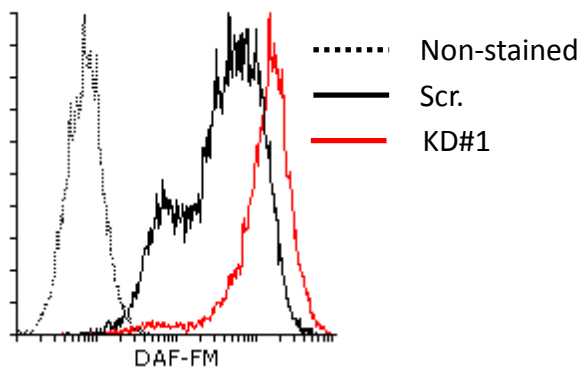
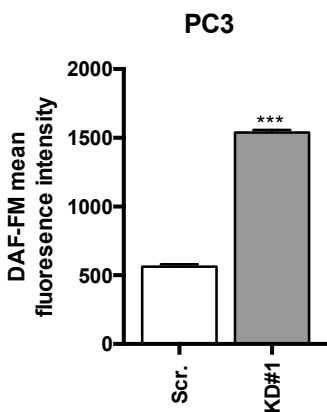


### **3.3 TRPML1 KD Results in the Accumulation of Reactive Oxygen and Nitrogen Species in PCa Cells**

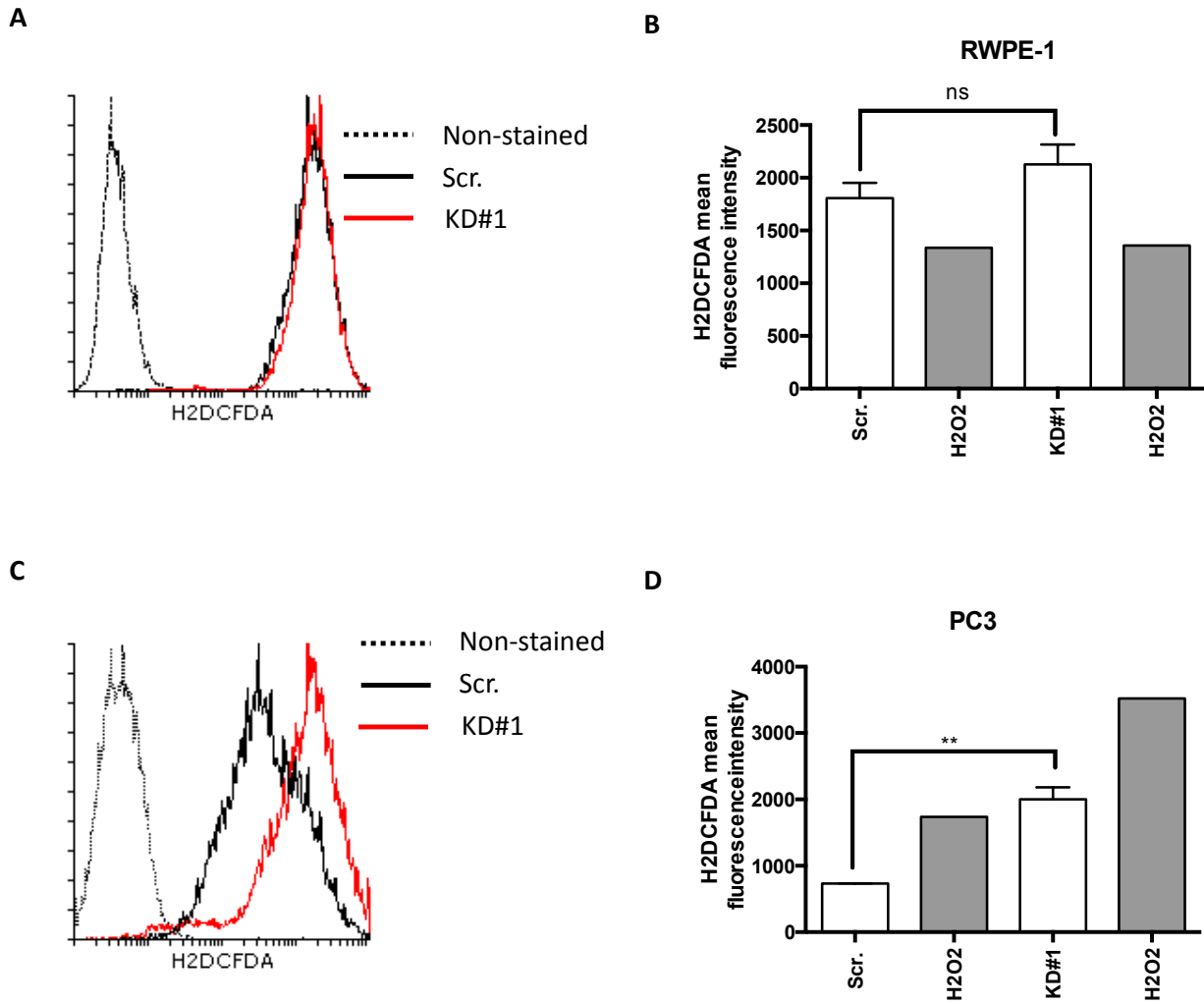
One of the major causes of DNA damage within cells is exposure to reactive oxygen and nitrogen species, a concept which has been exploited in many aspects of cancer therapy (e.g. pro-oxidant therapy)<sup>311</sup>. Considering our results so far and the presence of an active DNA damage response in TRPML1 KD cells, we next investigated the impact of TRPML1 KD on the production of ROS and NO. In accordance with our hypothesis, we observed an increase in the presence of ROS and NO in PC3 TRPML1 KD cells, but not in the normal, RWPE-1 TRPML1 KD cells as evidenced by the rightward shift in DAF-FM and H<sub>2</sub>DCFDA staining, respectively (Figs. 13 and 14). These results suggest that the accumulation of ROS and NO is potentially contributing to the DNA damage we have previously shown.

**Figure 13: Accumulation of nitric oxide (NO) following TRPML1 knockdown in PC3 cells.**

A and C) RWPE-1 and PC3 cells, respectively were first incubated for 48 hrs then stained with DAF-FM for the detection of intracellular nitric oxide (NO) and analyzed using flow cytometry. Cells were initially gated on the SSC and FSC then further gated on DAF-FM. Histograms were generated to represent the intensity of staining and thus, the amount of NO present within RWPE-1 and PC3 cells. A rightward shift in the histogram is indicative of an increase in the presence of NO which was quantified as MFI in the bar graphs in panels B and D. While RWPE-1 cells appear to not increase their NO production following the loss of TRPML1, PC3 cells showed an increase in NO production after TRPML1 KD. The significance of the difference between the scrambled control and KD groups of each cell line was calculated using a *t* test and depicted using asterisks (\*\*\*\* =  $p \leq 0.0001$ , \*\*\* =  $p \leq 0.0005$ , \*\* =  $p \leq 0.001$ , \* =  $p \leq 0.01$ , n.s =  $p > 0.05$ ). Three independent experiments ( $n= 3$ ) were conducted in triplicates to ensure the validity of results, but only one representative example is represented in this figure.

**A****B****C****D**

**Figure 14: Increased levels of reactive oxygen species (ROS) detected in TRPML1 KD PC3 cells.** A and C) Flow cytometry analysis of ROS levels in RWPE-1 and PC3 cells, respectively as determined by H<sub>2</sub>DCFDA staining. Cells were first incubated for 48 hrs prior to staining with H<sub>2</sub>DCFDA. H<sub>2</sub>O<sub>2</sub> was added as a positive control 15 minutes before the staining procedure. For analysis purposes, cells were gated on the SSC and FSC and then back gated on H<sub>2</sub>DCFDA. Histograms were generated from the H<sub>2</sub>DCFDA gated cells and represented as H<sub>2</sub>DCFDA MFI where a rightward shift is proportional to an increase in ROS production. The non-stained control (n.s), the scrambled and KD cells are represented by a dashed line, black and red lines, respectively. B and D) Quantitative representation of the MFI values generated by the Flowing software, including the H<sub>2</sub>O<sub>2</sub> positive controls. Statistical significance was calculated using a One-way ANOVA test and shown as asterisks above each bar (\*\*\*\* = p ≤ 0.0001, \*\*\* = p ≤ 0.0005, \*\* = p ≤ 0.001, \* = p ≤ 0.01, n.s = p > 0.05). The H<sub>2</sub>DCFDA experiments were performed in triplicates, three consecutive times, but only one sample experiment is depicted here.



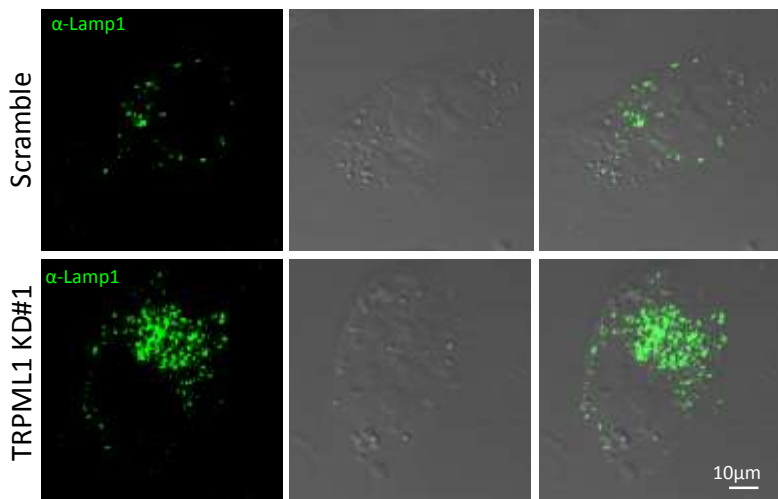
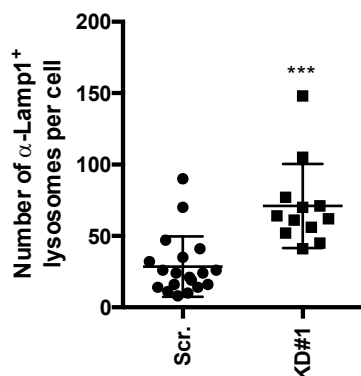
### **3.4 TRPML1 Knockdown Inhibits Autophagy Through the Activation of AKT**

ROS overproduction is often linked to accumulation of damaged mitochondria or ER stress, both of which are a consequence of abnormal autophagy. As mentioned in the Introduction, autophagy is a catabolic process heavily reliant on the proper functioning of the lysosome and in turn, the function of the lysosome is dependent on proper ion homeostasis. Hence, we hypothesized that the loss of TRPML1 may impair lysosomal functionality and therefore, hamper its ability to degrade biomolecules. Rather strikingly, the KD of TRPML1 led to an increase in lysosome biogenesis as indicated by the increase in the number of lysosomes in KD cells as compared to scrambled cells (Fig. 15A and B). We confirmed these results by quantifying the amount of the Lamp protein using western blot (Fig. 15C). These results allude to the possibility that the cell is attempting to compensate for the decreased lysosomal function by producing more lysosomes. However, the existence of such a compensatory mechanism remains to be addressed. Furthermore, to test whether the loss of TRPML1 leads to decreased autophagy and the subsequent accumulation of ROS and NO, we assessed the expression level of two commonly used autophagy markers, LC3 I/II and p62. LC3 I is converted to LC3 II during autophagosome maturation and correlates with the induction of autophagy. Our western blot results showed an increase in LC3 I and decrease in LC3 II in KD cells as compared to scrambled cells suggesting that these cells may have reduced activation of autophagy (Fig. 16A). To further confirm the absence of an active autophagic process in our TPRML1 KD cells, we quantified the protein level of p62, a protein that normally gets degraded during autophagy. As illustrated in Fig. 16A, p62 is accumulated in KD cells only.

Since the PI3K/AKT/mTOR and JNK pathway have been previously implicated in the modulation of the autophagic response, we quantified the expression of AKT and JNK in TRPML1 KD PC3 cells<sup>312</sup>. Interestingly, western blot analysis showed an increase in phosphorylated AKT with a minor increase in total AKT (Fig. 16B). We also found a decrease in phosphorylated JNK with no change in the level of total JNK (Fig. 16C). Taken together, these findings indicate a potential involvement of TRPML1 in the modulation of AKT and JNK expression, both of which have been implicated in autophagy.

**Figure 15: Increased lysosomal biogenesis is observed following knockdown of TRPML1.**

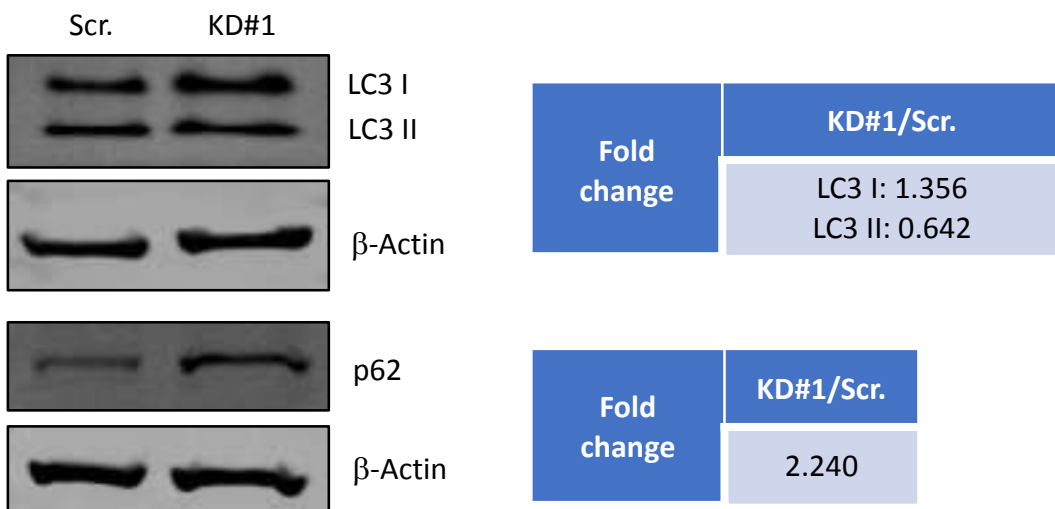
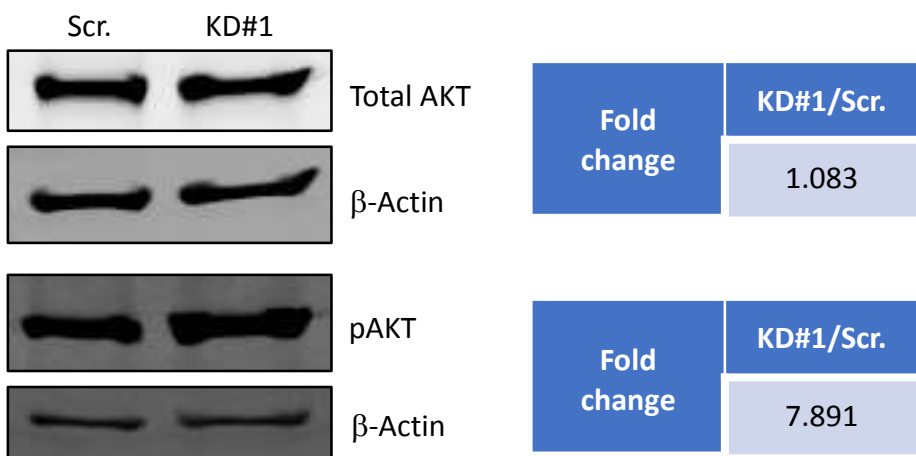
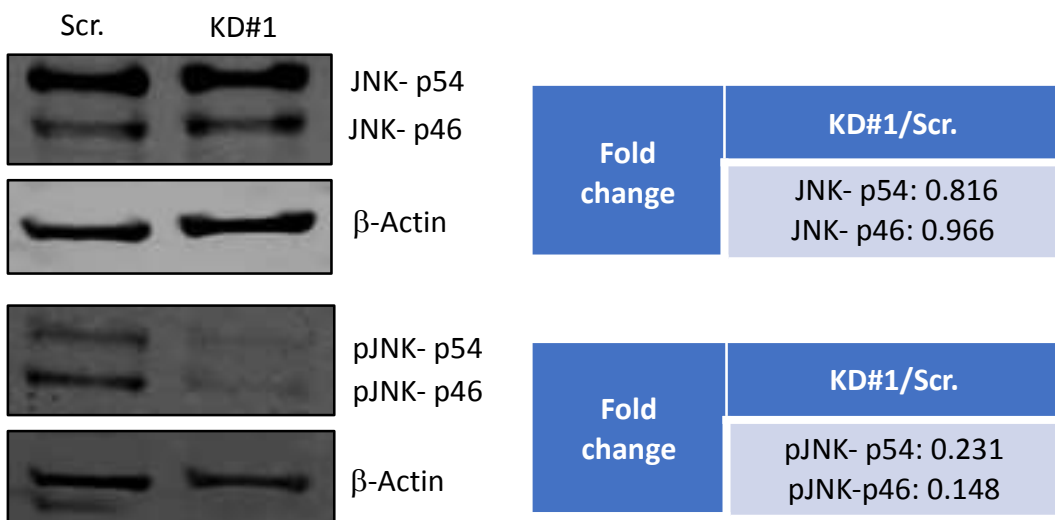
A)  $\alpha$ -Lamp1 staining of PC3 scrambled and TRPML1 KD cells analyzed by confocal microscopy and captured with the ZEN22012 software (Zeiss) then quantified with the ImageJ software. B) Confocal images were quantified and plotted as the number of lysosomes per individual cell. The number of lysosomes was assessed in 19 (n= 19) scrambled cells and 12 (n= 12) TRPML1 KD cells. As indicated by the increase in the number of lysosomes, TRPML1 KD cells appear to possess more lysosomes than their scrambled counterparts. C) The protein level of the Lamp protein in PC3 cells as quantified using western blotting and represented as the fold change (calculated as previously described in Fig. 12). The statistical significance of the confocal microscopy results was determined using a *t* test and represented with asterisks (\*\* = p ≤ 0.0001, \*\*\* = p ≤ 0.0005, \*\* = p ≤ 0.001, \* = p ≤ 0.01, n.s = p > 0.05). Confocal experiments were performed three times (n= 3) in duplicates while western blots were conducted three times (n= 3) with a single replicate per gel. However, only one representative figure is shown here.

**A****B**

Courtesy of Mengnan Xu

**C**

**Figure 16: TRPML1 modulates cell proliferation via autophagy inhibition and activation of AKT.** Western blot analysis of the protein levels of A) LC3 I/II and p62, B) total AKT and phosphorylated AKT (pAKT), C) total JNK and phosphorylated JNK (pJNK) in scrambled and TRPML1 knockdown PC3 cells. The corresponding fold changes were calculated as previously described in Fig. 12 and listed in tables adjacent to the western blot images. All western blots were performed three times ( $n= 3$ ) with one replicate per experiment.

**A****B****C**

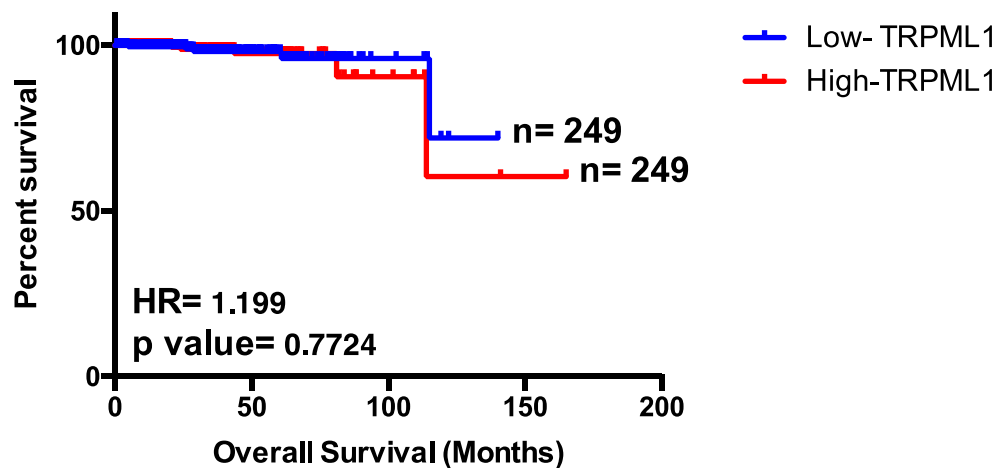
### **3.5 Analysis of TRPML1 as a Potential Biomarker for Prostate Cancer**

Despite technological advancements, the unavailability of reliable tests and biomarkers poses a major challenge for the diagnosis and management of prostate cancer. Currently, PSA is the most commonly used biomarker for PCa diagnosis; however, its use remains highly controversial with numerous studies suggesting that the implementation of PSA often leads to unnecessary biopsies and inaccurate diagnosis<sup>313</sup>. Hence, we aimed to assess the potential of TRPML1 as a biomarker for PCa using the online PCa databases available through cBioPortal. For this purpose, we accessed the TCGA provisional prostate cancer cohort. Patients were segregated into two groups based on a median cut-off: low TRPML1 (patients with mRNA expression below the calculated median value) and high TRPML1 (expression values higher than the median cut-off). Kaplan Meier survival analysis revealed that TRPML1 expression is not correlated with the overall survival (n= 498) or disease-free survival (n= 492) of PCa patients (Fig. 17A and B). Furthermore, we also investigated the possibility of an association between the expression TRPML1 and the clinical Gleason sum. Our results showed that there is no significant correlation between TRPML1 expression and the Gleason score suggesting that TRPML1 is not indicative of tumor grade or severity of the disease (Fig. 17C). In addition, gene alterations such as copy number and methylation are often detected in cancer cells and used as biomarkers to predict disease outcome or the risk of developing cancer. Given the importance of these genetic events in cancer cells, we sought to determine whether a relationship exists between TRPML1 copy number (amplification, diploid and deletion), methylation status and patient survival. As represented in Figure 18A and B, the copy number and methylation status of TRPML1 (low methylated vs. highly methylated TRPML1) does not form a significant correlation with overall patient survival.

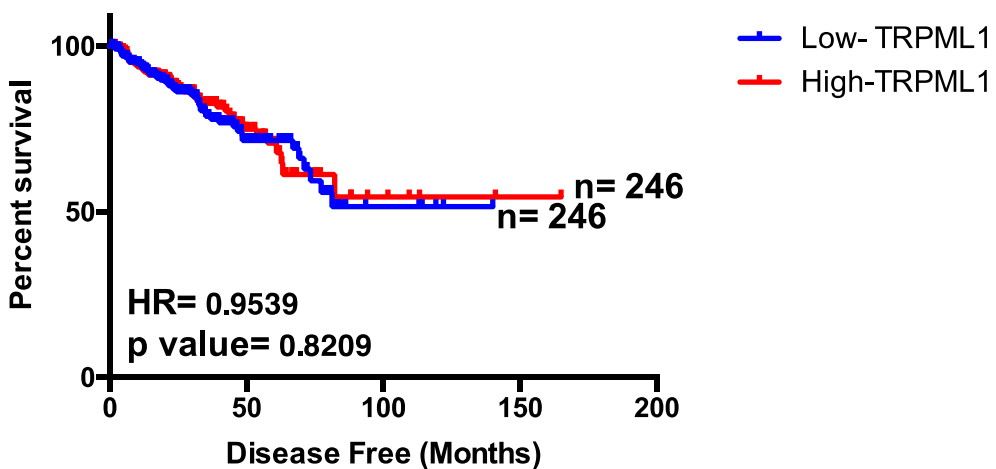
In our last attempt to establish the role of TRPML1 as a biomarker for PCa we conducted co-expression analysis between TRPML1 expression and known or emerging biomarkers. We found a statistically significant correlation between TRPML1 expression and KLK3, more commonly known as PSA, and CXCL8 (IL-8), a proinflammatory cytokine known to promote PCa cell survival (Fig. 19A and E). Our analysis also revealed that the expression of TRPML1 is not associated with other current and emerging PCa biomarkers such as PCA3, CD276 and TLR9 (Fig. 19B, C and D).

**Figure 17: Correlation analysis between TRPML1 expression and prostate cancer patient overall survival, disease-free survival and Gleason sum.** A and B) Kaplan Meier analysis of overall and disease-free survival of 498 and 492 patients, respectively from the prostate adenocarcinoma (TCGA, Provisional) cohort acquired from cBioPortal. A median cut-off for the mRNA expression level of TRPML1 was applied to divide the patients into low (n= 249 and 246) and high (n= 249 and 246) TRPML1 groups. The data was plotted as percent survival on the y axis against months of A) overall survival and B) disease-free survival along the x axis. C) Correlation analysis between the expression of TRPML1 and clinical Gleason sum in 236 patients from the prostate adenocarcinoma (TCGA, Cell 2015) dataset. Statistical significance for the survival curves was calculated as log rank p value (listed on the corresponding graphs). Pearson correlation analysis was performed to assess the strength of the relationship between TRPML1 expression and the clinical Gleason sum as shown on the representative graph in panel C.

A



B



C

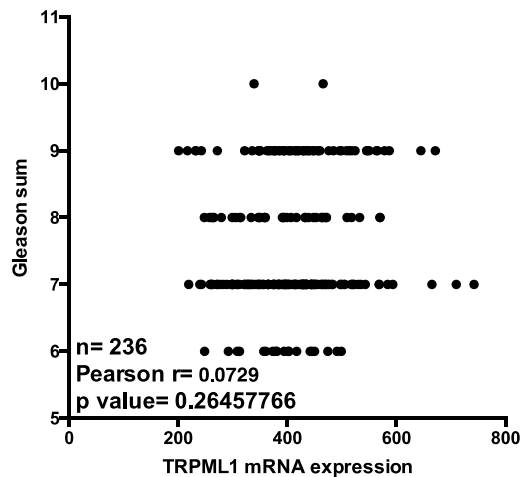
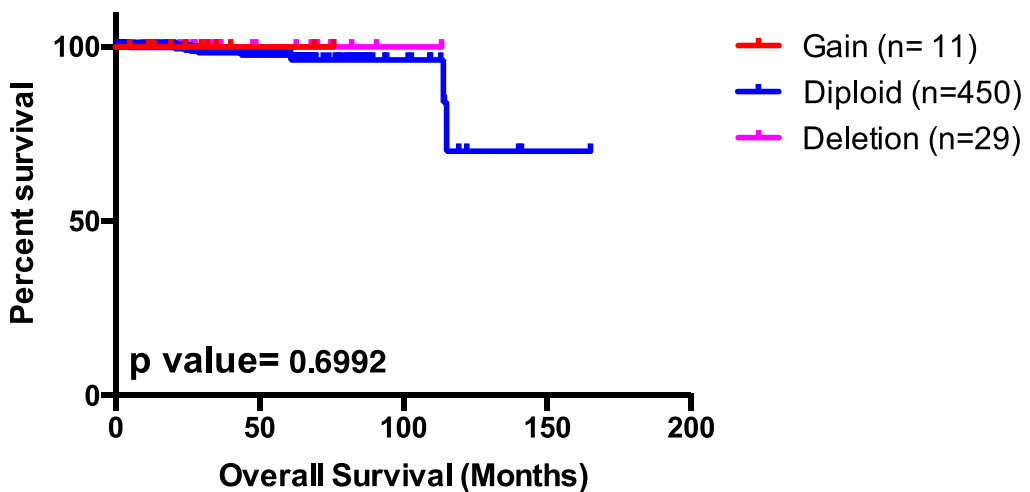


**Figure 18: Association between TRPML1 gene modifications and overall PCa patient survival.** A) Assessment of the correlation between TRPML1 gene modifications (gain, diploid and deletion) and overall survival in 490 patients from the prostate adenocarcinoma (TCGA, Provisional) cohort available on cBioPortal. Within this dataset, 11 PCa patients had a copy number change (gain), 450 possessed a diploid number of the TRPML1 gene and 29 patients were found to have deletions in the TRPML1 gene. Analysis revealed that TRPML1 gene alterations do not correlate with PCa patient survival. B) Kaplan Meier analysis of TRPML1 methylation status and overall prostate cancer patient survival showed no significant association. A median cut-off was used to segregate patients into low ( $n= 245$ ) and high ( $n= 245$ ) methylation groups. A log rank p value was used to determine the significance of the correlation between the variables.

A



B

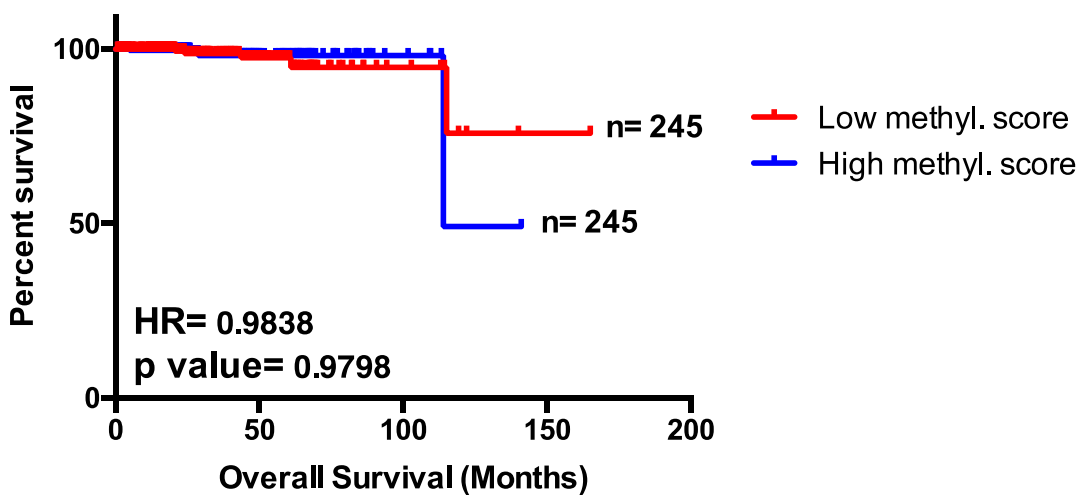
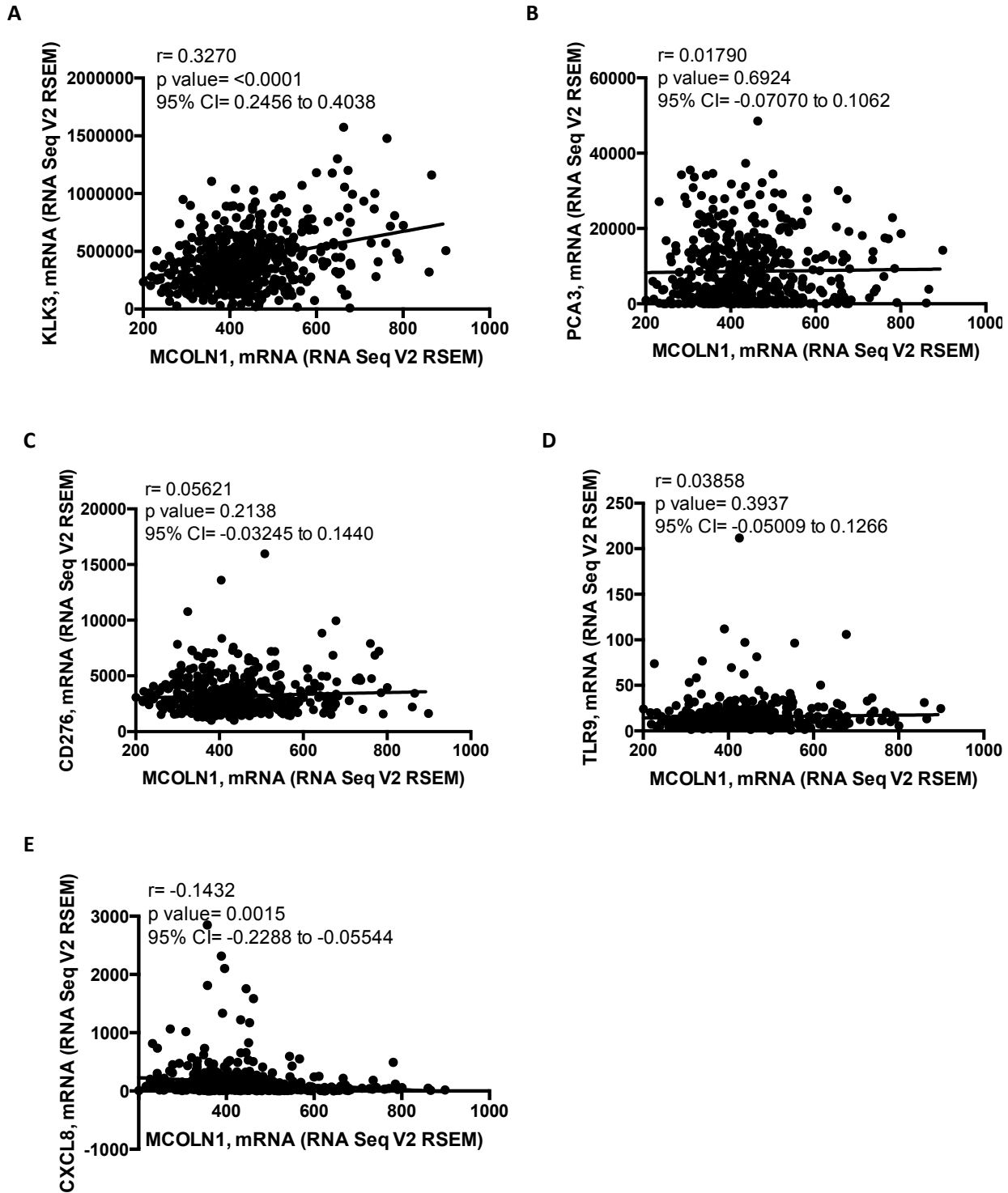


**Figure 19: TRPML1 co-expression with established and emerging PCa biomarkers. A-E**

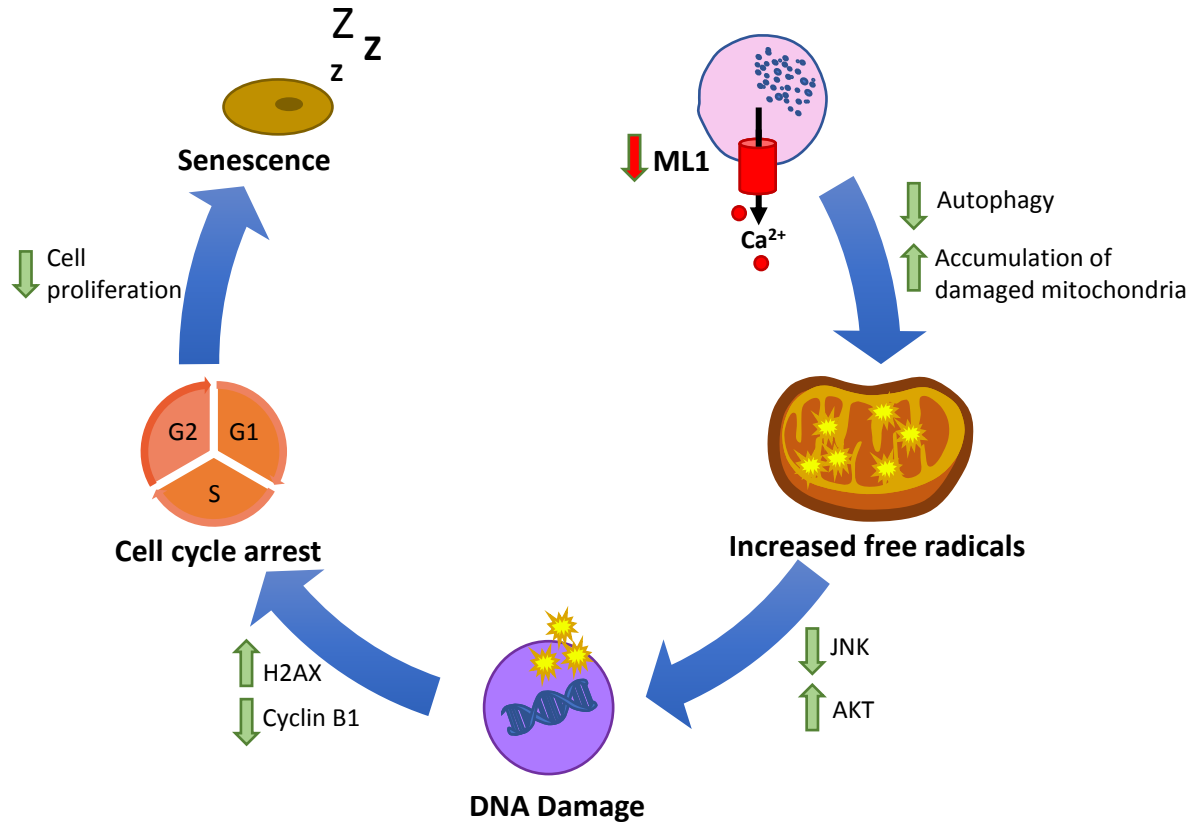
RNA Seq V2 REM gene expression data was acquired from cBioPortal (TCGA, Provisional dataset) and plotted using the GraphPad software. This dataset consisted of 499 PCa patients. The significance of the relationship between TRPML1 and the expression of other PCa biomarkers was assessed using the Pearson correlation coefficient as listed on each graph.



## CHAPTER IV: SUMMARY

To summarize the findings presented in this dissertation, the loss of TRPML1 decreases the functionality of lysosomes and their ability to degrade cellular material leading to the accumulation of damaged mitochondria and toxic material. This accumulation triggers the overproduction of ROS and NO which activate AKT. AKT and NO inhibit JNK; thus, further impairing the autophagy pathway and preventing the removal of unwanted material from the cell such as free radicals and damaged organelles, ultimately resulting in DNA damage, cell cycle arrest and the subsequent decrease in PCa cell proliferation (Fig. 20). Furthermore, we found no significant correlation between TRPML1 and overall PCa patient survival or disease-free survival. In addition, while the mRNA expression of TRPML1 did not correlate with the expression of PCA3, CD276 and TLR9, our univariate analysis revealed a positive relationship between TRPML1 expression and KLK3 (PSA) and CXCL8.

**Figure 20: Schematic representation of the proposed mechanism for the involvement of TRPML1 in mediating PCa cell proliferation.** The loss of TRPML1 hampers the efficiency of the autophagy process leading to the accumulation of unwanted cellular material. Due to decreased clearance of damaged mitochondria, misfolded proteins and other cellular waste, the cell enters a state of stress and starts overproducing ROS and NO. The free radicals damage nuclear DNA resulting in cell cycle arrest, decreased proliferation and ultimately, senescence.



## CHAPTER V: LIMITATIONS AND FUTURE DIRECTIONS

### 5.1 *In Vitro* Model

The cell lines used for the generation of data presented in this dissertation (PC3, DU145, PC-TU, PC-LC and RWPE-1) were once the gold standard for PCa research; however, these cell lines do not encompass the complexity of PCa. PC3 and DU145 are hormone insensitive and do not possess androgen receptors (AR) or PSA while the normal, RWPE-1 cells are hormone sensitive and express AR and PSA. Given that PCa is highly influenced by the presence of hormones, the use of these cell lines alone may not be representative of all prostate cancers (androgen dependent vs. independent). In addition, while data regarding the effect of sex hormones (or hormone receptors) on TRPML1 function is not yet available, the possibility of differences existing between channel activation and the presence or absence of hormones cannot be ignored. Nonetheless, hormone-sensitive PCa cell lines are commercially available (e.g. LNCaP) and should be used in future studies to determine whether TRPML1 has a similar effect on the proliferation capabilities of androgen-dependent cells. Furthermore, aside from differences in responsiveness to hormones, the doubling time varies across cell lines which can affect the significance of some results. For instance, PC3 and DU145 cells have a doubling time of approximately 34 hours while RWPE-1 cells divide once in 120 hours<sup>314</sup>. The difference in division rate could explain why we did not observe a decrease in the proliferation rate of RWPE-1 cells following TRPML1 KD. Additional experiments may investigate the role of TRPML1 in RWPE-1 cell proliferation at extended times points (e.g. more than 3 days) to establish if indeed, TRPML1 does not affect their ability to divide.

## **5.2 Specificity of ML-SI**

Another limiting factor in this study is the specificity of the ML-SI inhibitor. While research has demonstrated its ability to inhibit TRPML1, ML-SI can negatively impact the other two members of the TRPML family, TRPML2 and 3. Hence, the reduction in proliferation seen in Figs. 5 and 6 could be a manifestation of the loss of all three TRPML channels and not just TRPML1. However, our results demonstrated that TRPML1 alone (e.g. TRPML1 KD experiments) can decrease PCa cell proliferation, and as such, future studies should focus on the development of a specific TRPML1 inhibitor that could potentially be used as a treatment for cancer patients. In addition, double knockdown of TRPML1 and one of the other two members of the Mucolipin family may result in an even greater reduction in cell proliferation than TRPML1 alone.

## **5.3 Presence of TRPML1 in Newly Synthesized Lysosomes**

In the discussion section of this dissertation it was mentioned that TRPML1 knockdown PCa cells may be attempting to compensate for the lack of autophagy by inducing the synthesis of more lysosomes. These newly synthesized lysosomes were assumed to have a decreased expression of TRPML1 due to the knockdown of this channel in the host cell; however, this was not shown in the data presented in this dissertation and as such, it poses as an additional limitation. Here, we showed a decrease in calcium release from TRPML1 PCa KD cells as compared to their scrambled counterparts which points towards the idea that the lysosomes in these cells are deficient in their expression of TRPML1 since they did not respond to the TRPML1 agonist. Additional experiments such as lysosomal extraction and RT-qPCR analysis

of the lysosomal fraction should be performed to show the decreased TRPML1 expression in lysosomes following total TRPML1 knockdown.

#### **5.4 Assessment of Lysosomal Functionality**

The data presented in this dissertation showed a decrease in autophagy and alluded to the possibility of lysosomal function impairment as the causative agent. Further studies should investigate the functionality of the lysosomes to confirm the hypothesis that the downregulation of autophagy subsequent to the loss of TRPML1 is indeed due to dysfunctional lysosomes. This objective can be achieved by staining scrambled and knockdown PCa cells with the Lysotracker Red dye or Quinacrine to determine the pH of the lysosomes, a characteristic which is important for the proper functioning of the enzymes within the lysosome. Previous studies have shown that the intensity of the color of Lysotracker Red and Quinacrine is proportional to the pH inside the lysosome<sup>315</sup>. Such experiments can determine whether the lysosomes are performing at full capacity when TRPML1 is not present. Furthermore, one could speculate that the knockdown of TRPML1 would lead to an increase in lysosomal pH; thus, resulting in decreased enzyme activity and impaired degradation of unwanted material during autophagy. This decrease could be attributed to the role of TRPML1 in maintaining lysosomal pH through its activation by H<sup>+</sup>.

#### **5.5 Identification of Molecular Mechanism**

In the current study, we suggested that TRPML1 modulates PCa cell proliferation through the phosphorylation and subsequent activation of AKT. However, we have not presented data showing the effect of TRPML1 on other proteins within this pathway or other pathways that may be involved. Future studies should analyze the involvement of upstream and downstream

effectors of AKT such as PI3K, mTOR or PTEN in order to establish the exact mechanism behind the role of TRPML1 in mediating PCa cell proliferation. Other pathways involved in mediating cell proliferation such as ERK signalling should also be investigated as a potential contributor to the effects demonstrated in this dissertation. Moreover, the decrease in autophagy should be further confirmed by quantifying the protein or mRNA expression of ATGs.

## **5.6 Univariate Analysis vs. Multivariate Analysis**

Lastly, the implementation of a univariate analysis method to determine the potential of TRPML1 as a biomarker for PCa has its limitations. Many factors can affect the expression of a gene and, thus, influence results when performing a univariate analysis. For a more accurate representation of the relationship between TRPML1 expression, overall patient survival and/or expression of other biomarkers, a multivariate analysis approach should be used to account for confounding variables (e.g. age, comorbidities, life style, reason for death, etc.) that could affect the expression or activity of the ion channel in the patient cohort analyzed.

## CHAPTER VI: DISCUSSION

A recurrent theme throughout this dissertation was the emphasis on cell proliferation as a defining characteristic of cancer cells. Here, we demonstrated the effect of TRPML1 on prostate cancer cell proliferation through inhibition and specific shRNA gene knockdown. Although TRPML1 has not yet been identified as a therapeutic target for cancer, our results showed that inhibition and/or knockdown of TRPML1 can reduce PCa cell proliferation; thus, elucidating the potential for TRPML1 as an oncogene. Importantly, this dissertation shows, for the first time, the involvement of TRPML1 in cancer; however, other TRPML channels have also recently been investigated in the context of cancer progression. More specifically, a 2016 study was published by Morelli *et al.* outlining the role of TPRML2, the second member of the Mucolipin family as an important regulator of cell proliferation in glioma cells<sup>316</sup>. Similar to our data, the authors provided evidence suggesting that the loss of TPRML2 reduces glioma cell proliferation and induced apoptosis<sup>316</sup>. Interestingly, unlike the Morelli *et al.* paper, downregulation of TRPML1 did not induce apoptosis in prostate cancer cell lines. This alludes to the idea that TRPML channels may modulate cellular fate via different mechanisms.

The observed reduction in the proliferative rate of PCa cells was attributed to an accumulation of cells in the G2/M phase of the cell cycle which was confirmed by the upregulation of Cyclin B1 in TRPML1 KD cells. Due to its integral role in the cell cycle and consequently, cell division, Cyclin B1 is usually overexpressed in many cancers and often correlates with aggressive disease<sup>317-320</sup>. During the normal cell cycle, cells go through several checkpoints to ensure the integrity of their DNA prior to nuclear division in the Mitotic (M) phase. It is at these check points that cells harboring DNA damage are arrested and prevented

from proceeding to the subsequent phases of the cell cycle in order to avert aberrant cell division and the propagation of mutations. Our results indicated that the downregulation of TRPML1 resulted in increased levels of DNA damage proteins thus, explaining the enhanced accumulation of cells in the G2/M phase (Fig. 18). We also uncovered the potential source of DNA damage as the increased production of ROS and NO. In normal cell physiology, TRPML1 acts a sensor of ROS which, upon activation triggers the initiation of autophagy and lysosome biogenesis to mitigate the oxidative stress<sup>321</sup>. Hence, dysregulation in the function of TRPML1 impairs autophagy and leads to the accumulation of free radicals within the cell (Fig. 18)<sup>321</sup>. As mentioned in the introduction, accumulation of ROS is a major endogenous source of DNA damage; therefore, given our current knowledge on TRPML1 functionality as a ROS sensor and the results presented, we conclude that the knockdown of TRPML1 is likely disrupting its function as a ROS sensor thereby allowing the buildup of ROS leading to DNA damage.

Furthermore, TRPML1 is also important in mediating autophagosome-lysosome fusion, a step necessary for the degradation phase of the autophagic process<sup>289,322</sup>. Interestingly, in the current study we show an increase in lysosomal number with an accompanying decrease in autophagy following TRPML1 KD. This phenomenon can be justified by the inability of cells to undergo proper autophagy. The absence of TRPML1 from lysosomes may prevent the degradation of cytotoxic material and hence, allow for the accumulation of ROS within the cell. Notably, this suggests that the residual pool of TRPML1 channels remaining following the shRNA KD are activated by ROS, subsequently triggering the transcription of autophagy-related genes and the production of more lysosomes to sustain the increase in autophagosome formation. However, the newly synthesized lysosomes are more likely to lack TRPML1 (due to KD) which is necessary for the subsequent fusion with the autophagosome, ultimately resulting in

incomplete autophagy. Techniques such as CRISPR which can achieve complete knockout of the TRPML1 channel may explain the rationale above and determine whether residual TRPML1 levels are sustaining diminished levels of autophagy and increased lysosome biogenesis. Furthermore, due to the unavailability of a specific/suitable antibody against TRPML1, only the mRNA level of the channel was assessed.

Based on our functional analysis of TRPML1 in PCa we attempted to uncover the underlying molecular mechanism behind the effect of TPRML1 on proliferation. Our results showed an increase in total and phosphorylated AKT, a major effector of the PI3K pathway that is known to control cell proliferation and survival. Notably, Ushio-Fukai *et al.* demonstrated that ROS is an inducer of AKT activation<sup>323,324</sup>. As such, it is possible that the increase in AKT activation is likely a result of the increased presence of ROS within TRPML1 KD cells. Phosphorylation of AKT activates its downstream target mTOR, which in turn prevents the initiation of autophagy leading us to conclude that TRPML1 is potentially mediating cell proliferation through the activation of AKT. It should also be noted that during oxidative stress (e.g. presence of high levels of free radicals), AKT activation sensitizes cancer cells to oxidative apoptosis<sup>325</sup>. Although it is a widely held belief that AKT activation is often employed as an evasion mechanism for cancer cells to escape apoptosis, AKT cannot prevent ROS-induced cell death thus, triggering senescence (Fig. 17)<sup>325</sup>. In addition to the increase in AKT, we also detected a decrease in phosphorylated JNK. Previous literature has provided evidence for the existence of a cross talk between AKT and JNK suggesting that AKT can antagonize JNK signaling which in turn can reduce autophagy<sup>326,327</sup>. Moreover, several research groups have demonstrated that the overproduction of NO can disrupt JNK signaling through S-nitrosylation of cystine residues and inhibiting autophagosome formation; therefore, decreasing autophagy<sup>328-</sup>

<sup>331</sup>. Here, we have provided evidence that TRPML1 KD in PCa cells stimulates the formation of NO which provides a further explanation for the observed decrease in phosphorylated JNK and autophagy. Furthermore, S-nitrosylation negatively regulates PTEN allowing for the activation of AKT and the subsequent autophagy inhibition<sup>332,333</sup>. Therefore, it is plausible that together, TRPML1 KD- mediated activation of AKT and allowed inhibition of JNK may reduce the autophagic response.

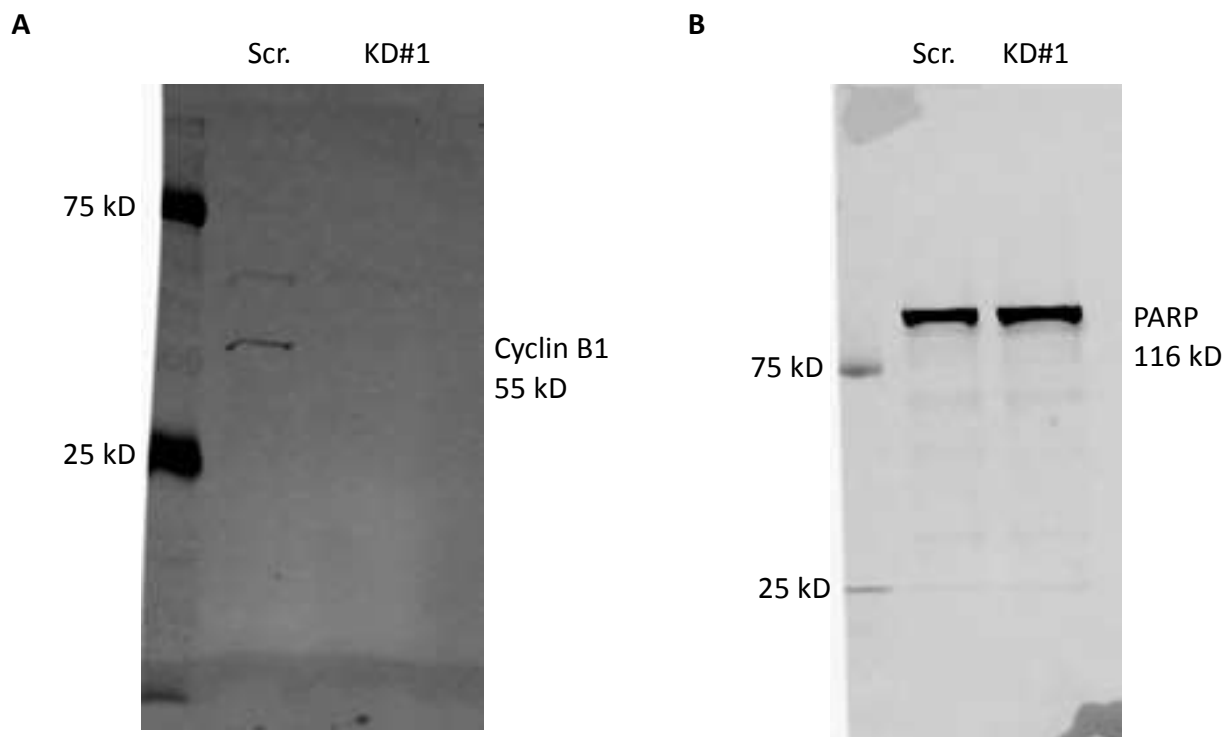
Given the mechanistic involvement of TRPML1 in regulating PCa cell proliferation, we attempted to establish TRPML1 as a potential biomarker for PCa. However, our results showed no statistically significant correlation between TRPML1 and overall survival or disease- free survival. The mRNA expression of TRPML1 was also not associated with the clinical Gleason sum, gene modifications or methylation status of TRPML1. We also investigated the expression of TRPML1 as part of the genetic signature of PCa by conducting co-expression analysis with known and emerging biomarkers. The univariate analysis performed on the presented PCa patient cohort revealed no relationship between TRPML1 mRNA expression and some biomarkers. Of note, the expression of TRPML1 did correlate with the expression of PSA and CXCL8 which may potentially serve as a gene signature for the early diagnosis of PCa in the future. In addition, the analysis of TRPML1 in conjunction with PSA for diagnostic purposes could increase the sensitivity and specificity of PSA testing and thus, lead to a more efficient diagnosis. Nonetheless, despite the apparent lack of a link with survival, whether TRPML1 protein levels are predictive of patient survival remains elusive. For instance, the protein level of members of the TRP family such as TRPML2, TRPM7 and TRPM8 have been shown as indicative of metastatic and advanced stage glioma and pancreatic cancer, respectively<sup>316,334,335</sup>. In addition, the mRNA and protein levels of TRPM8 were recently demonstrated to correlated

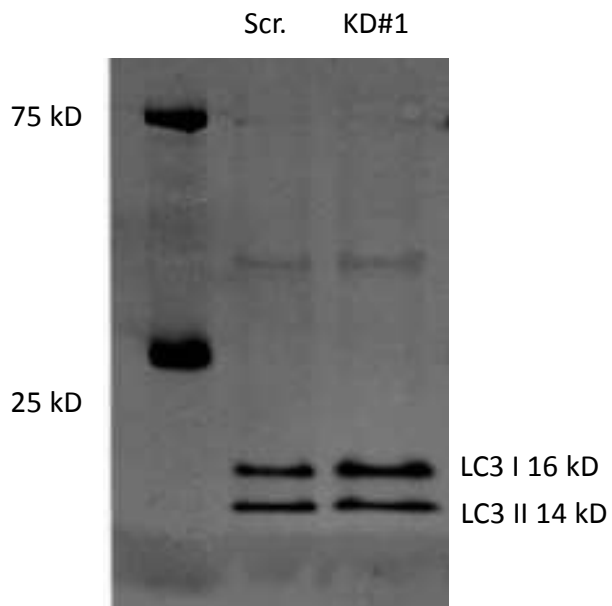
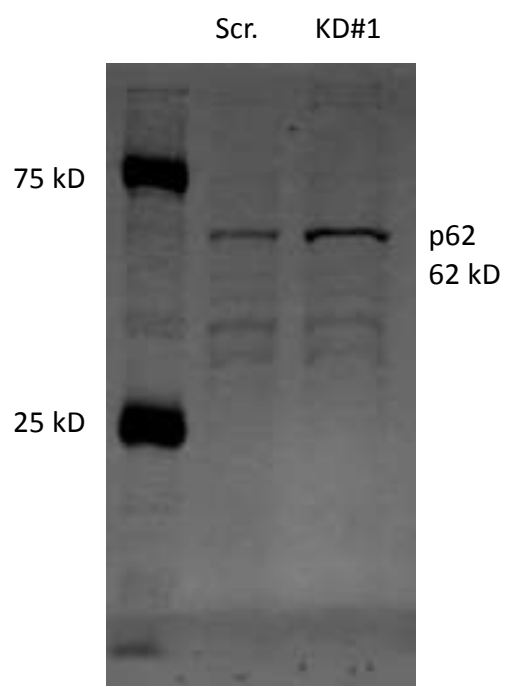
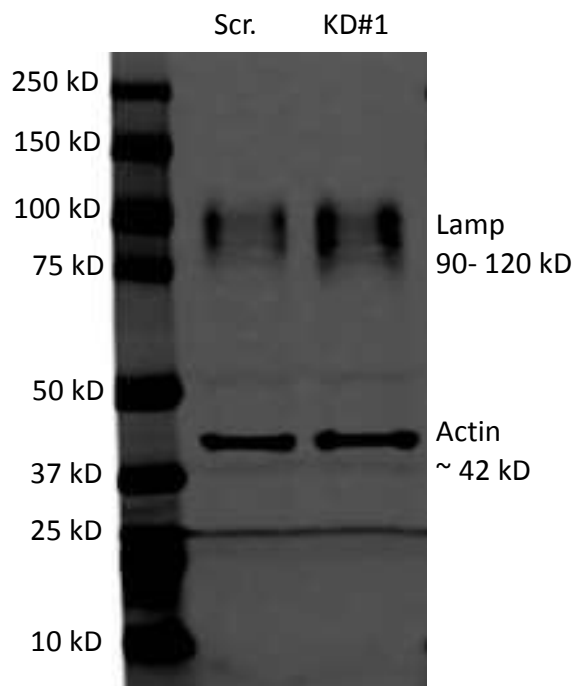
with poor overall survival in patients with osteosarcoma<sup>336</sup>. Therefore, although analysis of the mRNA level of TRPML1 did not result in a positive relationship with survival, studies investigating the protein level of this channel in PCa patients may uncover a different outcome.

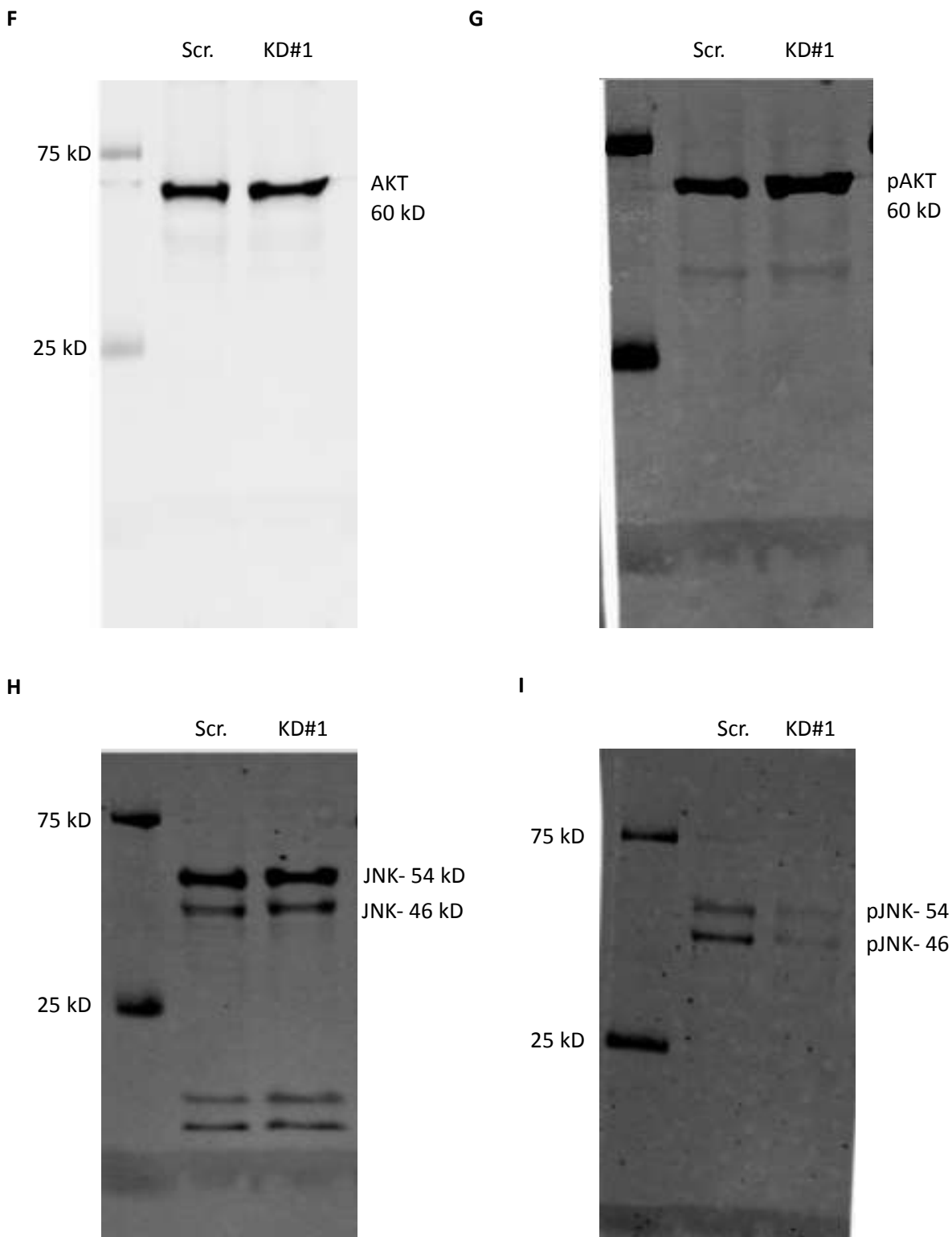
To conclude, this study provides novel evidence supporting the role of TPRML1 as a regulator of cell proliferation through the inhibition of autophagy via induction of DNA damage. This work sets the foundation for future research investigating the involvement of TPRML1 in the molecular mechanisms of cancer and its potential as an anticancer drug used alone or in combination with other DNA damage-inducing chemotherapeutics. The results presented in this dissertation highlight the importance of understanding ion channels as potential oncogenes as a means of improving current cancer treatments and more importantly, patient outcome and quality of life.

## APPENDIX A: SUPPLEMENTAL FIGURES

**Supplemental figure 1: Uncropped western blot images.** Panels A and B are the uncropped western blot images showing the protein ladder and the appropriate size of the Cyclin B1 (55 kD) and PARP (116 kD) protein bands that were used in Fig. 13 A and D, respectively. Panels C, D, E-I are the corresponding full blot images of the western images shown in Fig. 16 for proteins LC3 I/II (16 and 14 kD), p62 (62 kD), total AKT (60 kD), pAKT (60 kD), total JNK (54 and 46 kD) and pJNK (54 and 46 kD), respectively. Lastly, panel E shows the entire western blot membrane image used to show the increase in Lamp protein (90- 120 kD) in Fig. 15C.



**C****D****E**



## REFERENCES

1. Sudhakar, A. History of Cancer, Ancient and Modern Treatment Methods. *J. Cancer Sci. Ther.* **1**, 1–4 (2009).
2. Hajdu, S. I., Vadmal, M. & Tang, P. A note from history: Landmarks in history of cancer, part 7. *Cancer* **121**, 2480–2513 (2015).
3. Kottapurath Kunjumoideen MD. History of Cancer. *The SAGE Encyclopedia of Cancer and Society* 1-8 (2014).
4. Hassanpour, S. H. & Dehghani, M. Review of cancer from perspective of molecular. *J. Cancer Res. Pract.* **4**, 127–129 (2017).
5. Bujalkova, M., Straka, S. & Jureckova, A. Hippocrates' humoral pathology in nowaday's reflections. *Bratisl. Lek. Listy* **102**, 489–92 (2001).
6. Hajdu, S. I. Greco-Roman thought about cancer. *Cancer* **100**, 2048–2051 (2004).
7. Javier, R. T. & Butel, J. S. The History of Tumor Virology. *Cancer Res.* **68**, 7693–7706 (2008).
8. Olszewski, M. M. Concepts of Cancer from Antiquity to the Nineteenth Century. *Univ. Toronto Med. J.* **87**, 181–186 (2010).
9. Triolo, v. A. Nineteenth century foundations of cancer research advances in tumor pathology, nomenclature, and theories of oncogenesis. *Cancer Res.* **25**, 75–106 (1965).
10. Liedke, P. E. R. *et al.* Systemic administration of doxorubicin impairs aversively motivated memory in rats. *Pharmacol. Biochem. Behav.* **94**, 239–243 (2009).
11. Loeb, K. R. & Loeb, L. a. Significance of multiple mutations in cancer. *Carcinogenesis* **21**, 379–385 (2000).

12. Stratton, M. R., Campbell, P. J. & Futreal, P. A. The cancer genome. *Nature* **458**, 719–724 (2009).
13. De, S. & Ganesan, S. Looking beyond drivers and passengers in cancer genome sequencing data. *Ann. Oncol. Off. J. Eur. Soc. Med. Oncol.* **28**, 938–945 (2017).
14. Pesch, B. *et al.* Cigarette smoking and lung cancer-relative risk estimates for the major histological types from a pooled analysis of case-control studies. *Int. J. Cancer* **131**, 1210–1219 (2012).
15. Berwick, M. *et al.* Sun Exposure and Mortality From Melanoma. *JNCI J. Natl. Cancer Inst.* **97**, 195–199 (2005).
16. Durst, M., Gissmann, L., Ikenberg, H. & zur Hausen, H. A papillomavirus DNA from a cervical carcinoma and its prevalence in cancer biopsy samples from different geographic regions. *Proc. Natl. Acad. Sci.* **80**, 3812–3815 (1983).
17. Fallot, G., Neuveut, C. & Buendia, M.-A. Diverse roles of hepatitis B virus in liver cancer. *Curr. Opin. Virol.* **2**, 467–473 (2012).
18. Liu, X. *et al.* Cancer risk in patients with hepatitis C virus infection: a population-based study in Sweden. *Cancer Med.* **6**, 1135–1140 (2017).
19. Kim, S. S., Ruiz, V. E., Carroll, J. D. & Moss, S. F. Helicobacter pylori in the pathogenesis of gastric cancer and gastric lymphoma. *Cancer Lett.* **305**, 228–238 (2011).
20. Sharma, S., Kelly, T. K. & Jones, P. A. Epigenetics in cancer. *Carcinogenesis* **31**, 27–36 (2010).
21. Kulis, M. & Esteller, M. DNA methylation and cancer. *Adv. Genet.* **70**, 27–56 (2010).
22. Van Tongelen, A., Loriot, A. & De Smet, C. Oncogenic roles of DNA hypomethylation through the activation of cancer-germline genes. *Cancer Lett.* **396**, 130–137 (2017).

23. Ehrlich, M. DNA hypomethylation in cancer cells. *Epigenomics* **1**, 239–259 (2009).
24. Chandrasekhar, V. & Krishnamurti, C. George Papanicolaou (1883–1962): Discoverer of the Pap Smear. *J. Obstet. Gynecol. India* **68**, 232–235 (2018).
25. McGranahan, N. & Swanton, C. Clonal Heterogeneity and Tumor Evolution: Past, Present, and the Future. *Cell* **168**, 613–628 (2017).
26. Lipinski, K. A. *et al.* Cancer Evolution and the Limits of Predictability in Precision Cancer Medicine. *Trends in Cancer* **2**, 49–63 (2016).
27. Stanta, G. & Bonin, S. Overview on Clinical Relevance of Intra-Tumor Heterogeneity. *Front. Med.* **5**, 1-10 (2018).
28. Tellez-Gabriel, M., Ory, B., Lamoureux, F., Heymann, M.-F. & Heymann, D. Tumour Heterogeneity: The Key Advantages of Single-Cell Analysis. *Int. J. Mol. Sci.* **17**, 2142–2161 (2016).
29. Marusyk, A. & Polyak, K. Tumor heterogeneity: Causes and consequences. *Biochim. Biophys. Acta - Rev. Cancer* **1805**, 105–117 (2010).
30. Reya, T., Morrison, S. J., Clarke, M. F. & Weissman, I. L. Stem cells, cancer and cancer stem cells. *Nature* **414**, 105–111 (2001).
31. Nowell, P. The clonal evolution of tumor cell populations. *Science* **194**, 23–28 (1976).
32. Bintanja, R. & Selten, F. M. Future increases in Arctic precipitation linked to local evaporation and sea-ice retreat. *Nature* **509**, 479–482 (2014).
33. Burrell, R. A., McGranahan, N., Bartek, J. & Swanton, C. The causes and consequences of genetic heterogeneity in cancer evolution. *Nature* **501**, 338–345 (2013).
34. Cavallo, F., De Giovanni, C., Nanni, P., Forni, G. & Lollini, P.-L. The immune hallmarks of cancer. *Cancer Immunol. Immunother.* **60**, 319–326 (2011).

35. Hanahan, D. & Weinberg, R. A. Hallmarks of cancer: The next generation. *Cell* **144**, 646–647 (2011).
36. Rodgers, S. J., Ferguson, D. T., Mitchell, C. A. & Ooms, L. M. Regulation of PI3K effector signalling in cancer by the phosphoinositide phosphatases. *Biosci. Rep.* **37**, 1-18 (2017).
37. Vivanco, I. & Sawyers, C. L. The phosphatidylinositol 3-Kinase–AKT pathway in human cancer. *Nat. Rev. Cancer* **2**, 489–501 (2002).
38. Shaw, R. J. & Cantley, L. C. Ras, PI(3)K and mTOR signalling controls tumour cell growth. *Nature* **441**, 424–430 (2006).
39. Porta, C., Paglino, C. & Mosca, A. Targeting PI3K/Akt/mTOR Signaling in Cancer. *Front. Oncol.* **4**, 1-11 (2014).
40. Pirker, R. *et al.* Cetuximab plus chemotherapy in patients with advanced non-small-cell lung cancer (FLEX): an open-label randomised phase III trial. *Lancet* **373**, 1525–1531 (2009).
41. Manning, B. D. & Toker, A. AKT/PKB Signaling: Navigating the Network. *Cell* **169**, 381–405 (2017).
42. Mahajan, K. & Mahajan, N. P. PI3K-independent AKT activation in cancers: A treasure trove for novel therapeutics. *J. Cell. Physiol.* **227**, 3178–3184 (2012).
43. Meier, R., Alessi, D. R., Cron, P., Andjelković, M. & Hemmings, B. Mitogenic Activation, Phosphorylation, and Nuclear Translocation of Protein Kinase B. *J. Biol. Chem.* **272**, 30491–30497 (1997).
44. Memmott, R. M. & Dennis, P. A. Akt-dependent and -independent mechanisms of mTOR regulation in cancer. *Cell. Signal.* **21**, 656–664 (2009).

45. Stambolic, V. *et al.* Negative Regulation of PKB/Akt-Dependent Cell Survival by the Tumor Suppressor PTEN. *Cell* **95**, 29–39 (1998).
46. Georgescu, M.-M. PTEN Tumor Suppressor Network in PI3K-Akt Pathway Control. *Genes Cancer* **1**, 1170–1177 (2010).
47. Dillon, L. & Miller, T. Therapeutic Targeting of Cancers with Loss of PTEN Function. *Curr. Drug Targets* **15**, 65–79 (2014).
48. Naor, Z., Benard, O. & Seger, R. Activation of MAPK Cascades by G-protein-coupled Receptors: The Case of Gonadotropin-releasing Hormone Receptor. *Trends Endocrinol. Metab.* **11**, 91–99 (2000).
49. Son, Y., Kim, S., Chung, H.-T. & Pae, H.-O. Reactive Oxygen Species in the Activation of MAP Kinases. *Methods Enzymol* **528**, 27–48 (2013).
50. Han, M. S., Barrett, T., Brehm, M. A. & Davis, R. J. Inflammation Mediated by JNK in Myeloid Cells Promotes the Development of Hepatitis and Hepatocellular Carcinoma. *Cell Rep.* **15**, 19–26 (2016).
51. Ichijo, H. Induction of Apoptosis by ASK1, a Mammalian MAPKKK That Activates SAPK/JNK and p38 Signaling Pathways. *Science* **275**, 90–94 (1997).
52. Dérijard, B. *et al.* JNK1: A protein kinase stimulated by UV light and Ha-Ras that binds and phosphorylates the c-Jun activation domain. *Cell* **76**, 1025–1037 (1994).
53. Heasley, L. E. & Han, S. JNK regulation of oncogenesis. *Mol. Cells* **21**, 167–73 (2006).
54. Ashenden, M. *et al.* An In Vivo Functional Screen Identifies JNK Signaling As a Modulator of Chemotherapeutic Response in Breast Cancer. *Mol. Cancer Ther.* **16**, 1967–1978 (2017).

55. Seino, M. *et al.* Time-staggered inhibition of JNK effectively sensitizes chemoresistant ovarian cancer cells to cisplatin and paclitaxel. *Oncol. Rep.* **35**, 593–601 (2016).
56. Potapova, O. *et al.* c-Jun N-terminal Kinase Is Essential for Growth of Human T98G Glioblastoma Cells. *J. Biol. Chem.* **275**, 24767–24775 (2000).
57. Joo, S. S. & Yoo, Y.-M. Melatonin induces apoptotic death in LNCaP cells via p38 and JNK pathways: therapeutic implications for prostate cancer. *J. Pineal Res.* **47**, 8–14 (2009).
58. Sánchez, A. M. *et al.* Apoptosis induced by capsaicin in prostate PC-3 cells involves ceramide accumulation, neutral sphingomyelinase, and JNK activation. *Apoptosis* **12**, 2013–2024 (2007).
59. Kwon, G. T. *et al.* Isoliquiritigenin inhibits migration and invasion of prostate cancer cells: possible mediation by decreased JNK/AP-1 signaling. *J. Nutr. Biochem.* **20**, 663–676 (2009).
60. Tournier, C. The 2 Faces of JNK Signaling in Cancer. *Genes Cancer* **4**, 397–400 (2013).
61. Abe, M. K. *et al.* ERK8, a New Member of the Mitogen-activated Protein Kinase Family. *J. Biol. Chem.* **277**, 16733–16743 (2002).
62. Wortzel, I. & Seger, R. The ERK Cascade: Distinct Functions within Various Subcellular Organelles. *Genes Cancer* **2**, 195–209 (2011).
63. Yao, Z. & Seger, R. The ERK signaling cascade-Views from different subcellular compartments. *BioFactors* **35**, 407–416 (2009).
64. McCubrey, J. A. *et al.* Roles of the Raf/MEK/ERK pathway in cell growth, malignant transformation and drug resistance. *Biochim. Biophys. Acta - Mol. Cell Res.* **1773**, 1263–1284 (2007).

65. Ramos, J. W. The regulation of extracellular signal-regulated kinase (ERK) in mammalian cells. *Int. J. Biochem. Cell Biol.* **40**, 2707–2719 (2008).
66. Wellbrock, C., Karasarides, M. & Marais, R. The RAF proteins take centre stage. *Nat. Rev. Mol. Cell Biol.* **5**, 875–885 (2004).
67. Ryan, M. B., Der, C. J., Wang-Gillam, A. & Cox, A. D. Targeting RAS -mutant Cancers: Is ERK the Key? *Trends in Cancer* **1**, 183–198 (2015).
68. Eskelinen, E.-L. & Saftig, P. Autophagy: a lysosomal degradation pathway with a central role in health and disease. *Biochim. Biophys. Acta* **1793**, 664–673 (2009).
69. Klionsky, D. J. Autophagy: from phenomenology to molecular understanding in less than a decade. *Nat. Rev. Mol. Cell Biol.* **8**, 931–937 (2007).
70. Singh, S. S. *et al.* Dual role of autophagy in hallmarks of cancer. *Oncogene* **37**, 1142–1158 (2018).
71. Thorburn, A. Autophagy and Its Effects: Making Sense of Double-Edged Swords. *PLoS Biol.* **12**, 1-4 (2014).
72. Hippert, M. M., O'Toole, P. S. & Thorburn, A. Autophagy in cancer: Good, bad, or both? *Cancer Research* **66**, 9349-9351 (2006).
73. Meijer, A. J., Lorin, S., Blommaart, E. F. & Codogno, P. Regulation of autophagy by amino acids and MTOR-dependent signal transduction. *Amino Acids* **47**, 2037–2063 (2015).
74. Liou, W., Geuze, H. J., Geelen, M. J. H. & Slot, J. W. The Autophagic and Endocytic Pathways Converge at the Nascent Autophagic Vacuoles. *J. Cell Biol.* **136**, 61–70 (1997).
75. Lawrence, B. P. & Brown, W. J. Autophagic vacuoles rapidly fuse with pre-existing

- lysosomes in cultured hepatocytes. *J. Cell Sci.* **102**, 515–26 (1992).
76. Ohsumi, Y. Molecular dissection of autophagy: two ubiquitin-like systems. *Nat. Rev. Mol. Cell Biol.* **2**, 211–216 (2001).
77. Lee, Y.-K. & Lee, J.-A. Role of the mammalian ATG8/LC3 family in autophagy: differential and compensatory roles in the spatiotemporal regulation of autophagy. *BMB Rep.* **49**, 424–430 (2016).
78. Tanida, I., Ueno, T. & Kominami, E. LC3 and Autophagy. in *Methods in Molecular Biology* **445**, 77–88 (2008).
79. Bjørkøy, G. *et al.* Chapter 12 Monitoring Autophagic Degradation of p62/SQSTM1. in *Methods* **452**, 181–197 (2009).
80. Lippai, M. & Low, P. The role of the selective adaptor p62 and ubiquitin-like proteins in autophagy. *Biomed Res. Int.* **2014**, 1-11 (2014).
81. Sena, L. A. & Chandel, N. S. Physiological roles of mitochondrial reactive oxygen species. *Molecular Cell* **48**, 158-167 (2012).
82. Kotiadis, V. N., Duchen, M. R. & Osellame, L. D. Mitochondrial quality control and communications with the nucleus are important in maintaining mitochondrial function and cell health. *Biochimica et Biophysica Acta - General Subjects* **1840**, 1254-1265 (2014).
83. De Sá Junior, P. L. *et al.* The Roles of ROS in Cancer Heterogeneity and Therapy. *Oxidative Medicine and Cellular Longevity* **2017**, 1-12 (2017).
84. Liou, M.-Y. & Storz, P. Reactive oxygen species in cancer. *Free Radic Res.* **44**, 479-496 (2010).
85. Fleury, C., Mignotte, B. & Vayssi  re, J.-L. Mitochondrial reactive oxygen species in cell

- death signaling. *Biochimie* **84**, 131–141 (2002).
86. Chio, I. I. C. & Tuveson, D. A. ROS in Cancer: The Burning Question. *Trends Mol. Med.* **23**, 411–429 (2017).
87. Bolisetty, S. & Jaimes, E. Mitochondria and Reactive Oxygen Species: Physiology and Pathophysiology. *Int. J. Mol. Sci.* **14**, 6306–6344 (2013).
88. Di Meo, S., Reed, T. T., Venditti, P. & Victor, V. M. Role of ROS and RNS Sources in Physiological and Pathological Conditions. *Oxid. Med. Cell. Longev.* **2016**, 1–44 (2016).
89. Murphy, M. P. How mitochondria produce reactive oxygen species. *Biochem. J.* **417**, 1–13 (2009).
90. Yakes, F. M. & Van Houten, B. Mitochondrial DNA damage is more extensive and persists longer than nuclear DNA damage in human cells following oxidative stress. *Proc. Natl. Acad. Sci.* **94**, 514–519 (1997).
91. Zorov, D. B., Juhaszova, M. & Sollott, S. J. Mitochondrial Reactive Oxygen Species (ROS) and ROS-Induced ROS Release. *Physiol. Rev.* **94**, 909–950 (2014).
92. Luiking, Y. C., Engelen, M. P. & Deutz, N. E. Regulation of nitric oxide production in health and disease. *Curr. Opin. Clin. Nutr. Metab. Care* **13**, 97–104 (2010).
93. Epstein, F. H., Moncada, S. & Higgs, A. The L-Arginine-Nitric Oxide Pathway. *N. Engl. J. Med.* **329**, 2002–2012 (1993).
94. Zweier, J. L., Wang, P., Samoilov, A. & Kuppusamy, P. Enzyme-independent formation of nitric oxide in biological tissues. *Nat. Med.* **1**, 804–809 (1995).
95. Burke, A. J., Sullivan, F. J., Giles, F. J. & Glynn, S. A. The yin and yang of nitric oxide in cancer progression. *Carcinogenesis* **34**, 503–512 (2013).

96. Vahora, H., Khan, M. A., Alalami, U. & Hussain, A. The Potential Role of Nitric Oxide in Halting Cancer Progression Through Chemoprevention. *J. Cancer Prev.* **21**, 1–12 (2016).
97. Gallo, O. *et al.* Role of nitric oxide in angiogenesis and tumor progression in head and neck cancer. *J. Natl. Cancer Inst.* **90**, 587–96 (1998).
98. Huerta-Yepez, S. *et al.* Contribution of either YY1 or BclXL-induced inhibition by the NO-donor DETANONOate in the reversal of drug resistance, both in vitro and in vivo. YY1 and BclXL are overexpressed in prostate cancer. *Nitric Oxide* **29**, 17–24 (2013).
99. Hakem, R. DNA-damage repair; the good, the bad, and the ugly. *EMBO J.* **27**, 589–605 (2008).
100. Friedberg, E. C. DNA damage and repair. *Nature* **421**, 436–440 (2003).
101. Menck, C. F. & Munford, V. DNA repair diseases: what do they tell us about cancer and aging? *Genet. Mol. Biol.* **37**, 220–233 (2014).
102. Krejci, L., Altmannova, V., Spirek, M. & Zhao, X. Homologous recombination and its regulation. *Nucleic Acids Res.* **40**, 5795–5818 (2012).
103. Sung, P., Krejci, L., Van Komen, S. & Sehorn, M. G. Rad51 Recombinase and Recombination Mediators. *J. Biol. Chem.* **278**, 42729–42732 (2003).
104. Baumann, P. & West, S. C. Role of the human RAD51 protein in homologous recombination and double-stranded-break repair. *Trends Biochem. Sci.* **23**, 247–251 (1998).
105. Bryant, H. E. *et al.* Specific killing of BRCA2-deficient tumours with inhibitors of poly(ADP-ribose) polymerase. *Nature* **434**, 913–917 (2005).
106. Ko, H. L. & Ren, E. C. Functional Aspects of PARP1 in DNA Repair and Transcription. *Biomolecules* **2**, 524–548 (2012).

107. Jagtap, P. & Szabó, C. Poly(ADP-ribose) polymerase and the therapeutic effects of its inhibitors. *Nat. Rev. Drug Discov.* **4**, 421–440 (2005).
108. Rouleau, M., Patel, A., Hendzel, M. J., Kaufmann, S. H. & Poirier, G. G. PARP inhibition: PARP1 and beyond. *Nat. Rev. Cancer* **10**, 293–301 (2010).
109. Li, G.-M. Mechanisms and functions of DNA mismatch repair. *Cell Res.* **18**, 85–98 (2008).
110. Modrich, P. & Lahue, R. Mismatch Repair in Replication Fidelity, Genetic Recombination, and Cancer Biology. *Annu. Rev. Biochem.* **65**, 101–133 (1996).
111. Genschel, J., Bazemore, L. R. & Modrich, P. Human Exonuclease I Is Required for 5' and 3' Mismatch Repair. *J. Biol. Chem.* **277**, 13302–13311 (2002).
112. Wei, K. Inactivation of Exonuclease 1 in mice results in DNA mismatch repair defects, increased cancer susceptibility, and male and female sterility. *Genes Dev.* **17**, 603–614 (2003).
113. Fukui, K. DNA Mismatch Repair in Eukaryotes and Bacteria. *J. Nucleic Acids* **2010**, 1–16 (2010).
114. Reenan, R. A. & Kolodner, R. D. Isolation and characterization of two *Saccharomyces cerevisiae* genes encoding homologs of the bacterial HexA and MutS mismatch repair proteins. *Genetics* **132**, 963–73 (1992).
115. Scharer, O. D. Nucleotide Excision Repair in Eukaryotes. *Cold Spring Harb. Perspect. Biol.* **5**, 1-19 (2013).
116. de Laat, W. L., Jaspers, N. G. J. & Hoeijmakers, J. H. J. Molecular mechanism of nucleotide excision repair. *Genes Dev.* **13**, 768–785 (1999).
117. Sugasawa, K. A multistep damage recognition mechanism for global genomic nucleotide

- excision repair. *Genes Dev.* **15**, 507–521 (2001).
118. Mu, D. *et al.* Reconstitution of Human DNA Repair Excision Nuclease in a Highly Defined System. *J. Biol. Chem.* **270**, 2415–2418 (1995).
119. Fousteri, M. & Mullenders, L. H. Transcription-coupled nucleotide excision repair in mammalian cells: molecular mechanisms and biological effects. *Cell Res.* **18**, 73–84 (2008).
120. Noll, D. M., Mason, T. M. & Miller, P. S. Formation and Repair of Interstrand Cross-Links in DNA. *Chem. Rev.* **106**, 277–301 (2006).
121. Deans, A. J. & West, S. C. DNA interstrand crosslink repair and cancer. *Nat. Rev. Cancer* **11**, 467–480 (2011).
122. Sarkar, S., Davies, A. A., Ulrich, H. D. & McHugh, P. J. DNA interstrand crosslink repair during G1 involves nucleotide excision repair and DNA polymerase  $\zeta$ . *EMBO J.* **25**, 1285–1294 (2006).
123. Xie, S.-H. *et al.* DNA damage and oxidative stress in human liver cell L-02 caused by surface water extracts during drinking water treatment in a waterworks in China. *Environ. Mol. Mutagen.* **51**, 229–35 (2010).
124. De Silva, I. U., McHugh, P. J., Clingen, P. H. & Hartley, J. A. Defining the Roles of Nucleotide Excision Repair and Recombination in the Repair of DNA Interstrand Cross-Links in Mammalian Cells. *Mol. Cell. Biol.* **20**, 7980–7990 (2000).
125. Hashimoto, S., Anai, H. & Hanada, K. Mechanisms of interstrand DNA crosslink repair and human disorders. *Genes Environ.* **38**, 1-8 (2016).
126. Lieber, M. R. The Mechanism of Double-Strand DNA Break Repair by the

- Nonhomologous DNA End-Joining Pathway. *Annu. Rev. Biochem.* **79**, 181–211 (2010).
127. Sharma, V. *et al.* Oxidative stress at low levels can induce clustered DNA lesions leading to NHEJ mediated mutations. *Oncotarget* **7**, 25377–25390 (2016).
128. Calderwood, S. K. A critical role for topoisomerase IIb and DNA double strand breaks in transcription. *Transcription* **7**, 75–83 (2016).
129. Pastwa, E. & Malinowski, M. Non-Homologous DNA End Joining in Anticancer Therapy. *Curr. Cancer Drug Targets* **7**, 243–250 (2007).
130. Elmore, S. Apoptosis: A Review of Programmed Cell Death. *Toxicol. Pathol.* **35**, 495–516 (2007).
131. Fulda, S. & Debatin, K.-M. Extrinsic versus intrinsic apoptosis pathways in anticancer chemotherapy. *Oncogene* **25**, 4798–4811 (2006).
132. Hengartner, M. O. The biochemistry of apoptosis. *Nature* **407**, 770–776 (2000).
133. Saelens, X. *et al.* Toxic proteins released from mitochondria in cell death. *Oncogene* **23**, 2861–2874 (2004).
134. Jin, Z. & El-Deiry, W. S. Overview of cell death signaling pathways. *Cancer Biol. Ther.* **4**, 147–171 (2005).
135. Papaliagkas, V., Anogianaki, A., Anogianakis, G. & Ilonidis, G. The proteins and the mechanisms of apoptosis: a mini-review of the fundamentals. *Hippokratia* **11**, 108–113 (2007).
136. Tsujimoto, Y. Role of Bcl-2 family proteins in apoptosis: apoptosomes or mitochondria? *Genes to Cells* **3**, 697–707 (1998).
137. Hardwick, J. M. & Soane, L. Multiple Functions of BCL-2 Family Proteins. *Cold Spring Harb. Perspect. Biol.* **5**, 1-22 (2013).

138. Cory, S. & Adams, J. M. The Bcl2 family: regulators of the cellular life-or-death switch. *Nat. Rev. Cancer* **2**, 647–656 (2002).
139. Walczak, H. & Krammer, P. H. The CD95 (APO-1/Fas) and the TRAIL (APO-2L) Apoptosis Systems. *Exp. Cell Res.* **256**, 58–66 (2000).
140. Aaron, L., Franco, O. E. & Hayward, S. W. Review of Prostate Anatomy and Embryology and the Etiology of Benign Prostatic Hyperplasia. *Urol. Clin. North Am.* **43**, 279–288 (2016).
141. Radmayr, C. *et al.* 5-alpha-reductase and the development of the human prostate. *Indian J. Urol.* **24**, 309-312 (2008).
142. Bhavsar, A. & Verma, S. Anatomic Imaging of the Prostate. *Biomed Res. Int.* **2014**, 1–9 (2014).
143. McNeal, J. E. The zonal anatomy of the prostate. *Prostate* **2**, 35–49 (1981).
144. McNeal, J. E., Redwine, E. A., Freiha, F. S. & Stamey, T. A. Zonal Distribution of Prostatic Adenocarcinoma. *Am. J. Surg. Pathol.* **12**, 897–906 (1988).
145. Cohen, R. J. *et al.* Central Zone Carcinoma of the Prostate Gland: A Distinct Tumor Type With Poor Prognostic Features. *J. Urol.* **179**, 1762–1767 (2008).
146. Fair, W. R. & Cordonnier, J. J. The ph of Prostatic Fluid: A Reappraisal and Therapeutic Implications. *J. Urol.* **120**, 695–698 (1978).
147. Stenman, U.-H., Leinonen, J., Zhang, W.-M. & Finne, P. Prostate-specific antigen. *Semin. Cancer Biol.* **9**, 83–93 (1999).
148. Mattsson, J. M. *et al.* Proteolytic Activity of Prostate-Specific Antigen (PSA) towards Protein Substrates and Effect of Peptides Stimulating PSA Activity. *PLoS One* **9**, 1-12 (2014).

149. Alwaal, A., Breyer, B. N. & Lue, T. F. Normal male sexual function: emphasis on orgasm and ejaculation. *Fertil. Steril.* **104**, 1051–1060 (2015).
150. Costello, L. C. & Franklin, R. B. Prostatic fluid electrolyte composition for the screening of prostate cancer: a potential solution to a major problem. *Prostate Cancer Prostatic Dis.* **12**, 17–24 (2009).
151. Verze, P., Cai, T. & Lorenzetti, S. The role of the prostate in male fertility, health and disease. *Nat. Rev. Urol.* **13**, 379–386 (2016).
152. Prostate Cancer Statistics. 1 (2017). Available at: <http://www.cancer.ca/en/cancer-information/cancer-type/prostate/statistics/?region=sk>. (Accessed: 5th April 2018)
153. Bashir, M. N. Epidemiology of Prostate Cancer. *Asian Pacific J. Cancer Prev.* **16**, 5137–5141 (2015).
154. Zhou, C. K. *et al.* Prostate cancer incidence in 43 populations worldwide: An analysis of time trends overall and by age group. *Int. J. Cancer* **138**, 1388–1400 (2016).
155. Hassanipour-Azgomi, S. *et al.* Incidence and mortality of prostate cancer and their relationship with the Human Development Index worldwide. *Prostate Int.* **4**, 118–124 (2016).
156. Torre, L. A. *et al.* Global cancer statistics, 2012. *CA. Cancer J. Clin.* **65**, 87–108 (2015).
157. Neupane, S., Bray, F. & Auvine, A. National economic and development indicators and international variation in prostate cancer incidence and mortality: an ecological analysis. *World J. Urol.* **35**, 851–858 (2017).
158. Gaudreau, P.-O., Saad, F., Stagg, J. & Soulieres, D. The Present and Future of Biomarkers in Prostate Cancer: Proteomics, Genomics, and Immunology Advancements. *Biomark. Cancer* **8**, 15-33 (2016).

159. Litwin, M. S. & Tan, H.-J. The Diagnosis and Treatment of Prostate Cancer. *JAMA* **317**, 2532 (2017).
160. PDQ Adult Treatment Editorial Board. Prostate Cancer Treatment (PDQ®): Health Professional Version. *PDQ Cancer Information Summaries* (2018). Available from: <https://www.ncbi.nlm.nih.gov/books/NBK65915/>. (Accessed: 20th July 2018).
161. Lilja, H. *et al.* Prostate-specific antigen in serum occurs predominantly in complex with alpha 1-antichymotrypsin. *Clin. Chem.* **37**, 1618–25 (1991).
162. Carter, H. B. Prostate Cancers in Men with Low PSA Levels — Must We Find Them? *N. Engl. J. Med.* **350**, 2292–2294 (2004).
163. Moon, T. D., Neal, D. E. & Clejan, S. Prostate specific antigen and prostatitis II. PSA production and release kinetics in vitro. *Prostate* **20**, 113–116 (1992).
164. Adhyam, M. & Gupta, A. K. A Review on the Clinical Utility of PSA in Cancer Prostate. *Indian Journal of Surgical Oncology* **3**, 120–129 (2012).
165. Vickers, A. J. *et al.* Prostate specific antigen concentration at age 60 and death or metastasis from prostate cancer: case-control study. *BMJ* **341**, 4521–4590 (2010).
166. Singer, E. A. & DiPaola, R. S. Our shifting understanding of factors influencing prostate-specific antigen. *Journal of the National Cancer Institute* **105**, 1264–1265 (2013).
167. Henry, N. L. & Hayes, D. F. Cancer biomarkers. *Molecular Oncology* **6**, 140–146 (2012).
168. Lord, S., Lee, C. & Simes, R. J. The role of prognostic and predictive markers in cancer. *Cancer Forum* **32**, 1-4 (2008).
169. Catalona, W. J. *et al.* Measurement of prostate-specific antigen in serum as a screening test for prostate cancer. *N. Engl. J. Med.* **324**, 1156–61 (1991).
170. Gretzer, M. B. & Partin, A. W. PSA levels and the probability of prostate cancer on

- biopsy. *Eur. Urol. Suppl.* **1**, 21–27 (2002).
171. Catalona, W. J. *et al.* Comparison of percent free PSA, PSA density, and age-specific PSA cutoffs for prostate cancer detection and staging. *Urology* **56**, 255–260 (2000).
172. Benson, M. C., Whang, I. S., Olsson, C. A., McMahon, D. J. & Cooner, W. H. The use of prostate specific antigen density to enhance the predictive value of intermediate levels of serum prostate specific antigen. *J. Urol.* **147**, 817–21 (1992).
173. Ferro, M. *et al.* Prostate Health Index (Phi) and Prostate Cancer Antigen 3 (PCA3) Significantly Improve Prostate Cancer Detection at Initial Biopsy in a Total PSA Range of 2-10 ng/ml. *PLoS One* **8**, 1-7 (2013).
174. Blanchet, J., Stephan, C., Vincendeau, S., Houlgatte, A. & Semjonow, A. [-2]proPSA and prostate health index (PHI) improve detection of prostate cancer at initial and repeated biopsies in young men ( $\leq$  60 year old) preferentially detecting clinically significant cancer. *Biochim. Clin.* **37**, 158-174 (2013).
175. Lazzeri, M. *et al.* Clinical performance of serum prostate-specific antigen isoform [-2]proPSA (p2PSA) and its derivatives, %p2PSA and the prostate health index (PHI), in men with a family history of prostate cancer: Results from a multicentre European study, the PROMEtheuS . *BJU Int.* **112**, 313–321 (2013).
176. Punnen, S. *et al.* The 4Kscore Predicts the Grade and Stage of Prostate Cancer in the Radical Prostatectomy Specimen: Results from a Multi-institutional Prospective Trial. *Eur. Urol. Focus* **3**, 94–99 (2017).
177. Punnen, S., Pavan, N. & Parekh, D. J. Finding the Wolf in Sheep's Clothing: The 4Kscore Is a Novel Blood Test That Can Accurately Identify the Risk of Aggressive Prostate

- Cancer. Rev. Urol. **17**, 3–13 (2015).
178. Vickers, A. J. *et al.* A panel of kallikrein marker predicts prostate cancer in a large, population-based cohort followed for 15 years without screening. *Cancer Epidemiol. Biomarkers Prev.* **20**, 255–261 (2011).
179. Crawford, E. D. *et al.* Diagnostic performance of PCA3 to detect prostate cancer in men with increased prostate specific antigen: A prospective study of 1,962 cases. *J. Urol.* **188**, 1726–1731 (2012).
180. Durand, X., Moutereau, S., Xylinas, E. & De La Taille, A. Progensa<sup>TM</sup> PCA3 test for prostate cancer. *Expert Rev. Mol. Diagn.* **11**, 137–144 (2011).
181. Wei, W., Leng, J., Shao, H. & Wang, W. High PCA3 scores in urine correlate with poor-prognosis factors in prostate cancer patients. *Int. J. Clin. Exp. Med.* **8**, 16606–16612 (2015).
182. Roobol, M. J. *et al.* Performance of prostate cancer antigen 3 (PCA3) and prostate-specific antigen in prescreened men: Reproducibility and detection characteristics for prostate cancer patients with high PCA3 scores ( $\geq 100$ ). *Eur. Urol.* **58**, 893–899 (2010).
183. McDunn, J., Stirdvant, S., Ford, L. & Wolfert, R. Metabolomics and its application to the development of clinical laboratory tests for prostate cancer. *J. Int. Fed. Clin. Chem. Lab. Med.* **26**, 92–104 (2015).
184. Khan, A. P. *et al.* The Role of Sarcosine Metabolism in Prostate Cancer Progression. *Neoplasia* **15**, 491–501 (2013).
185. Lebastchi, A. H. *et al.* Michigan Prostate Score (Mips): an Analysis of a Novel Urinary Biomarker Panel for the Prediction of Prostate Cancer and Its Impact on Biopsy Rates. *J. Urol.* **197**, 128 (2017).

186. Tomlins, S. A. *et al.* Urine TMPRSS2:ERG Plus PCA3 for Individualized Prostate Cancer Risk Assessment. *Eur. Urol.* **70**, 45–53 (2016).
187. Klein, E. A. *et al.* A 17-gene assay to predict prostate cancer aggressiveness in the context of gleason grade heterogeneity, tumor multifocality, and biopsy undersampling. *Eur. Urol.* **66**, 550–560 (2014).
188. Knezevic, D. *et al.* Analytical validation of the Oncotype DX prostate cancer assay - a clinical RT-PCR assay optimized for prostate needle biopsies. *BMC Genomics* **14**, 1-12 (2013).
189. Sharma, J. *et al.* Elevated IL-8, TNF- $\alpha$ , and MCP-1 in men with metastatic prostate cancer starting androgen-deprivation therapy (ADT) are associated with shorter time to castration-resistance and overall survival. *Prostate* **74**, 820–828 (2014).
190. Kumar, S. *et al.* IL-8 and CRP as Predictive Markers in Prostate Cancer. *Int. J. Radiat. Oncol.* **99**, E251 (2017).
191. Väisänen, M. R., Jukkola-Vuorinen, A., Vuopala, K. S., Selander, K. S. & Vaarala, M. H. Expression of Toll-like receptor-9 is associated with poor progression-free survival in prostate cancer. *Oncol. Lett.* **5**, 1659–1663 (2013).
192. Benzon, B. *et al.* Correlation of B7-H3 with androgen receptor, immune pathways and poor outcome in prostate cancer: An expression-based analysis. *Prostate Cancer Prostatic Dis.* **20**, 28–35 (2017).
193. Castellanos, J. R. *et al.* B7-H3 role in the immune landscape of cancer. *Am J Clin Exp Immunol* **6**, 66–75 (2017).
194. Wang, X. *et al.* Autoantibody Signatures in Prostate Cancer. *N. Engl. J. Med.* **353**, 1224–1235 (2005).

195. Mintz, P. J. *et al.* Discovery and horizontal follow-up of an autoantibody signature in human prostate cancer. *Proc. Natl. Acad. Sci.* **112**, 2515–2520 (2015).
196. Chen, N. & Zhou, Q. The evolving Gleason grading system. *Chin. J. Cancer Res.* **28**, 58–64 (2016).
197. Turker, P. *et al.* Presence of high grade tertiary Gleason pattern upgrades the Gleason sum score and is inversely associated with biochemical recurrence-free survival. *Urol. Oncol. Semin. Orig. Investig.* **31**, 93–98 (2013).
198. Brierley, J. The evolving TNM cancer staging system: an essential component of cancer care. *Can. Med. Assoc. J.* **174**, 155–156 (2006).
199. Barbieri, C. E. *et al.* The Mutational Landscape of Prostate Cancer. *Eur. Urol.* **64**, 567–576 (2013).
200. Cairns, P. *et al.* Frequent inactivation of PTEN/MMAC1 in primary prostate cancer. *Cancer Res.* **57**, 4997–5000 (1997).
201. Phin, S., Moore, M. W. & Cotter, P. D. Genomic Rearrangements of PTEN in Prostate Cancer. *Front. Oncol.* **3**, 1-9 (2013).
202. Taylor, B. S. *et al.* Integrative Genomic Profiling of Human Prostate Cancer. *Cancer Cell* **18**, 11–22 (2010).
203. Chen, M. *et al.* Identification of PHLPP1 as a Tumor Suppressor Reveals the Role of Feedback Activation in PTEN-Mutant Prostate Cancer Progression. *Cancer Cell* **20**, 173–186 (2011).
204. Sun, X. *et al.* Genetic alterations in the PI3K pathway in prostate cancer. *Anticancer Res.* **29**, 1739–1743 (2009).

205. Barbieri, C. E. *et al.* Exome sequencing identifies recurrent SPOP, FOXA1 and MED12 mutations in prostate cancer. *Nat. Genet.* **44**, 685–689 (2012).
206. Meek, D. W. The p53 response to DNA damage. *DNA Repair (Amst.)*. **3**, 1049–1056 (2004).
207. Beltran, H. *et al.* Targeted Next-generation Sequencing of Advanced Prostate Cancer Identifies Potential Therapeutic Targets and Disease Heterogeneity. *Eur. Urol.* **63**, 920–926 (2013).
208. Kumar, A. *et al.* Exome sequencing identifies a spectrum of mutation frequencies in advanced and lethal prostate cancers. *Proc. Natl. Acad. Sci.* **108**, 17087–17092 (2011).
209. Grasso, C. S. *et al.* The mutational landscape of lethal castration-resistant prostate cancer. *Nature* **487**, 239–243 (2012).
210. Hughes, I. A. *et al.* Androgen insensitivity syndrome. *Lancet* **380**, 1419–1428 (2012).
211. Tomlins, S. A. *et al.* ETS Gene Fusions in Prostate Cancer: From Discovery to Daily Clinical Practice. *Eur. Urol.* **56**, 275–286 (2009).
212. Tomlins, S. A. Recurrent Fusion of TMPRSS2 and ETS Transcription Factor Genes in Prostate Cancer. *Science (80-. ).* **310**, 644–648 (2005).
213. Liu, W. *et al.* Identification of novel CHD1-associated collaborative alterations of genomic structure and functional assessment of CHD1 in prostate cancer. *Oncogene* **31**, 3939–3948 (2012).
214. Saraon, P., Drabovich, A. P., Jarvi, K. A. & Diamandis, E. P. Mechanisms of Androgen-Independent Prostate Cancer. *EJIFCC* **25**, 42–54 (2014).
215. Dillard, P. R., Lin, M.-F. & Khan, S. A. Androgen-independent prostate cancer cells acquire the complete steroidogenic potential of synthesizing testosterone from cholesterol.

*Mol. Cell. Endocrinol.* **295**, 115–120 (2008).

216. Hospital, B. I. Treatment of Androgen-Independent Prostate Cancer. *Oncologist* **1**, 30–35 (1996).
217. Parker, C., Gillessen, S., Heidenreich, A. & Horwich, A. Cancer of the prostate: ESMO Clinical Practice Guidelines for diagnosis, treatment and follow-up. *Ann. Oncol.* **26**, 69–77 (2015).
218. Chang, A. J., Autio, K. A., Roach, M. & Scher, H. I. High-risk prostate cancer—classification and therapy. *Nat. Rev. Clin. Oncol.* **11**, 308–323 (2014).
219. Klotz, L. & Emberton, M. Management of low risk prostate cancer—active surveillance and focal therapy. *Nat. Rev. Clin. Oncol.* **11**, 324–334 (2014).
220. Yang, S. L., Cao, Q., Zhou, K. C., Feng, Y. J. & Wang, Y. Z. Transient receptor potential channel C3 contributes to the progression of human ovarian cancer. *Oncogene* **28**, 1320–1328 (2009).
221. Aydar, E., Yeo, S., Djamgoz, M. & Palmer, C. Abnormal expression, localization and interaction of canonical transient receptor potential ion channels in human breast cancer cell lines and tissues: a potential target for breast cancer diagnosis and therapy. *Cancer Cell Int.* **9**, 1-12 (2009).
222. Ding, X. *et al.* Essential Role of TRPC6 Channels in G2/M Phase Transition and Development of Human Glioma. *JNCI J. Natl. Cancer Inst.* **102**, 1052–1068 (2010).
223. Guilbert, A. *et al.* Expression of TRPC6 channels in human epithelial breast cancer cells. *BMC Cancer* **8**, 1-11 (2008).
224. Park, Y. R. *et al.* Data-driven Analysis of TRP Channels in Cancer: Linking Variation in

Gene Expression to Clinical Significance. *Cancer Genomics Proteomics* **13**, 83–90 (2016).

225. Middelbeek, J. *et al.* TRPM7 Is Required for Breast Tumor Cell Metastasis. *Cancer Res.* **72**, 4250–4261 (2012).
226. Yee, N. Role of TRPM7 in Cancer: Potential as Molecular Biomarker and Therapeutic Target. *Pharmaceuticals* **10**, 1-15 (2017).
227. Ma, X. *et al.* Transient receptor potential channel TRPC5 is essential for P-glycoprotein induction in drug-resistant cancer cells. *Proc. Natl. Acad. Sci.* **109**, 16282–16287 (2012).
228. Wang, T. *et al.* Inhibition of Transient Receptor Potential Channel 5 Reverses 5-Fluorouracil Resistance in Human Colorectal Cancer Cells. *J. Biol. Chem.* **290**, 448–456 (2015).
229. Zhang, P. *et al.* TRPC5-induced autophagy promotes drug resistance in breast carcinoma via CaMKK $\beta$ /AMPK $\alpha$ /mTOR pathway. *Sci. Rep.* **7**, 1-13 (2017).
230. Tsavaler, L., Shapero, M. H., Morkowski, S. & Laus, R. Trp-p8, a novel prostate-specific gene, is up-regulated in prostate cancer and other malignancies and shares high homology with transient receptor potential calcium channel proteins. *Cancer Res.* **61**, 3760–3769 (2001).
231. Gkika, D., Flourakis, M., Lemonnier, L. & Prevarska, N. PSA reduces prostate cancer cell motility by stimulating TRPM8 activity and plasma membrane expression. *Oncogene* **29**, 4611–4616 (2010).
232. Zhang, L. & Barritt, G. J. Evidence that TRPM8 Is an Androgen-Dependent Ca<sup>2+</sup>

Channel Required for the Survival of Prostate Cancer Cells. *Cancer Res.* **64**, 8365–8373 (2004).

233. de la Torre-Martínez, R. *et al.* Synthesis, high-throughput screening and pharmacological characterization of  $\beta$ -lactam derivatives as TRPM8 antagonists. *Sci. Rep.* **7**, 1-13 (2017).
234. Grolez, G. & Gkika, D. TRPM8 Puts the Chill on Prostate Cancer. *Pharmaceuticals* **9**, 1-8 (2016).
235. Berg, K. D. *et al.* TRPM4 protein expression in prostate cancer: a novel tissue biomarker associated with risk of biochemical recurrence following radical prostatectomy. *Virchows Arch.* **468**, 345–355 (2016).
236. Monet, M. *et al.* Role of Cationic Channel TRPV2 in Promoting Prostate Cancer Migration and Progression to Androgen Resistance. *Cancer Res.* **70**, 1225–1235 (2010).
237. Fixemer, T., Wissenbach, U., Flockerzi, V. & Bonkhoff, H. Expression of the Ca<sup>2+</sup>-selective cation channel TRPV6 in human prostate cancer: a novel prognostic marker for tumor progression. *Oncogene* **22**, 7858–7861 (2003).
238. Sánchez, M. G. *et al.* Expression of the transient receptor potential vanilloid 1 (TRPV1) in LNCaP and PC-3 prostate cancer cells and in human prostate tissue. *Eur. J. Pharmacol.* **515**, 20–27 (2005).
239. Sagredo, A. I. *et al.* TRPM4 regulates Akt/GSK3- $\beta$  activity and enhances  $\beta$ -catenin signaling and cell proliferation in prostate cancer cells. *Mol. Oncol.* **12**, 151–165 (2018).
240. Bainton, D. The Discovery of Lysosomes. *J. Cell Biol.* **91**, 66–76 (1981).
241. Cooper, G. M. & Hausman, R. E. The Cell: A Molecular Approach 2nd Edition. in *Sinauer Associates* **87**, 603-604 (2007).
242. Kolter, T. & Sandhoff, K. Principles of lysosomal membrane digestion: Stimulation of

Sphingolipid Degradation by Sphingolipid Activator Proteins and Anionic Lysosomal Lipids. *Annu. Rev. Cell Dev. Biol.* **21**, 81–103 (2005).

243. Schröder, B. A., Wrocklage, C., Hasilik, A. & Saftig, P. The proteome of lysosomes. *Proteomics* **10**, 4053–4076 (2010).
244. Braulke, T. & Bonifacino, J. S. Sorting of lysosomal proteins. *Biochim. Biophys. Acta - Mol. Cell Res.* **1793**, 605–614 (2009).
245. Saftig, P. & Klumperman, J. Lysosome biogenesis and lysosomal membrane proteins: trafficking meets function. *Nat. Rev. Mol. Cell Biol.* **10**, 623–635 (2009).
246. Mindell, J. A. Lysosomal Acidification Mechanisms. *Annu. Rev. Physiol.* **74**, 69–86 (2012).
247. Lieberman, A. P. *et al.* Autophagy in lysosomal storage disorders. *Autophagy* **8**, 719–730 (2012).
248. Ballabio, A. & Gieselmann, V. Lysosomal disorders: From storage to cellular damage. *Biochimica et Biophysica Acta - Molecular Cell Research* **1793**, 684–696 (2009).
249. Andrejewski, N. *et al.* Normal Lysosomal Morphology and Function in LAMP-1-deficient Mice. *J. Biol. Chem.* **274**, 12692–12701 (1999).
250. Zhong, X. Z., Yang, Y., Sun, X. & Dong, X.-P. Methods for monitoring Ca<sup>2+</sup> and ion channels in the lysosome. *Cell Calcium* **64**, 20–28 (2017).
251. Sterea, A. M., Almasi, S. & El Hiani, Y. The hidden potential of lysosomal ion channels: A new era of oncogenes. *Cell Calcium* **72**, 91–103 (2018).
252. Luzio, J. P., Pryor, P. R. & Bright, N. A. Lysosomes: fusion and function. *Nat. Rev. Mol. Cell Biol.* **8**, 622–632 (2007).
253. Morgan, A. J., Platt, F. M., Lloyd-Evans, E. & Galione, A. Molecular mechanisms of

- endolysosomal Ca<sup>2+</sup> signalling in health and disease. *Biochem. J.* **439**, 349–74 (2011).
254. Dong, X. P., Wang, X. & Xu, H. TRP channels of intracellular membranes. *Journal of Neurochemistry* **113**, 313–328 (2010).
255. Sardiello, M. *et al.* A Gene Network Regulating Lysosomal Biogenesis and Function. *Science* **325**, 473-477 (2009).
256. Boya, P. Lysosomal Function and Dysfunction: Mechanism and Disease. *Antioxid. Redox Signal.* **17**, 766–774 (2012).
257. Lange, P. F., Wartosch, L., Jentsch, T. J. & Fuhrmann, J. C. ClC-7 requires Ostm1 as a β-subunit to support bone resorption and lysosomal function. *Nature* **440**, 220–223 (2006).
258. Chakraborty, K., Leung, K. H. & Krishnan, Y. High luminal chloride in the lysosome is critical for lysosome function. *Elife* **6**, 1–21 (2017).
259. Platt, F. M., Boland, B. & van der Spoel, A. C. Lysosomal storage disorders: The cellular impact of lysosomal dysfunction. *J. Cell Biol.* **199**, 723–734 (2012).
260. Jardim, L. B., Villanueva, M. M., Souza, C. F. M. de & Netto, C. B. O. Clinical aspects of neuropathic lysosomal storage disorders. *J. Inherit. Metab. Dis.* **33**, 315–329 (2010).
261. Berman, E. R., Livni, N., Shapira, E., Merin, S. & Levij, I. S. Congenital corneal clouding with abnormal systemic storage bodies: A new variant of mucolipidosis. *J. Pediatr.* **84**, 519–526 (1974).
262. Chen, C. C. *et al.* A small molecule restores function to TRPML1 mutant isoforms responsible for mucolipidosis type IV. *Nat. Commun.* **5**, 1-10 (2014).
263. Slaugenhaupt, S. a *et al.* Mapping of the Mucolipidosis Type IV Gene to Chromosome 19p and Definition of Founder Haplotypes. *Am. J. Hum. Genet.* **65**, 773–778 (1999).

264. Sun, M. *et al.* Mucolipidosis type IV is caused by mutations in a gene encoding a novel transient receptor potential channel. *Hum. Mol. Genet.* **9**, 2471–2478 (2000).
265. Bargal, R. *et al.* Identification of the gene causing mucolipidosis type IV. *Nat. Genet.* **26**, 118–23 (2000).
266. Onyenwoke, R. U. *et al.* The mucolipidosis IV  $\text{Ca}^{2+}$  channel TRPML1 (MCOLN1) is regulated by the TOR kinase. *Biochem. J.* **470**, 331–342 (2015).
267. Venugopal, B. *et al.* Chaperone-mediated autophagy is defective in mucolipidosis type IV. *J. Cell. Physiol.* **219**, 344–353 (2009).
268. COSENS, D. J. & MANNING, A. Abnormal Electroretinogram from a Drosophila Mutant. *Nature* **224**, 285–287 (1969).
269. Hardie, R. C. & Minke, B. The trp gene is essential for a light-activated  $\text{Ca}^{2+}$  channel in Drosophila photoreceptors. *Neuron* **8**, 643–651 (1992).
270. Kaneko, Y. & Szallasi, A. Transient receptor potential (TRP) channels: A clinical perspective. *British Journal of Pharmacology* **171**, 2474–2507 (2014).
271. Clapham, D. E., Runnels, L. W. & Strübing, C. The trp ion channel family. *Nat. Rev. Neurosci.* **2**, 387–396 (2001).
272. Venkatachalam, K. & Montell, C. TRP Channels. *Annu. Rev. Biochem.* **76**, 387–417 (2007).
273. Pedersen, S. F., Owsianik, G. & Nilius, B. TRP channels: An overview. *Cell Calcium* **38**, 233–252 (2005).
274. Cheng, X., Shen, D., Samie, M. & Xu, H. Mucolipins: Intracellular TRPML1-3 channels. *FEBS Letters* **584**, 2013–2021 (2010).
275. Schmiege, P., Fine, M., Blobel, G. & Li, X. Human TRPML1 channel structures in open

- and closed conformations. *Nature* **550**, (2017).
276. Shen, D. *et al.* Lipid storage disorders block lysosomal trafficking by inhibiting a TRP channel and lysosomal calcium release. *Nat. Commun.* **3**, (2012).
277. Grimm, C. *et al.* Small Molecule Activators of TRPML3. *Chem. Biol.* **17**, 135–148 (2010).
278. Grimm, C., Hassan, S., Wahl-Schott, C. & Biel, M. Role of TRPML and Two-Pore Channels in Endolysosomal Cation Homeostasis. *J. Pharmacol. Exp. Ther.* **342**, 236–244 (2012).
279. Grimm, C., Barthmes, M. & Wahl-Schott, C. TRPML3. *Handb. Exp. Pharmacol.* **222**, 659–674 (2014).
280. Li, M. *et al.* Structural basis of dual Ca<sup>2+</sup>/pH regulation of the endolysosomal TRPML1 channel. *Nat. Struct. Mol. Biol.* **24**, 205–213 (2017).
281. Dong, X. P. *et al.* Activating mutations of the TRPML1 channel revealed by proline-scanning mutagenesis. *J. Biol. Chem.* **284**, 32040–32052 (2009).
282. Vergarajauregui, S. & Puertollano, R. Two di-leucine motifs regulate trafficking of mucolipin-1 to lysosomes. *Traffic* **7**, 337–353 (2006).
283. Miedel, M. T., Weixel, K. M., Bruns, J. R., Traub, L. M. & Weisz, O. A. Posttranslational cleavage and adaptor protein complex-dependent trafficking of mucolipin-1. *J. Biol. Chem.* **281**, 12751–12759 (2006).
284. LaPlante, J. M. *et al.* Identification and characterization of the single channel function of human mucolipin-1 implicated in mucolipidosis type IV, a disorder affecting the lysosomal pathway. *FEBS Lett.* **532**, 183–187 (2002).
285. Dong, X.-P. *et al.* The type IV mucolipidosis-associated protein TRPML1 is an

- endolysosomal iron release channel. *Nature* **455**, 992–996 (2008).
286. Dong, X. *et al.* PI(3,5)P<sub>2</sub> controls membrane trafficking by direct activation of mucolipin Ca<sup>2+</sup> release channels in the endolysosome. *Nat. Commun.* **1**, 1–11 (2010).
287. Bach, G. Mucolipin 1: Endocytosis and cation channel - A review. *Pflugers Archiv European Journal of Physiology* **451**, 313–317 (2005).
288. Alexander, S. P. H., Mathie, a & Peters, J. a. *Guide to Receptors and Channels, 2nd edition (2007 Revision)*. *British journal of pharmacology* **150**, (2007).
289. Wang, W. *et al.* Up-regulation of lysosomal TRPML1 channels is essential for lysosomal adaptation to nutrient starvation. *Proc. Natl. Acad. Sci.* **112**, E1373–E1381 (2015).
290. Settembre, C. *et al.* TFEB Links Autophagy to Lysosomal Biogenesis. *Science*. **332**, 1429–1433 (2011).
291. Soyombo, A. A. *et al.* TRP-ML1 regulates lysosomal pH and acidic lysosomal lipid hydrolytic activity. *J. Biol. Chem.* **281**, 7294–7301 (2006).
292. Zhang, L. *et al.* TRPML1 Participates in the Progression of Alzheimer's Disease by Regulating the PPAR $\gamma$ /AMPK/Mtor Signalling Pathway. *Cell. Physiol. Biochem.* **43**, 2446–2456 (2017).
293. Miller, A. *et al.* Mucolipidosis Type IV Protein TRPML1-Dependent Lysosome Formation. *Traffic* **16**, 284–297 (2015).
294. Fehrenbacher, N. *et al.* Sensitization to the lysosomal cell death pathway by oncogene-induced down-regulation of lysosome-associated membrane proteins 1 and 2. *Cancer Res.* **68**, 6623–6633 (2008).
295. Serrano-Puebla, A. & Boya, P. Lysosomal membrane permeabilization in cell death: new

- evidence and implications for health and disease. *Ann. N. Y. Acad. Sci.* **1371**, 30–44 (2016).
296. Samie, M. A. *et al.* The tissue-specific expression of TRPML2 (MCOLN-2) gene is influenced by the presence of TRPML1. *Pflugers Arch. Eur. J. Physiol.* **459**, 79–91 (2009).
297. Sun, L., Hua, Y., Vergarajauregui, S., Diab, H. I. & Puertollano, R. Novel Role of TRPML2 in the Regulation of the Innate Immune Response. *J. Immunol.* **195**, 4922–32 (2015).
298. Puertollano, R. & Kiselyov, K. TRPMLs : in sickness and in health. *Am. J. Physiol. Renal Physiol.* **296**, 1245-1254 (2009).
299. Hirschi, M. *et al.* Cryo-electron microscopy structure of the lysosomal calcium-permeable channel TRPML3. *Nature* **550**, 411-414 (2017).
300. Guo, Z., Grimm, C., Becker, L., Ricci, A. J. & Heller, S. A Novel Ion Channel Formed by Interaction of TRPML3 with TRPV5. *PLoS One* **8**, 8–10 (2013).
301. Di Palma, F. *et al.* Mutations in Mcoln3 associated with deafness and pigmentation defects in varitint-waddler (Va) mice. *Proc. Natl. Acad. Sci. U. S. A.* **99**, 14994–14999 (2002).
302. Gkika, D. & Prevarskaya, N. TRP channels in prostate cancer: the good, the bad and the ugly? *Asian J. Androl.* **13**, 673–676 (2011).
303. Tiscornia, G., Singer, O. & Verma, I. M. Production and purification of lentiviral vectors. *Nat. Protoc.* **1**, 241–5 (2006).
304. Livak, K. J. & Schmittgen, T. D. Analysis of Relative Gene Expression Data Using Real-

- Time Quantitative PCR and the 2– $\Delta\Delta$ CT Method. *Methods* **25**, 402–408 (2001).
305. Kishore, J., Goel, M. & Khanna, P. Understanding survival analysis: Kaplan-Meier estimate. *Int. J. Ayurveda Res.* **1**, 274 (2010).
306. Gao, J. *et al.* Integrative Analysis of Complex Cancer Genomics and Clinical Profiles Using the cBioPortal. *Sci. Signal.* **6**, pl1-pl1 (2013).
307. Cerami, E. *et al.* The cBio Cancer Genomics Portal: An Open Platform for Exploring Multidimensional Cancer Genomics Data: Figure 1. *Cancer Discov.* **2**, 401–404 (2012).
308. Kilpatrick, B. S., Yates, E., Grimm, C., Schapira, A. H. & Patel, S. Endo-lysosomal TRP mucolipin-1 channels trigger global ER Ca<sup>2+</sup> release and Ca<sup>2+</sup> influx. *J. Cell Sci.* **129**, 3859–3867 (2016).
309. Löbrich, M. & Jeggo, P. A. The impact of a negligent G2/M checkpoint on genomic instability and cancer induction. *Nat. Rev. Cancer* **7**, 861–869 (2007).
310. Nielsen, I., Andersen, A. H. & Bjergbæk, L. Studying repair of a single protein-bound nick in vivo using the Flp-nick system. *Methods Mol. Biol.* **920**, 393–415 (2012).
311. Trachootham, D., Alexandre, J. & Huang, P. Targeting cancer cells by ROS-mediated mechanisms: a radical therapeutic approach? *Nat. Rev. Drug Discov.* **8**, 579–591 (2009).
312. Sridharan, S., Jain, K. & Basu, A. Regulation of Autophagy by Kinases. *Cancers (Basel)*. **3**, 2630–2654 (2011).
313. Lin, K., Lipsitz, R., Miller, T. & Janakiraman, S. Benefits and Harms of Prostate-Specific Antigen Screening for Prostate Cancer: An Evidence Update for the U.S. Preventive Services Task Force. *Ann. Intern. Med.* **149**, 192 (2008).
314. Cunningham, D. & You, Z. In vitro and in vivo model systems used in prostate cancer research. *J. Biol. Methods* **2**, 1-28 (2015).

315. Pierzyńska-Mach, A., Janowski, P. A. & Dobrucki, J. W. Evaluation of acridine orange, LysoTracker Red, and quinacrine as fluorescent probes for long-term tracking of acidic vesicles. *Cytom. Part A* **85**, 729–737 (2014).
316. Morelli, M. B. *et al.* Overexpression of transient receptor potential mucolipin-2 ion channels in gliomas: role in tumor growth and progression. *Oncotarget* **7**, 43654–43668 (2016).
317. Altonen, K. *et al.* High cyclin B1 expression is associated with poor survival in breast cancer. *Br. J. Cancer* **100**, 1055–1060 (2009).
318. Hassan, K. A., El-naggar, A. K., Soria, J., Liu, D. & Hong, W. K. Clinical Significance of Cyclin B1 Protein Expression in Squamous Cell Carcinoma of the Tongue Clinical Significance of Cyclin B1 Protein Expression in Squamous Cell Carcinoma of the Tongue 1. *J. Clin. Oncol.* **19**, 2458–2462 (2001).
319. LI, W. *et al.* Prognostic significance of claudin-1 and cyclin B1 protein expression in patients with hypopharyngeal squamous cell carcinoma. *Oncol. Lett.* **11**, 2995–3002 (2016).
320. Weng, L. *et al.* Identification of cyclin B1 and Sec62 as biomarkers for recurrence in patients with HBV-related hepatocellular carcinoma after surgical resection. *Mol. Cancer* **11**, 1-10 (2012).
321. Zhang, X. *et al.* MCOLN1 is a ROS sensor in lysosomes that regulates autophagy. *Nat. Commun.* **7**, 1-12 (2016).
322. Ahuja, M., Park, S., Shin, D. M. & Muallem, S. TRPML1 as lysosomal fusion guard. *Channels* **10**, 261–263 (2016).
323. Pan, J. *et al.* Reactive Oxygen Species-Activated Akt/ASK1/p38 Signaling Pathway in

- Nickel Compound-Induced Apoptosis in BEAS 2B Cells. *Chem. Res. Toxicol.* **23**, 568–577 (2010).
324. Chetram, M. A. *et al.* ROS-mediated activation of AKT induces apoptosis via pVHL in prostate cancer cells. *Mol. Cell. Biochem.* **376**, 63–71 (2013).
325. Nogueira, V. *et al.* Akt Determines Replicative Senescence and Oxidative or Oncogenic Premature Senescence and Sensitizes Cells to Oxidative Apoptosis. *Cancer Cell* **14**, 458–470 (2008).
326. Yan, H., Gao, Y. & Zhang, Y. Inhibition of JNK suppresses autophagy and attenuates insulin resistance in a rat model of nonalcoholic fatty liver disease. *Mol. Med. Rep.* **15**, 180–186 (2017).
327. Jin, H.-O. *et al.* Inhibition of JNK-mediated autophagy enhances NSCLC cell sensitivity to mTORC1/2 inhibitors. *Sci. Rep.* **6**, 1-11 (2016).
328. Sarkar, S. *et al.* Complex Inhibitory Effects of Nitric Oxide on Autophagy. *Mol. Cell* **43**, 19–32 (2011).
329. Shen, C., Yan, J., Erkocak, O. F., Zheng, X.-F. & Chen, X.-D. Nitric oxide inhibits autophagy via suppression of JNK in meniscal cells. *Rheumatology* **53**, 1022–1033 (2014).
330. Park, H.-S., Huh, S.-H., Kim, M.-S., Lee, S. H. & Choi, E.-J. Nitric oxide negatively regulates c-Jun N-terminal kinase/stress-activated protein kinase by means of S-nitrosylation. *Proc. Natl. Acad. Sci.* **97**, 14382–14387 (2000).
331. Plenquette, S., Romagny, S., Laurens, V. & Bettaieb, A. S-nitrosylation in TNF superfamily signaling pathway: Implication in cancer. *Redox Biol.* **6**, 507–515 (2015).

332. Kwak, Y.-D. *et al.* NO signaling and S-nitrosylation regulate PTEN inhibition in neurodegeneration. *Mol. Neurodegener.* **5**, 1-12 (2010).
333. Zhu, L. *et al.* NOS1 S-nitrosylates PTEN and inhibits autophagy in nasopharyngeal carcinoma cells. *Cell Death Discov.* **3**, 1-10 (2017).
334. Yee, N. S., Chan, A. S., Yee, J. D. & Yee, R. K. TRPM7 and TRPM8 Ion Channels in Pancreatic Adenocarcinoma: Potential Roles as Cancer Biomarkers and Targets. *Scientifica (Cairo)*. **2012**, 1–8 (2012).
335. Yee, N. *et al.* Aberrantly Over-Expressed TRPM8 Channels in Pancreatic Adenocarcinoma: Correlation with Tumor Size/Stage and Requirement for Cancer Cells Invasion. *Cells* **3**, 500–516 (2014).
336. Zhao, W. & Xu, H. High expression of TRPM8 predicts poor prognosis in patients with osteosarcoma. *Oncol. Lett.* **12**, 1373–1379 (2016).